Université de Lille

Doctoral School **Ecole Doctorale Sciences Pour l'Ingénieur Université Lille Nord-de-France - 072**

University Department **Institut de Recherche sur les Composants logiciels et matériels pour l'Information et la Communication Avancée**

Thesis defended by **Nícolas de Araújo Moreira**

Defended on **11th July, 2019**

In order to become Doctor from Université de Lille

Academic Field **Sciences for Engineering**

Speciality **Electronics, microelectronics, nanoelectronics and microwaves**

Thesis Title

On heterogeneous networks under non-Gaussian interferences:
experimental and theoretical aspects

Thesis supervised by Laurent Clavier

Committee members

Referees	Olivier Berder	ENSSAT/IRISA	
	Jean-Yves Baudais	IETR/INSA Rennes	
Examiners	Virginie Degardin	Professor at IEMN	Committee President
	Leonardo Sampaio Cardoso	INSA Lyon	
	Nathalie Mitton	INRIA Lille-Nord Europe	
	Ahcène Bounceur	Université de Bretagne Occidentale	
Supervisor	Laurent Clavier	IMT Lille Douai	

Université de Lille

Doctoral School **Ecole Doctorale Sciences Pour l'Ingénieur Université Lille Nord-de-France - 072**

University Department **Institut de Recherche sur les Composants logiciels et matériels pour l'Information et la Communication Avancée**

Thesis defended by **Nícolas de Araújo Moreira**

Defended on **11th July, 2019**

In order to become Doctor from Université de Lille

Academic Field **Sciences for Engineering**

Speciality **Electronics, microelectronics, nanoelectronics and microwaves**

Thesis Title

On heterogeneous networks under non-Gaussian interferences:
experimental and theoretical aspects

Thesis supervised by Laurent Clavier

Committee members

Referees	Olivier Berder	ENSSAT/IRISA	
	Jean-Yves Baudais	IETR/INSA Rennes	
Examiners	Virginie Degardin	Professor at IEMN	Committee President
	Leonardo Sampaio Cardoso	INSA Lyon	
	Nathalie Mitton	INRIA Lille-Nord Europe	
	Ahcène Bounceur	Université de Bretagne Occidentale	
Supervisor	Laurent Clavier	IMT Lille Douai	

Université de Lille

École doctorale **Ecole Doctorale Sciences Pour l'Ingénieur Université Lille Nord-de-France - 072**

Unité de recherche **Institut de Recherche sur les Composants logiciels et matériels pour l'Information et la Communication Avancée**

Thèse présentée par **Nícolas de Araújo Moreira**

Soutenue le **11 juillet 2019**

En vue de l'obtention du grade de docteur de l'Université de Lille

Discipline **Sciences pour l'Ingénieur**

Spécialité **Electronique, microélectronique, nanoélectronique et micro-ondes**

Titre de la thèse

Réseaux de capteurs sous interférence non-Gaussienne :
aspects expérimentaux et théoriques

Thèse dirigée par Laurent Clavier

Composition du jury

Rapporteurs	Olivier Berder	ENSSAT/IRISA	
	Jean-Yves Baudais	IETR/INSA Rennes	
Examinateurs	Virginie Degardin	professeur à l'IEMN	président du jury
	Leonardo Sampaio Cardoso	INSA Lyon	
	Nathalie Mitton	INRIA Lille-Nord Europe	
	Ahcène Bounceur	Université de Bretagne Occidentale	
Directeur de thèse	Laurent Clavier	IMT Lille Douai	

This thesis has been prepared at

Institut de Recherche sur les Composants logiciels et matériels pour l'Information et la Communication Avancée

Parc Scientifique de la Haute Borne
50, avenue Halley
B.P. 70478
59658 Villeneve d'Ascq
France

☎   (33)(0)3 62 53 15 00
✉   seretariat@iria.univ-lille1.fr
Web Site   http://www.ircica.univ-lille1.fr/

To my family

Combati o bom combate, acabei a carreira, guardei a fé.

<div align="right">2 Timóteo 7</div>

O sertanejo é, antes de tudo, um forte.

<div align="right">Euclides da Cunha</div>

ON HETEROGENEOUS NETWORKS UNDER NON-GAUSSIAN INTERFERENCES:
experimental and theoretical aspects

Abstract

Internet of Things represents a technical challenge for 5G communications due to its characteristic heterogeneity: the 2.4 GHz ISM band, for example, is shared between different kind of technologies, such Wifi, Bluetooth and Zigbee. In addition to the loss of quality of communication, recent studies show that interference increases significantly the energy consumption. So, dealing with interference becomes an important task to ensure successfull data transmission. The present thesis approaches two aspects of heterogeneous networks. The first part presents an experimental study on the nature of interference between IEEE 802.11 and IEEE 802.15.4 devices, its impacts on the communication reliability and proposes a statistical description of it. The main conclusion of this part is that, on this context, the interference may present a non-Gaussian behavior, more precisely, an impulsive behavior. Recent theoretical works allied with these experimental results show that the α-stable distribution is more adequate to represent impulsive noises. It means that the, once optimal, classical communication architectures based on the Gaussian assumption, particularly the Least Squares based channel estimation and linear receiver, is not optimal anymore, presenting a significant loss of performance. The second part presents a robust MIMO architecutre based on Alamouti coding, supervised channel estimation based on Least Absolute Deviation and p-norm receiver with an estimator for p. The proposed approach outperforms the classical method.

Keywords: internet of things, sensor netowrks, non-gaussian interference

Réseaux de capteurs sous interférence non-Gaussienne :
aspects expérimentaux et théoriques

Résumé

L'Internet des Objets représente un défi technique pour la communication 5G à cause de sa hétérogénéité caractéristique : la bande 2.4 GHz ISM, par exemple, est partagée entre différentes types de technologies, comme Wifi, Bluetooth et Zigbee. En plus de la perte de qualité de communication, des études récents montrent que l'interférence augmente de façon significative la consommation d'énergie. Donc, traiter l'interférence devient un tâche important pour assurer la réussite de la transmission de donnés. Cette thèse s'approche de deux aspects différents des réseaux hétérogènes. La première partie présente un étude expérimentale sur la nature de l'interférence entre dispositifs IEEE 802.11 et 802.15.4, ses impacts dans la fiabilité de la communication et propose une description statistique. La conclusion principale est que, dans ce contexte, l'interférence présente un comportement non-Gaussien, plus précisément, impulsif. Des travaux théoriques récents alliés avec ces résultats expérimentaux montrent que la distribution α-stable est plus convenable pour représenter bruits impulsives. Cela signifie que, une fois optimal, les architectures de communication classiques basé sur assomption Gaussienne, particulièrement le méthode des moindres carrés et le récepteur linéaire, ne sont plus optimales et présentent une perte de performance significative. La deuxième partie présente une architecture MIMO basé sur codage Alamouti, estimation de canal supervisée basé sur méthode *Least Absolute Deviation* et récepteur p-norme avec une estimation de p. L'architecture proposée présente une performance supérieure au méthode classique.

Mots clés : internet des objets, réseaux de capteurs, interférences non-gaussiennes

Remerciements

Before all, I would like to express my most sincere gratitude to all those who helped me during this thesis and contributed to the elaboration and success of this work.

First of all, I would like thank Prof. Laurent CLAVIER for the opportunity given, accepting me as PhD student, guiding me, and for his contributions, kindness and (enourmous) patiance. Thank you very much for your advises, contributions and attention which allowed the good development of this thesis.

Thanks also to Mr. Olivier BERDER and Mr. Jean-Yves BAUDAIS for accepting to write the report. Thanks for the also jury members Ms. Virginie DEGARDIN, Mr. Leonardo CARDOSO, Ms. Nathalie MITTON and Mr. Ahcène BOUNCEUR for their availability and for accepting to evaluate this work.

I would like to thank also Mr. Antoine SUGITA for all his help, kindness and attention while helping me with all administrative procedures. In addition, I thank Prof. Tuami LASRI, Prof. Henry HAPPY, Malika HABBAS and Malika DEBUYSSCHERE.

Thanks also for the Director of IRCICA, Prof. Nathalie ROLLAND, the leader of CSAM team, Prof. Christophe LOYEZ, the secratary fo IRCICA Peggy Stankowski, and staff of IRCICA Michel SOULANGE and Ahmed BEN ABDESE-LAM and also Anne-Sophie BEURET.

Thank you very much for all my friends and colleagues from IRCICA for helping me with ideas, opinions, tips, helping with experiments, sharing knowledge, etc.: Viktor TOLDOV, Roman IGUAL PEREZ, Xin YAN, Rahul VYAS, Umber NOREEN, Zheng CE, Angeson TESFAY, Achile, Ashenafi FEKEDE, Yasser MESTRAH, Bernard VERBEKE, Salvatore GUZZO BONIFACIO, Kevin CARPENTIER, Kamel GUERCHOUCHE, Laura GUERIN, Aymeric PASTRE, Rédha KASSI, Sebastien JACOB, Anne SAVARD and Emilie SORET.

I wold like also to thank Prof. Manuel ARDOUIN for giving me the great opportunity of working at at Institut Mines-Télécom Lille Douai. Thanks also for

Acronyms

A | B | C | D | E | F | G | I | L | M | N | O | P | Q | R | S | T | U | W | Z

A

ADC Analog-Digital Converter. 10, 19
AOR Asymptotically Optimal Receiver. 99
AWGN Additive White Gaussian Noise. 35, 74
AZMNL Algebric-tailed Zero-Memory Nonlinearity. 88, 89

B

BER Bit Error Rate. xxx, 49, 76, 103–105
BLAST Bell-Labs Layered Space Time. 74, 75
BPSK Binary Phase Shift Keying. 13

C

CF Characteristic Function. 38, 42, 51, 53, 79
CSS Chirp Spread Spectrum. 13

D

DSSS Direct Sequence Spread Spectrum. 13

E

EMI Eletromagnetic Interference. 39, 47

F

FFT Fast Fourier Transform. 53, 54
FLOM Fractional Lower-Order Moments. xxiv, 55, 58, 59, 133, 137, 139, 140, 150
FPGA Field Programmable Gate Array. 95

G

GAR Genie-Aided Receiver. 99, 105
GGD Generalized Gaussian Distributions. 37
GGM Generalized Gaussian Model. 85
GPIO General Purpose Input-Output. 19
GSM Global System for Mobile Communications. 66
GUI Graphical User Interface. xxx, 101, 103

I

i.i.d. Independent and Identically Distributed. 35, 42, 47, 51, 59, 72, 93, 143
IoT Internet of Things. 5, 7, 9, 10, 13, 14, 29, 61, 64, 75
IP Internet Protocol. 26
IR Impulse Radio. 49
ISM Industrial, Scientific and Medical. 5

L

LAD Least Absolute Deviation. 7, 96, 105, 111
LLR Log-Likelihood Ratio. xxx, 87, 89, 90
LoS Line-of-Sight. 68
LPWAN Low Power Wide Area Network. 6, 11, 13, 68
LS Least Squares. 6, 7, 73, 96, 105, 111, 138

M

MAC medium access control. 5, 42
MAI Multiple Access Interference. 14, 37, 49
MAP Maximum a Posteriori. 78, 99
MDR Minimum-Distance Receiver. 99
MIMO Multiple-Input and Multiple-Output. xxiv, xxx, 6, 68–71, 73, 75, 111, 150
ML Maximum Likelihood. 58, 72, 74, 75, 78, 80, 94, 98, 99
MPI Multi-Path Interference. 14
MRC Maximal-Ratio Combining. 74, 81, 84, 85, 91
MSE Mean-Square-Error. 89

N

NG Natural Gradient. 96
NI National Instruments. xxix, 17, 18
NIG Normal Inverse Gaussian. 86, 91

O

xxii

WSN Wireless Sensor Networks. xxiii, xxix, 9–12, 14, 16, 18–20, 22, 24–26, 28–30, 32, 34, 149

Z

ZF Zero-Forcing. 74
ZOS Zero-Order Statistics. xxv, 139, 142, 151

Summary

List of Tables

List of Figures

List of Symbols

$\mathbb{C}$: Set of complex numbers

$\mathbb{R}$: Set of real numbers

j: imaginary unit, $\sqrt{-1}$

N_T: Number of transmitting antennas

N_R: Number of receiving antennas

N_I: Number of interferers

P: Power

P_t: Power of transmitting antenna P_r: Power of receiving antenna

G_t: Gain of transmitting antenna, in dB

G_r: Gain of receiving antenna, dB

R: Radius of a circle C

d: Distance

η: Pathloss

$\mathcal{O}$: Set of interferers

f_c: Carrier frequency

λ: Number of interferer per unit area (density of the network)

$\mathcal{Q}$: Variable which includes diverse propagation effects such as multipath fading and shadowing

$\mathbf{X}_{N_s,N_T}$: Sent symbols matrix (random matrix), $\mathbf{X} \in \mathbf{C}^{N_s \times N_T}$

$\mathbf{X}_{N_s,1}^{(i)}$: Symbols transmitted over the i-th transmitting antenna, $\mathbf{X}_{N_s,i} \in \mathbf{X}_{N_s,N_T}, i \in \mathbb{N}_*$

$\mathbf{Y}_{N_s,N_R}$: Received symbols matrix (random matrix), $\mathbf{Y} \in \mathbf{C}^{N_s \times N_R}$

$\mathbf{Y}_{N_s,1}^{(m)}$: Symbols received over the m-th transmitting antenna, $\mathbf{Y}_{N_s,1} \in \mathbf{Y}_{N_s,N_R}, i \in \mathbb{N}_*$

$\mathbf{H}_{N_T,N_R}$: Received symbols matrix (random matrix), $\mathbf{H} \in \mathbf{C}^{N_T \times N_R}$

$h_{i,m}$: Complex gain and represents the fading channel coefficient between the

i-th transmitting antenna and the m-th receiver antenna, $i = 1...,N_T, m = 1...,N_R$

$\mathbf{N}_{N_s,N_R}$: Noise matrix (random matrix), $\mathbf{N} \in \mathbf{C}^{N_s \times N_R}$

$\mathbf{T}$: Training sequence matrix (previously known matrix), $\mathbf{T} \in \mathbf{C}^{N_s \times N_T}$

L: Size of training sequence

$\mathcal{S}, \mathcal{X}$: Codemap (set of symbols that can be transmitted)

s: Symbol, $s \in \mathbb{C}, s \in \mathcal{S}$

T: Period of a symbol

t: Time

π_i: Probability that x_i was transmitted

$\mathbb{P}$: Probability function

f_X: Probability density function for the random variable X

$\varphi(\cdot)$: Characteristic function

$\mathbb{E}$: Expected value

μ: Average value of a random variable

σ: Standard deviation of a random variable

α: Characteristic exponent for an α-stable distribution. For Normal inverse Gaussian, is inversely related to the heaviness, $\alpha \in]0, 2]$

β: Symmetry parameter for an α-stable distribution, or shape parameter for Generalized Gaussian distribution, $\beta \in]-1, 1]$

γ: Dispersion for an α-stable distribution, $\gamma > 0$

δ: Location parameter for an α-stable distribution

ρ_G^2: Gaussian noise power for Middleton class A model

ρ_I^2: Impulsive noise power for Middleton class A model

A: Intensity of impulsive interference on Middleton class A model

$\mathcal{A}$: Scaling factor for Generalized Gaussian distribution, $\mathcal{A} > 0$

κ: term used to adapt Myriad filter to get near-optimal performance

$\| \cdot \|_p$: p-norm

$(\cdot)^*$: Complex conjugate

$\mathcal{R}$: Real part of a complex variable

$\mathcal{I}$: Imaginary part of a complex variable

$(\cdot)^H$: Hermitian of a complex matrix

$(\cdot)^T$: Transpose of a real matrix

$(\cdot)^\dagger$: Pseudo-inverse

$(\hat{\cdot})$: Estimation of variable or matrix

$\mathbb{I}$: Heaviside function

Ω: Decision region

$\overline{\Omega}$: Complementary region

Γ: Gamma function

$\psi(\cdot)^{(m)}$: Polygamma function

$K_0(\cdot)$: Zero-order first kind modified Bessel function

$K_1(\cdot)$: Modified second kind Bessel function with index 1

$\Phi(\cdot)$: The confluent-hypergeometric function

$\mathcal{C}$: Light speed

$\mathcal{L}$: Wave length

General Introduction

The concept of Internet of Things (IoT) refers to the transparent connection of apparatuses, sensors, objects, buildings, machines, vehicles, etc. via fixed and wireless sensor networks [Wei12]. It will play in a near future an essential role in the evolution of telecommunications [Gu12; Yan15].

Telecom operators are investing a lot of money in IoT, either on the NB-IoT standard or Orange or Bouygues which have deployed LoRa networks. New players like SigFox also made their way on the market. As a consequence, the quantity of IoT devices increases significantly: up to 50 billion objects may be connected through wireless networks in 2020, using the license free Industrial, Scientific and Medical (ISM) bands. Such band does not offer a very wide spectrum, forcing many technologies to share these bands. As an example, the 2.4 GHz ISM band is used by 802.11b (Wifi), 802.15.1(Bluetooth) and 802.15.4 (ZigBee and 6LoWPAN), resulting in a congested and overloaded band. Consequently, interference becomes a strong limiting factor [Mye+07; YXG11; Yoo+06; YWL07].

A significant part of the energy consumption is due to the Radio-Frequency (RF) circuit. The authors in [Tol+16] show that the energy consumption may increase up to 4.8 times depending on the level of interference present on the environment. In this case, the interference mitigation and the development of systems exhibiting a robust behaviour when facing interference become two priority problems for IoT, more precisely for sensor networks.

This challenge due to high nodes density is even more difficult to address due to the energy constraints faced by the deployed nodes that are suppose to have a life time of several years, if not decades. To avoid too much interference, frequently, the Medium Access Control (MAC) protocol is based on carrier sense

approaches. However if listening to a device using the same protocol as yourself is one thing, it can be inefficient when it comes to listening to other types of devices. Also, some recent approaches called LPWAN (e.g. SigFOX, LoRA) question the efficiency of carrier sensing. Indeed, what the transmitter hears is not necessarily significantly correlated to what the receiver hears.

One way to increase the robustness is the spatial diversity with Multiple Input Multiple Output (MIMO) technologies. In most of the studies concerning MIMO system, the noise is assumed to be Gaussian. One efficient way to estimate the channel matrix $\hat{\mathbf{H}}$ is to use a Least Squares (LS) estimator. The transmitted symbol can then be optimally detected using Euclidean distance. This is efficient as long as the Gaussian assumption is respected, but in many papers, interference has been shown to exhibit an impulsive behaviour [LS95; Ega+17; WPS09; MCA12]. Under the presence of such impulsive interference, the system will present a significant loss of performance, so, new solutions must be proposed assuming more realistic models. To model network interference, some works propose the Symmetric α Stable model as a more adequate model [Ega+17; WPS09]. This choice can be seen as the result of the Generalized Central Limit Theorem and stable distributions allow to represent a higher variability in the interference than what is allowed by the Gaussian representation and recently some experimental works support this solution [MCA12].

Objectives

Our approach assumes a system with simple access scheme, ALOHA for instance, under the presence of impulsive interference. The first objective of this thesis is to try to characterize experimentally the environment. The second objective is to design a simple, low power and reliable communication scheme for an environment dominated by dynamic non-Gaussian interference.

To increase reliability we propose to implement a MIMO communication system. Robustness is increased trough spatial diversity. However, we do not want to increase significantly the energy consumption nor the complexity (and the cost) at the transmitter side, even if we allow a complexity increase at the receiver, inspired by the star topology of LPWAN. A relevant solution is

then to adopt an Alamouti scheme, which improves the signal quality at the receiver, so increasing reliability, without increasing the global transmitted power; besides it does not require any channel state knowledge at the transmitter side and consequently does not require any feedback from the receiver, being very adequate to the IoT context.

In this context however, channel estimation is still needed at the receiving side. The impulsive interference significantly impacts the channel estimation method. Besides, it is also important to discuss the distance metric that is used to make the decision in the detection part. An adequate choice can significantly improve the receiver performance. In this work, we are going to replace Least Squares (LS) estimator by the Least Absolute Deviation (LAD) for channel estimation. This is clearly better suited for environments with impulsive noise. Similarly, the Euclidean distance is replaced by p-norm receiver which shows a large flexibility and techniques rather simple to estimate the parameter p.

Contributions

The main contributions of the present thesis are:

1. experimental study of interference and its impact on traditional communications;

2. design of a robust communication strategy based on spatial diversity;

3. design of an adapted receiver that includes channel estimation and an adapted decision for impulsive interference (decision strategy optimization), including estimation method for the p value used for the p-norm receiver. We present the performance of the global scheme and show its significant improvement in comparison to a scheme designed for Gaussian noise.

Organization of this thesis

The present thesis is divided on two parts. The first one tries to characterize and model the interference between IEEE 802.11 (Wifi) and IEEE 802.15.4 (Zigbee). This part gives an overview on Wireless Sensor Networks and discusses the co-existence of different technologies on 2.4 GHz ISM band, explains the experimental setup to characterize the interference under heterogeneous environments and presents an statistical analysis of the distribution of interference. Based on the experimental results, this chapter ends presenting the main properties of α-stable results.

The second part proposes a robust receiver design using space diversity, comparing its performance with the existing classical approaches.

Related papers

- Victor Toldov, Román José Igual-Pérez, Rahul Vyas, Laurent Clavier, Nathalie Mitton and Nícolas de Araújo Moreira *Experimental evaluation of interference impact on the energy consumption in wireless sensor networks*, IRACON 2nd MC Meeting and 1st Technical Meeting, Lille, France. May-June. 2016.

- Nícolas de Araújo Moreira, Victor Toldov, Román José Igual-Pérez, Rahul Vyas, Nathalie Mitton, and Laurent Clavier, *Heterogeneous networks: experimental study of interference between IEEE 802.11 and IEEE 802.15.4 technologies*,Journées Scientifiques URSI France 2017, pp. 9-16, Feb. 2017.

- Nícolas de Araújo Moreira and Laurent Clavier, *Multiple antenna receiver under impulsive SαS noise*, IEEE Wireless Communications and Networking Conference (WCNC) 2019, Marrakech, Apr. 2019.

Chapter 1

Coexistence of WSNs and interference characterization

The objective of this chapter is to present in details the impact of interference of IEEE 802.11 (Wifi) technology on IEEE 802.15.4 (Zigbee) packets and its relation with energy consumption and batteries life time, combining experiments, through a system capable of listening to 2.4 GHz ISM frequency, and theoretical results to understand the change that IoT will bring in the communication environment.

1.1 Wireless Sensor Networks

Since several decades, mankind developed an interest in observing and acquiring environmental parameters for industrial or scientific purposes, such as ecological control and studies (forest fire detection, pollution surveillance, etc.), intelligent houses (illumination and temperature control), roads surveillance and traffic security [Mas12]. This part of the Internet of Things is taking more and more importance nowadays but still face numerous challenges to fully impact our everyday life. Two of these challenges are robustness and lifetime. Difficult to ensure, those two aspects are crucial for an easy and large scale deployment of IoT but they could also suffer from their potential success. Indeed, an increase in the number and density of nodes will result in an increase in the interference

level. Interference deeply impacts the reliability of communications and also the energy efficiency of the network. In the following we describe the main aspects of an IoT or more specifically a Wireless Sensor Network (WSN).

1.1.1   Architectures and components of a WSNs

The heterogeneous nature of the nodes and their miniaturization pushed the development of Systems on Chip (SoC), which integrate a wide variety of subsystems: digital, analogical, Radio-Frequency (RF), etc [Mas12]. A node of a sensor network contains one or more sensors, a microprocessor/microcontroller, a wireless communication circuit and a power source that can be separated in four units: data acquisition, signal processing, communication and energy unities (see Fig. 1.1).

Figure 1.1 – Node Block Diagram.
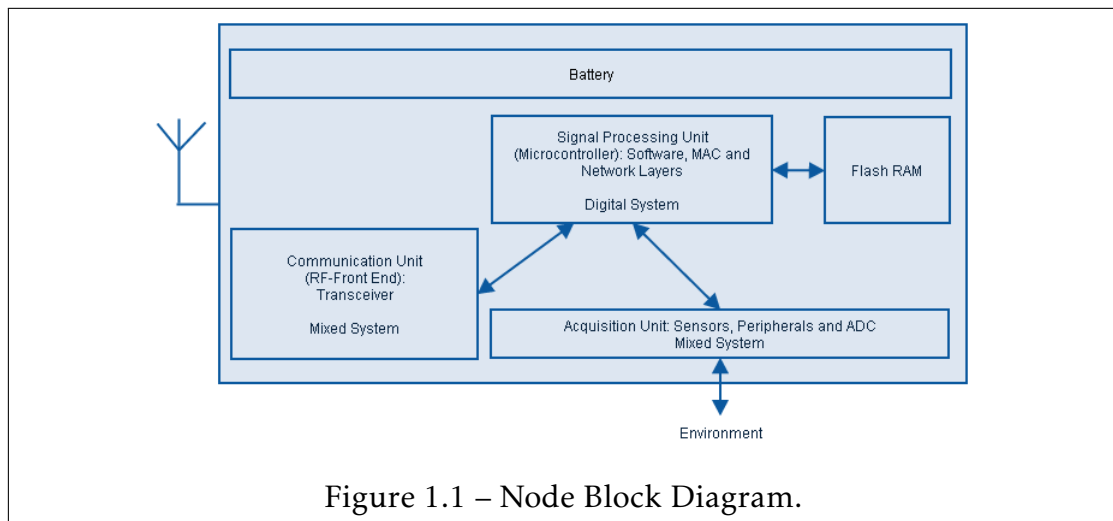
- The **data acquisition unit** is composed by one or several sensors which are responsible of the physical measurements and, generally, an Analog-Digital Converter (ADC) to transfer the measured date to the signal processing unit.

- The **signal processing unit** is composed by a processor and, possibly, memory. It has two interfaces, one with the data acquisition unit and another

with the communication unit. Is responsible data analysis according to applications, etc. [Mas12].

- The **communication unit** is responsible for the data transmission and reception via wireless links. It can contain a digital processing part and an analog part for its different functions (amplification, coding/decoding, compression equalization, filtering, synchronization, estimation). It is also responsible of multiple access protocols, routing algorithms...

- The **Energy unit** can simply be a battery or can also include some energy harvesting schemes. It is in charge of furnishing the necessary energy to all the other units.

1.1.2 WSN organisations.

WSN can be classified as event-driven, where one or several nodes detect an event and report it to a monitoring station, or demand-driven, where sensors remain silent until they receive a request from the monitoring station [CS04].

In a WSN, it is frequent to have nodes that play different roles so that we can have a hierarchical organization. In that case some nodes are end-nodes with limited capabilities, only transmitting what information they collect. Other nodes can act as relays. They both transmit their own information but also the one from other nodes, too far away to reach the sink in one hop. The sink or gateway is the collecting point, connected to the cloud via any types of link (fiber, radio,...). The network is then organized in a multihop and cooperative manner. Many standards are issued from such ideas, the most famous being Zigbee or Z-wave for instance (right picture in Fig. 1.2). Some other strategies were to group nodes in clusters in a master/slave manner. Slaves communicate with the master and masters take in charge the transmission, possibly via multihops, to the destination. Such a strategy was proposed for instance by Bluetooth.

However, more recently, to overcome the energy challenge that is difficult when routing is complex in multihop networks, star topologies have been proposed in LPWANs (left picture in Fig. 1.2). Using robust waveform design,

long range communications are possible with low power at the transmitter side. Both ultra narrow band communication or wider bandwidth (with Chirp Spread Spectrum for instance) can be used to make transmissions on ranges of several kilometers, and even tenth of kilometers in open areas.

Figure 1.2 – Types of topologies.
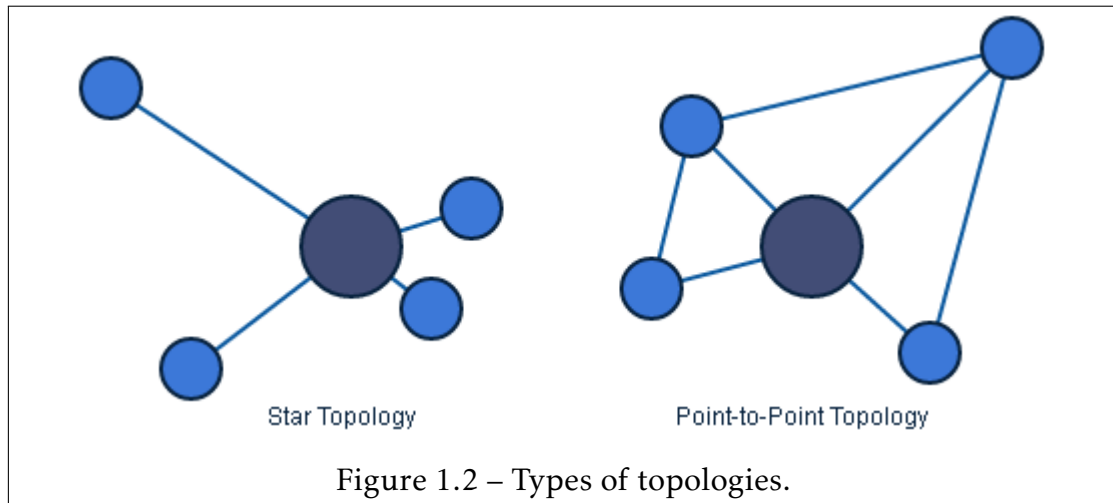
1.1.3   Standards

Two main families of standards can be found in commercial deployment of WSN:

- The multihop, *ad hoc*, configuration is mainly represented by the IEEE 802.15.4 standard. It defines several PHY layer options for short range communications (tens to hundreds of meters). The MAC and routing layers are left to the users. The most famous protocol based on this standard is certainly Zigbee, but others exist like Z-Wave, En-Ocean or 6LowPAN. Most of these protocols are intended for local area networks and are used in buildings. Bluetooth is also able to support multihop communications to ensure some increased coverage. It is based on the IEEE 802.15.1 standard and the network should organize in clusters to ensure the cooperative data transfer. In both cases, the multiple point to point communications that can arise at simultaneous times despite the carrier sensing approach used at the MAC layer, imperfect in wireless context, generate interference that will have to be handled at the receiver.

- Single hop strategies have emerged around 2010 with SigFox bringing old concepts to a new life. LoRa is a second famous solution proposing such a strategy. This star approach is more similar to cellular network but with very simple and low cost terminals so that scheduling is not possible. SigFox and LoRa use ALOHA MAC layer. This simple scheme is a source of interference that will have to be handled at the receiver.

LoRa is a LPWAN protocol for IoT applications. LoRa is a recent LPWAN technology based on spread spectrum technique with a wider band. LoRA uses the entire channel bandwidth to broadcast a signal which makes it resistant to channel noise, long term relative frequency, Doppler effects, multipath fading, jamming attacks and difficult to decode by an eavesdropper. The characteristics of LoRa are based on Code Rate , Spreading Factor and Bandwidth [NBC17].

The transmitter generates chirp signals by varying their frequency over time and keeping phase between adjacent symbols constant. Receiver can decode even a severely attenuated signal 19.5 dBs below the noise level. Chirp Spread Spectrum (CSS) is a particular type of Direct Sequence Spread Spectrum (DSSS) and allows to send one bit per each chirp. It takes much larger bandwidth for transmission than actually required for the considered data rate [NBC17].

The spread spectrum modulation technique implied in LoRa assures an increased link budget as well as better immunity to network interferences. LoRa utilizes wider band usually of 125 kHz or more to broadcast the signal. LoRa allows the usage of scalable bandwidth of 125 kHz, 250 kHz or 500 kHz. But, spreading a narrowband signal over wider band makes less efficient use of spectrum until the end devices utilize orthogonal sequences and/or different channels which result higher overall system capacity [NBC17].

SigFox supports narrowband (or ultra narrowband) technology with standard Differential BPSK, which allows the receiver to only listen in a very small part of the spectrum that avoids the noise impact. It requires an inexpensive endpoint radio and a more sophisticated base station to manage the network. These transmissions use unlicensed frequency bands [NBC17].

1.1.4   Challenges in WSNs

WSNs are facing several challenges that are delaying the expected growth and many possible applications. For instance we can mention environmental difficulties for sensor deployment, ensuring a sufficient coverage, the miniaturization of the nodes, the energy constraints and the increasing level of interference, etc. These challenges are more or less crucial depending on the application, but they can generally be related to the reliability, life time and latency constraints of the application. We are mainly considering the two first aspects.

- **Reliability**: it is difficult to guarantee the successful transmission of a packet in wireless communications. This is especially true in the IoT context where transmitters are very low cost and have to spare their energy as much as they can. The consequence is that channel state information is unknown at the transmitter side and orthogonality of channels cannot be ensured. As a consequence, in addition to the traditional Multipath Interference (MPI) due to the wireless channel, Multiple Access Interference (MAI) also arises. MPIs are due to the propagation in multiple paths originated from reflections that arrive and overlap at the receiver. Many different signal processing algorithms and techniques are available to deal with MPI, e.g., equalization. They usually rely on channel estimation which will be studied in the next chapter. MAI is the main focus of this work. We state that MAI can no longer be accurately modelled with a Gaussian distribution. To ensure robustness it is important to better model this type of interference and to accordingly design the receiver. These will constitute the main contributions of this chapter and the following one.

- **Lifetime**: The energy is a crucial constraint in sensor networks. Nodes usually operates with batteries and they have to last as long as possible. Recharging the batteries can be a solution but if this does not imply a human manipulation. Even if circuits are becoming low power, the RF circuits are still the most consuming parts. As we will see, once again the transmission schemes adopted in WSN generate interference which reduces reliability and, in the same time, increases consumption. This shows once

again that it is essential to understand how interference behaves and how we can modify the transmission/reception strategy to mitigate its effects.

1.2   The IEEE 802.15.4 technology and interference with IEEE 802.11

The objective of this chapter is to present in details the impact of interference of IEEE 802.11 (Wifi) technology on IEEE 802.15.4 (Zigbee) packets and its relation with energy consumption and duration of batteries, combining experiments and theoretical results to understand the changing communication environments, through a system capable of listening to 2.4 GHz ISM frequency. IEEE 802.15.4, also known as Zigbee, was designed to present low-complexity, extremely low-power and inexpensive wireless communication technology and became a common technology for wireless sensor networks [Pet+06; Tje07; Shi+06].

The IEEE 802.15.4 physical layer offers a total of 27 channels, one in the 868MHz band, 10 in the 915 MHz band and 16 in the 2.4 GHz band. The bit rates on these frequencies are 20 kbps, 40 kbps and 250 kbps, respectively [Pet+06] [Tje07].

The IEEE 802.15.4 supports the following PHY options: 868/915 MHz PHY, known as low-band, use BPSK modulation, whereas the 2.4 GHz PHY, known as high-band, uses OQPSK modulation[Pet+06] [Tje07]. It can reach up to 75 m [Tje07].

A more detailed description of IEEE 802.15.4 standard can be found in [Ada06] and [Erg04], a technical comparison between IEEE 802.15.4, IEEE 802.11, IEEE 802.15.1 and IEEE 802.15.6 is shown in [Tje07] and [Cav+14]. The following table summarizes the main characteristics and allows to compare Wifi, Zigbee and Bluetooth technologies.

	Wifi (WLAN)	Zigbee	Bluetooth
Specification	IEEE 802.11	IEEE 802.15.4	IEEE 802.15.1
Channels and Bandwidth	900 Hz, 2.4 GHz 3.6 GHz, 5 GHz, 60 GHz	868 MHz (27 channels) 915 MHz (10 channels) 2.4 GHz (16 channels)	2.4 GHz
Data Rate	11 Mbps (802.11b) 54 Mbps (802.11g)	20 kbps (for 868 MHz band) 40 kbps (for 915 MHz band) 250 kbps (for 2.4 GHz band)	up to 1 Mbps
Transmission Technique	CSMA/CA OFDM (802.11a) DSSS+CCK (802.11b) OFDM + CCK (802.11g) MIMO OFDM (802.11n/ac)	BPSK (868/915 MHz) OQPSK (2.4 GHz)	FHSS
Transmission Range	100 m	75 m	10 m

Table 1.1 – Main characteristics and allows to compare Wifi, Zigbee and Blue-tooth technologies.

1.3 Coexistence between IEEE 802.15.4 and IEEE 802.11 devices

The 2.4 GHz ISM band is shared between different kind of devices using different communication standards, see Figure 1.3. It is important to understand and evaluate the coexistence problems and limitations on this band. As we can see in Fig. 1.3, for the IEEE 802.11 and IEEE 802.15.4, the channel width is, respectively, 22 MHz and 5 MHz.

For a better comprehension of the impact of interference, We proposed the following experiment: a TelosB (ZigBee based node) module used in [Tol+16] for channel sniffing was replaced by the high performance National Instruments Universal Software Radio Peripheral (NIUSRP) 2942R. The USRP was placed close to a XBee node which sends a 100-bytes payload and a smart-phone with the Bluetooth module activated placed at 2 m distant. The smart-phone communicates via Bluetooth with another smart-phone in the same room. Figure 1.4 shows the amplitude (y-axis) vs. time (x-axis) of the signal received on the IEEE 802.15.4 channel 12, centred at 2.410 GHz. It is possible to identify a long IEEE 802.15.4 packet (the Zigbee packet), a small IEEE 802.11 control packet coming from a nearby WIFI access point and a short IEEE 802.15.1 pulse coming from the phone. Although the Bluetooth packet is much shorter, it corrupts the IEEE 802.15.4 packet, forcing the XBee node to stay in active mode for a re-transmission and, consequently, increasing the energy consumption and decreasing the lifetime of the node. Is important to note that the noise presents an impulsive behaviour. Even if carrier sensing is used, this will be difficult to be sensed by Zigbee transceivers. The heterogeneity of future networks will increase such difficulties resulting in a unavoidable level of interference.
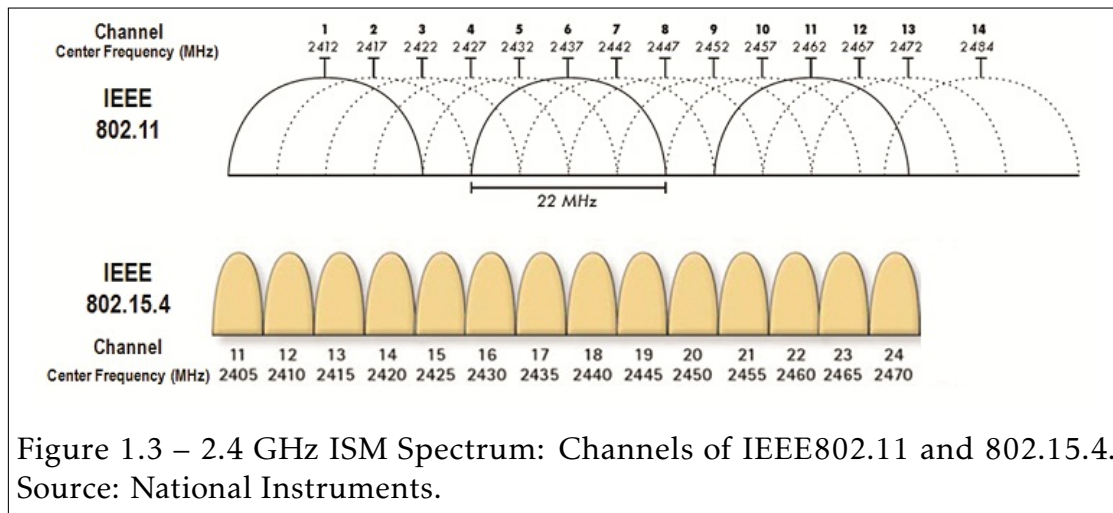
Figure 1.3 – 2.4 GHz ISM Spectrum: Channels of IEEE802.11 and 802.15.4. Source: National Instruments.
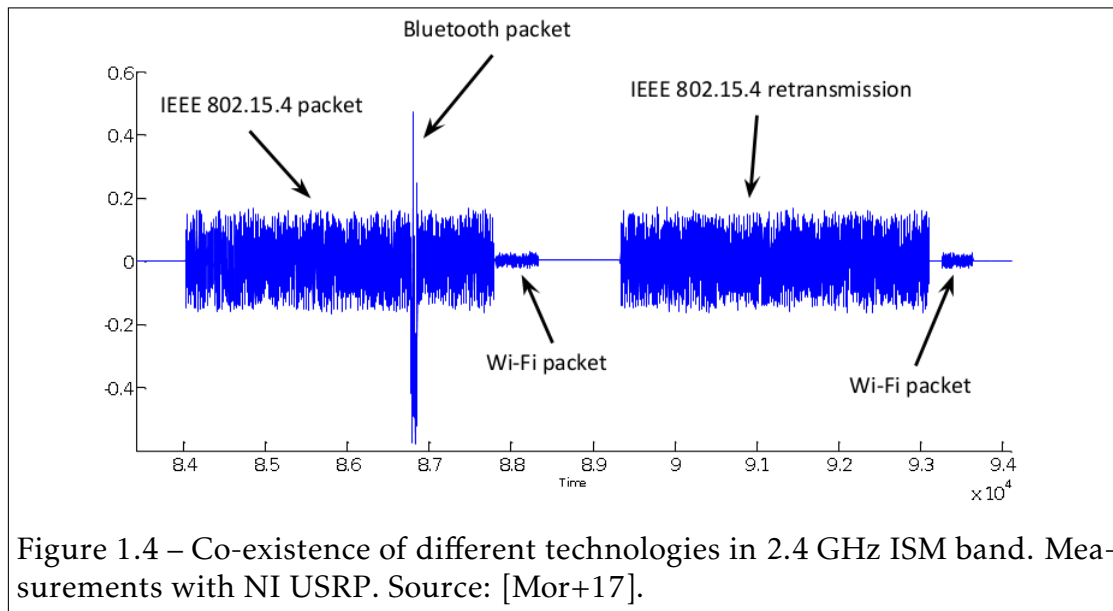
Figure 1.4 – Co-existence of different technologies in 2.4 GHz ISM band. Measurements with NI USRP. Source: [Mor+17].

Many other studies have shown that IEEE 802.15.4 is vulnerable to interference by other wireless technologies working in the same band such as IEEE 802.11 and IEEE 802.15.1 [Pet+06]. Studies ([Pet+06] [Yoo+06]) state that IEEE802.15.4 network has negligible or no impact on IEEE 802.11's performance, however, IEEE 802.11 can have a considerable impact on the IEEE 802.15.4 performance [Shi+06]. About the last case, [Abr+14] shows similar results for different scenarios.

[Yoo+06] shows that if the distance between IEEE 802.15.4 and 802.11b is larger than 8m, the interference of IEE 802.11b does not affect the performance of 802.15.4. If the frequency offset is larger than 7 MHz, the interference of IEEE 802.11b on IEEE 802.15.4 is negligible. [Pet+06] also confirms that there should be at least a 7 MHz offset between carrier frequencies for a satisfactory performance of Zigbee. Detailed studies about co-existence of IEEE 802.15.4 at 2.4 GHz can be found also in [NXP13] and [YXG11].

In [Mor+17], we discuss the coexistence of IEEE 802.15.4 network surrounded by other types of networks, specially 802.11 devices, and the impulsiveness of interferences in such scenarios, where linear receivers are not adapted, and compare the complexity and performance of some non linear detection models.

1.4   The SYNERGIE platform

In order to study the impact of interference on energy consumption, a platform called SYNERGIE was developed in IRCICA laboratory to calculate and measure energy consumption of each electronic component in a WSN node separately a rate of 1500 samples per second. This platform is based on commercially available low cost and low power hardware to evaluate the impact of interference on energy consumption on 2.4 GHz band based networks. The block diagram is shown in Figures 1.5 and 1.6 and the board on Figures 1.7 and 1.8. It is composed by a AT-mega328p microcontroller, which contains an embedded 10-bit Analog-to-Digital-Converter (ADC) and five operational amplifiers XCT1086 able to acquire up to five independent measurements. The SYNERGIE platform is connected to the node through a General Purpose Input-Output (GPIO) lines, responsible for the synchronization between the different states of device and the energy consumption data, and also connected to SYNERGIE platform through a resistor interface through terminals the platform measures the voltage. The measurements are transmitted to a computer via serial connection. More detailed explanations about SYNERGIE platform can be found on [Tol+16].

Figure 1.5 – Synergie Platform block diagram.

Figure 1.6 – Synergie Platform block diagram.

Figure 1.7 – Synergie platform boards.
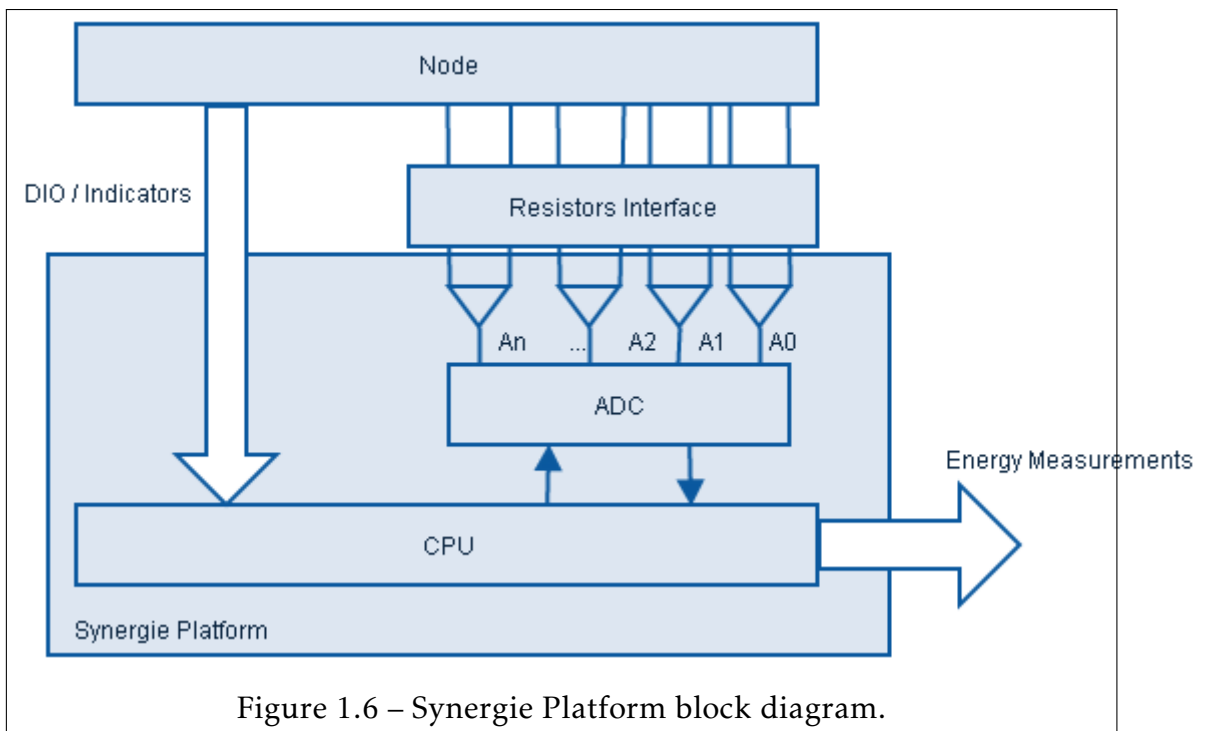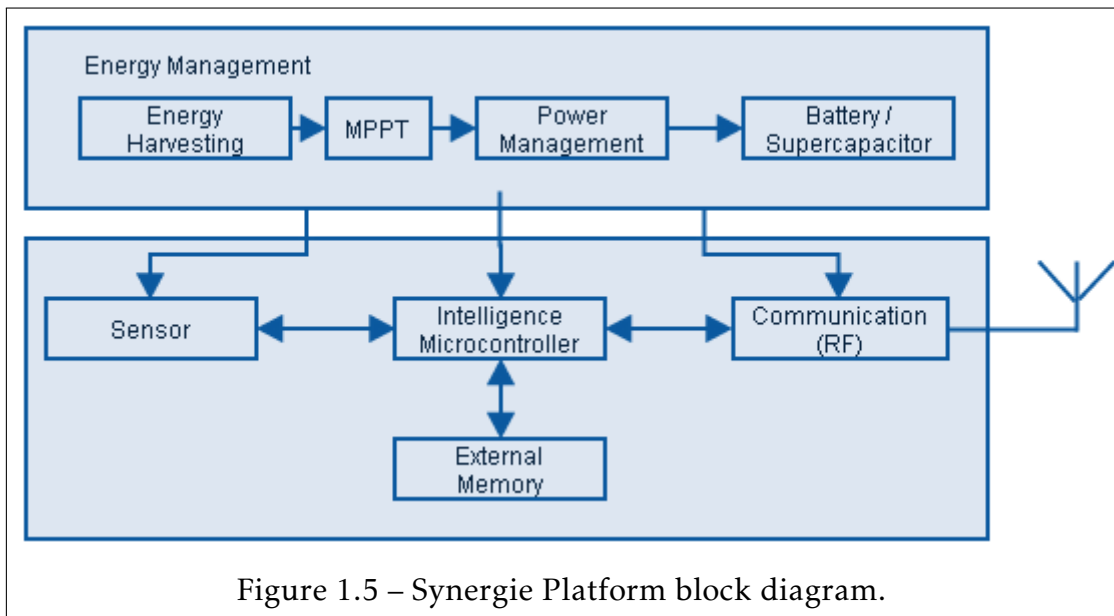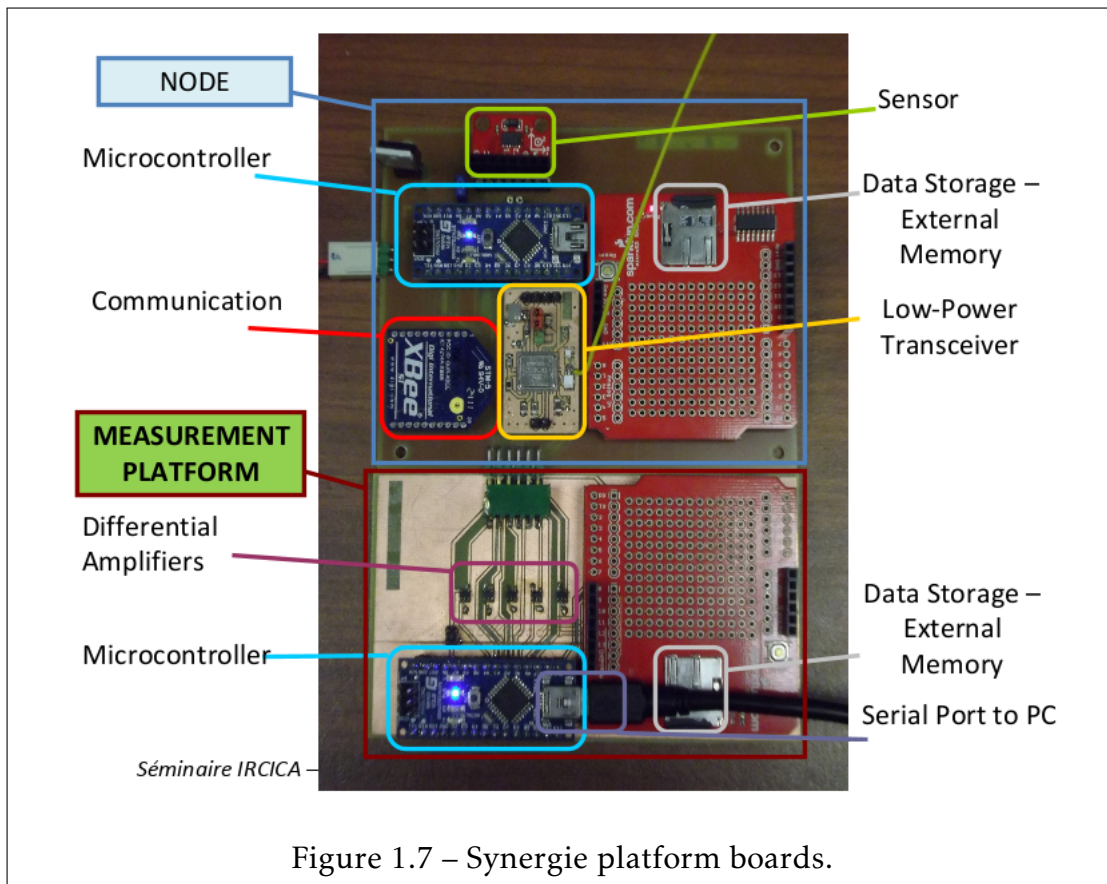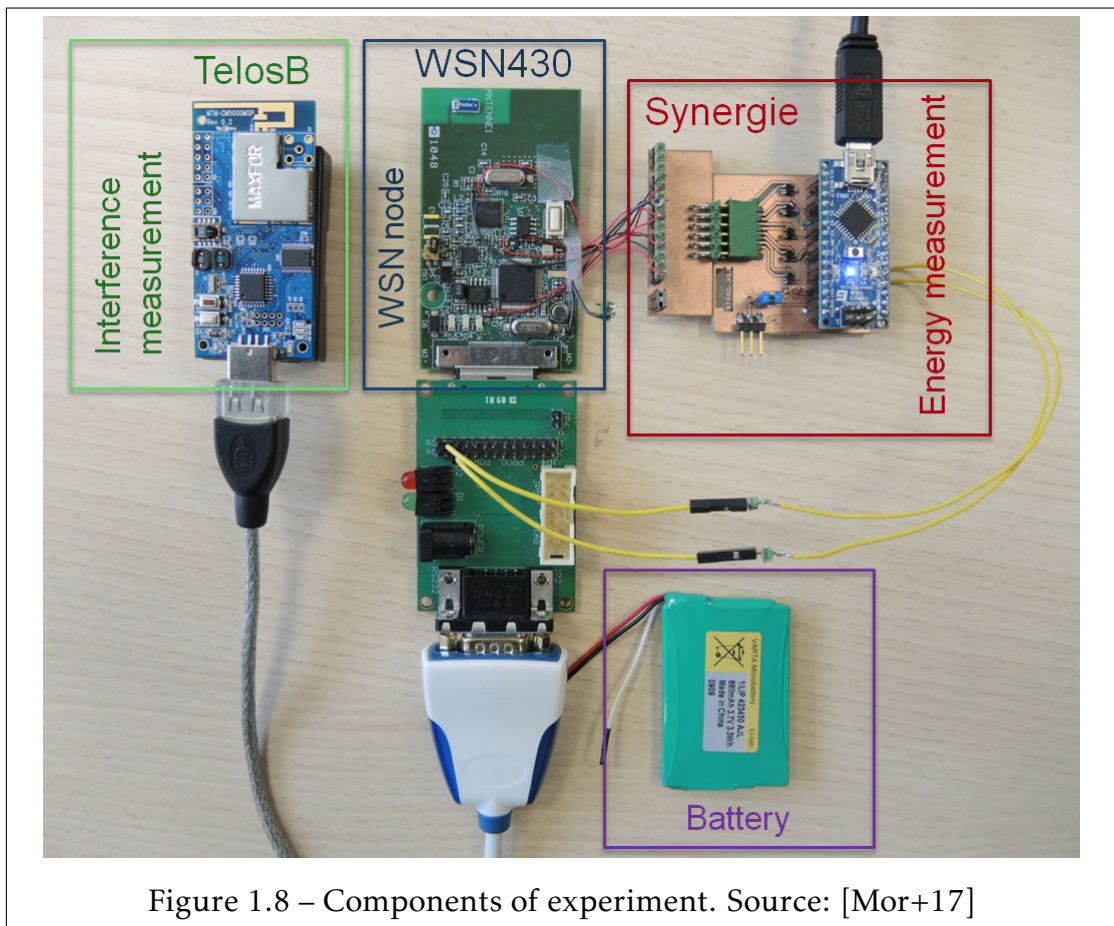
Figure 1.8 – Components of experiment. Source: [Mor+17]

1.5   Energy consumption and interference

Based on the Synergie platform, the quantitative relation between the interference level and the energy consumption is studied. The reliability is also considered by making a difference between four cases, as shown in Fig. 1.9:

1. packet successfully sent on first trial, with reception of ACK,

2. packet successfully sent (or reception of ACK) on second attempt,

3. packet successfully sent (or reception of ACK) on third attempt,

4. failure on sending packet (or no ACK).

Figure 1.9 – Transmission cases.
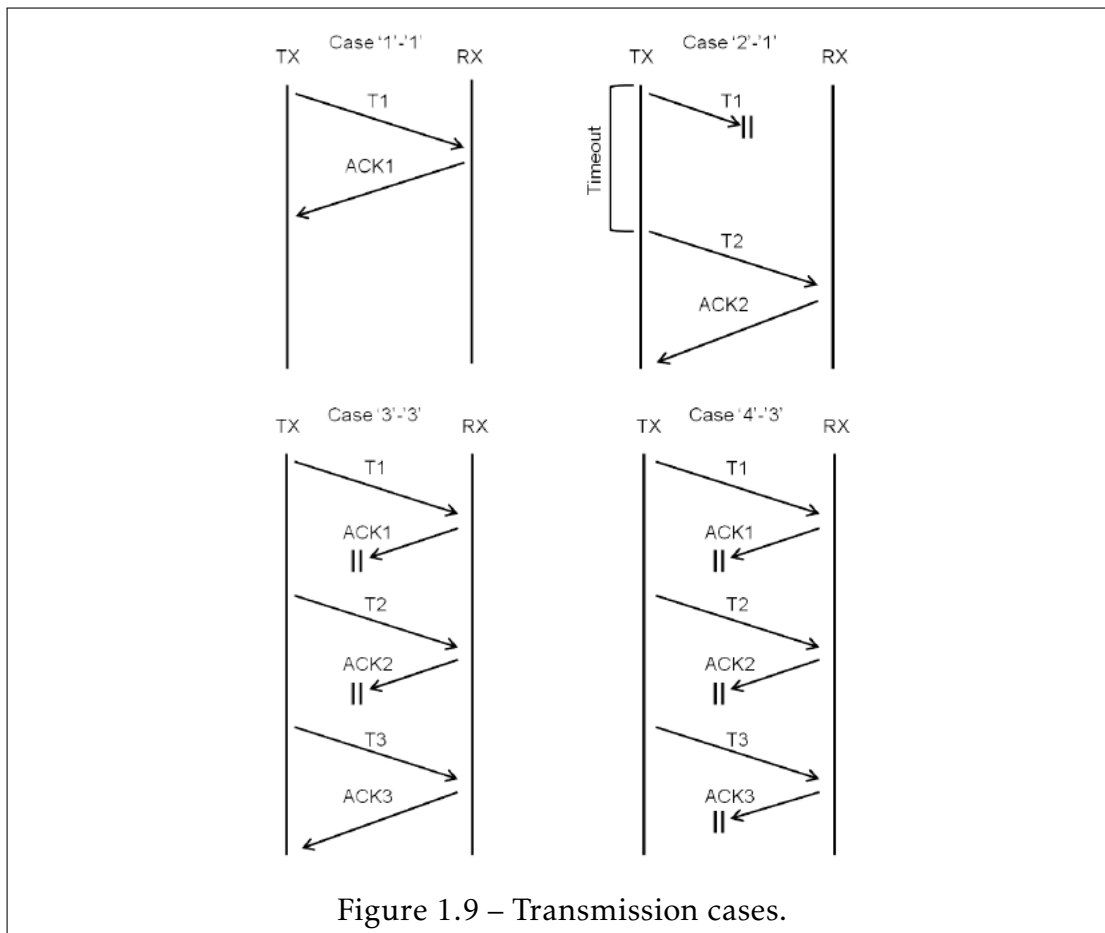
The main results of this work are shown in Figure 1.10, where we observe the energy used to transmit one packet as a function of the Received Signal Strength (RSS, as measured by a Zigbee module). The different makers indicate the number of times the packet has been re-transmitted, referring to the four cases previously described: red stars represent case 1, black stars case 2, green stars case 3 and the blue ones case 4. The protocol was set such that after three unsuccessful trials (no ACKnowledgment was received) the packet was dropped so that the blue stars (case 4) indicate packets that were lost (or eventually, but it happens less often, the ACKs were lost whereas the packet was indeed successfully received). As it is possible to see, case 1 is more frequent under low level of interference and the case 4 is quite rare. As the level of interference increases, the number of failing cases also increases.

Figure 1.10 shows that when interference gets high, not only the reliability is decreased as shown by the number of lost packets, but also the energy consumption significantly increases up to about 4.8 times for the full transmission of one packet, when compared to scenarios without interference. Due to the very low probability of success, it may be not interesting to try to send a packet a third time after two unsuccessful attempts - in our scenario, such a re-transmission policy happened to be very inefficient. The MAC layer usually attempts to minimize interference (at least in local area networks like those based on IEEE 802.15.4). Conversely, the PHY layer designs solutions to adapt and tolerate a certain level of interference. To incorporate these aspects, MAC protocols should be modified. This could significantly improve the network efficiency and the spatial reuse of the resource [Tol+16].

Figure 1.10 – Interference in WSN: Interference level, consumption and reliability measurements on transmitter side.
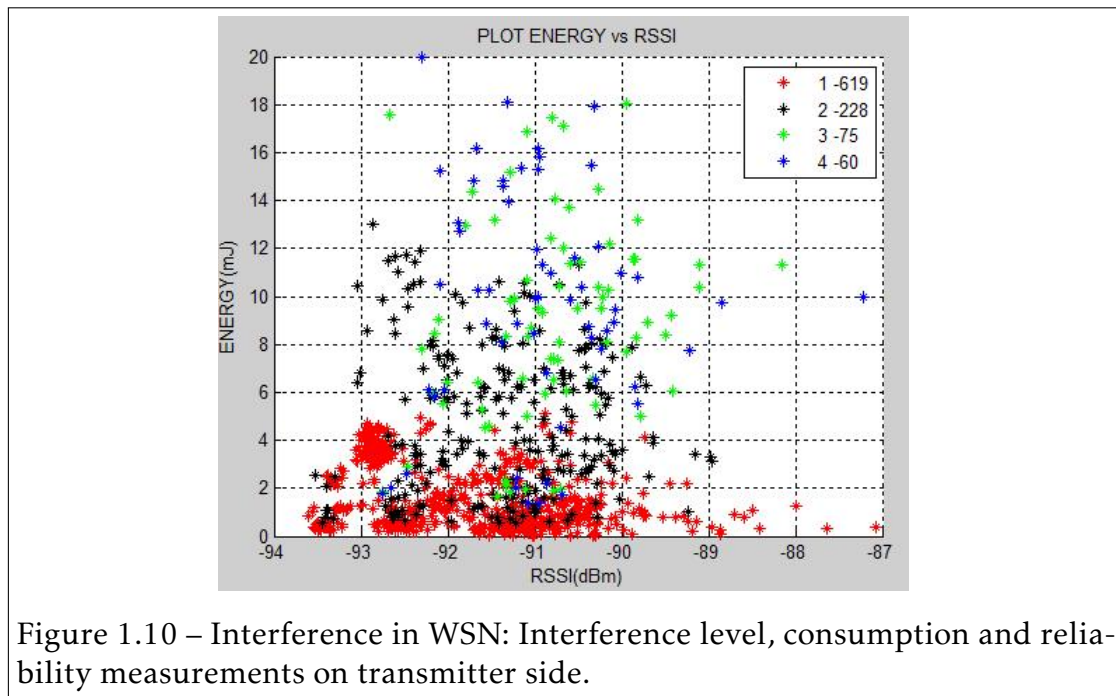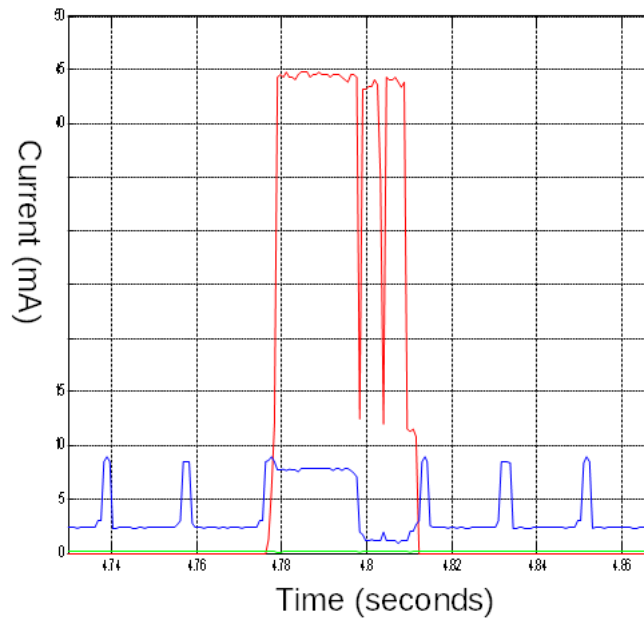
Figure 1.11 – Current consumed, in mA, on a WSN node in each componet. The red, blue and green curve indicates the current consumed by the RF, microcontroller and sensor components, respectively on transmitter side.

Previous results were obtained using TelosB to measure the received signal strength and the level of interference, using a similar approach than the one used for the carrier sensing. The goal was to analyze in a Zigbee network interference created by other Zigbee nodes. The Figure 1.12 shows a typical interference acquisition with TelosB. What we can comment from this figure is that TelosB does not allow very accurate measurements. Both RSSI and energy consumption are given at a *macroscopic* level but the sampling rate is low and the obtained results can not be used for more accurate analysis.
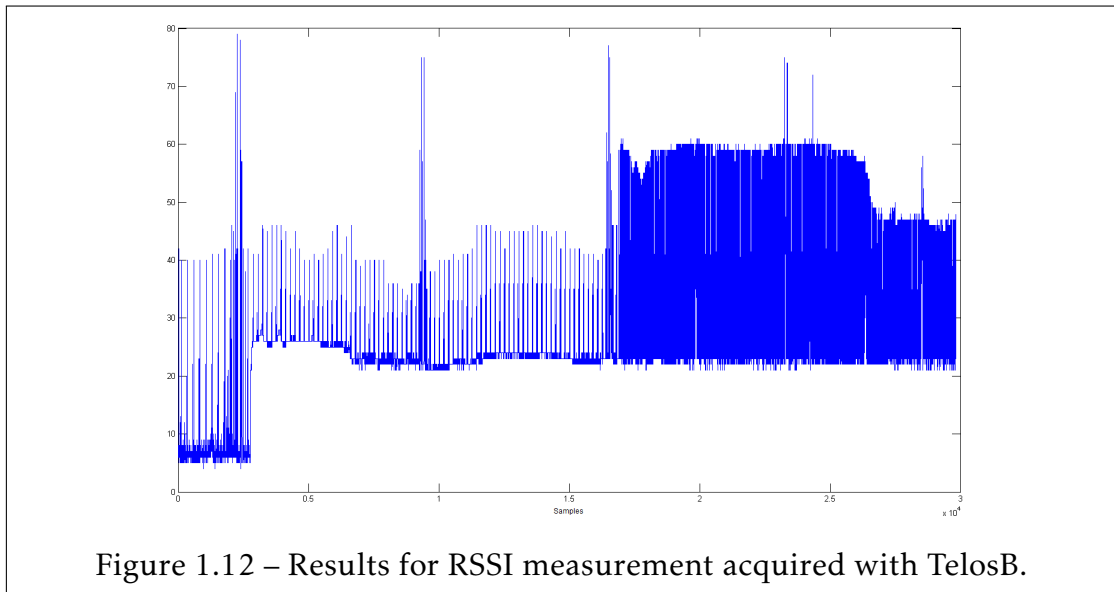
Figure 1.12 – Results for RSSI measurement acquired with TelosB.

Indeed, to calculate the RSSI, the TelosB uses a 128 μs frame. By definition, $RSSI = -10\log(I^2 + Q^2)$. This needs to be compared to a WIFI packet duration which is about. This long sampling period when compared to the length of a IEEE 802.11 packet results in a RSSI, which is an average over many samples acquired among which only a few really correspond to the WIFI packet, the others corresponding to an idle channel. This significantly reduces the interest of the information contained in the RSSI. This can be seen when looking at the difference of the power consumption per packet as a function of the measured RSSI when interferes are IEEE 802.15 devices or IEEE 802.11 devices. The crosses when interference is from Zigbee devices is much clearer. Different areas can be delineated depending on the number of active devices. The cloud point is much more diffused in the WIFI case, one of the reason being the bad match between the sensing process and the packets to be sensed.

1.6   Experimental Setup

To have more control of interference flow through WiFi network, we used the D-ITG (Distributed Internet Traffic Generator) software installed on a notebook. It is a PC-based software able to produce IPv4 and IPv6 packets used for measure,

for example, common performance metrics. It allows to accurately control the sequence of generated traffic. D-ITG can also generate traffic according to stochastic models [BDP12]. Our setup is shown in Figure 1.13. The sensors were 5.5 m distant from the USRP antenna.

Figure 1.13 – Experimental setup for experiment with D-ITG.

Figure 1.14 – XBee node, National Instruments USRP 2942R and PXI.
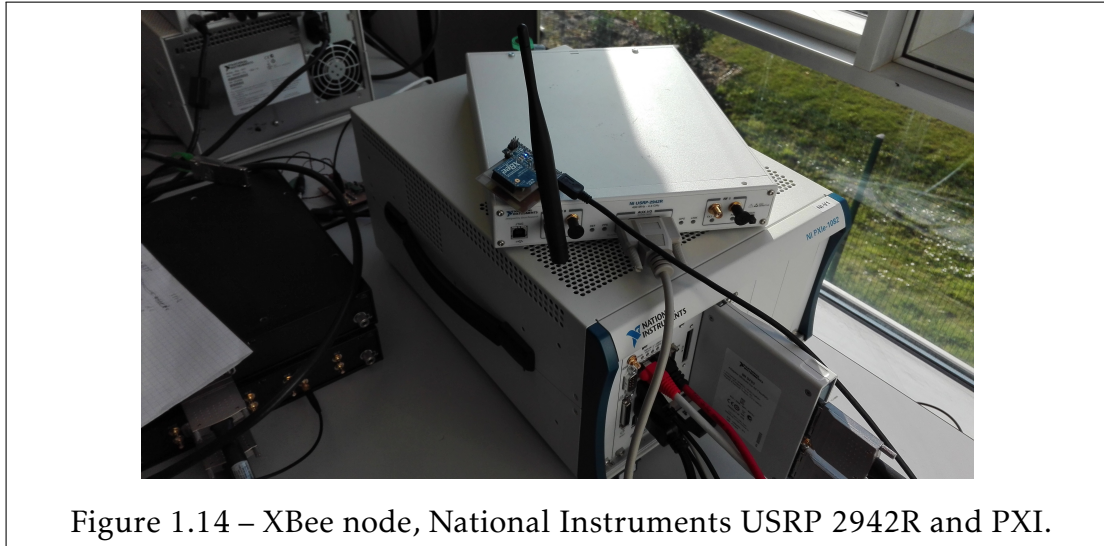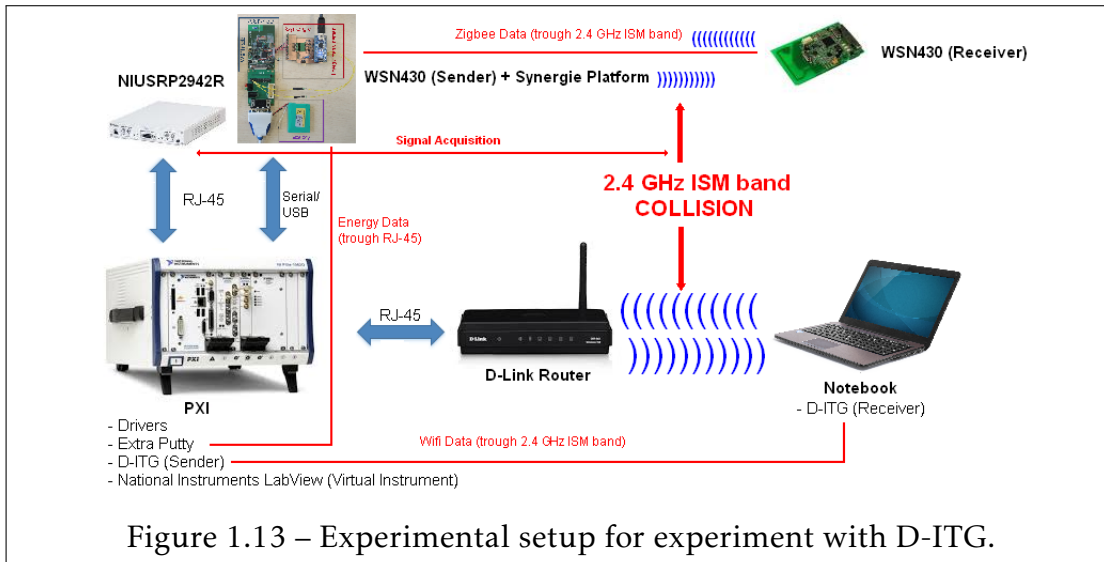
1.6.1   Results and discussion

The Figure 1.15 shows 25 ms of the "I" component measured by the USRP. We identify on this figures the repeated transmission of IEEE 802.15.4 packets and the more sporadic transmissions from the IEEE 802.11. Fig. 1.15 shows the same set of data but transformed to the RSSI.

The results show the size of Wifi Packet and Zigbee packet. Since the Wifi signal is much smaller than a Zigbee signal, the probability to loose a Zigbee packet due to a collision is high. It is important to note that each trial means an additional energy consumption as it was already shown in [Tol+16] and, consequently, reduces the lifetime of the node.

According to the specification of IEEE 802.15.4, the device tries to send the packet up to three attempts. Each attempt is shown by the higher vertical lines shown on Figure 1.15. Under a interference free environment, the average of RSSI is about -40.70dB, while under Wifi interference, the RSSI increases up to -30 dB (26.29%). Once that TelosB calculates the average over a long sampling period and the short period of a WiFi packet, the RSSI obtained was not accurate (that does not occur when using USRP2942R), because its sampling period is 128 μs against 22 ns of USRP2942R. Due to its high sampling frequency, the presented result is the given RSSI is much more feasible, giving a precise information about when and how the interference occurs being possible to distinguish WiFi and ZigBee packets and to detect the exact moment of the interference.

Due to the high sampling frequency of USRP2942R, is possible to verify in detail the nature of a IEEE 802.11 packet. The result obtained is shown in Fig. 1.16 and suggests that a Wifi packet, seen by a Zigbee receiver, is an impulsive signal. It means that a Gaussian model is inadequate to describe the behavior of a Wifi signal and more realistic models are needed. Is possible to see also the duration of a Wifi packet.

Figure 1.15 – Data and RSSI of 2.4 GHz ISM band acquired by USRP2942R with 1MHz band.

Figure 1.16 – Wifi packet.
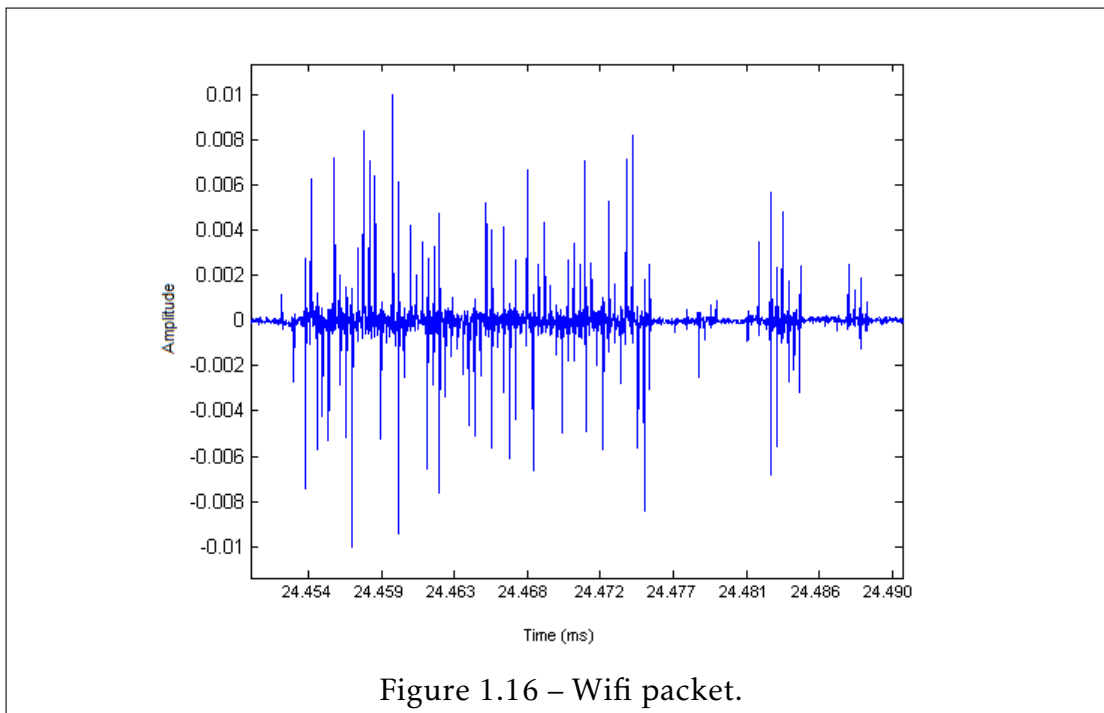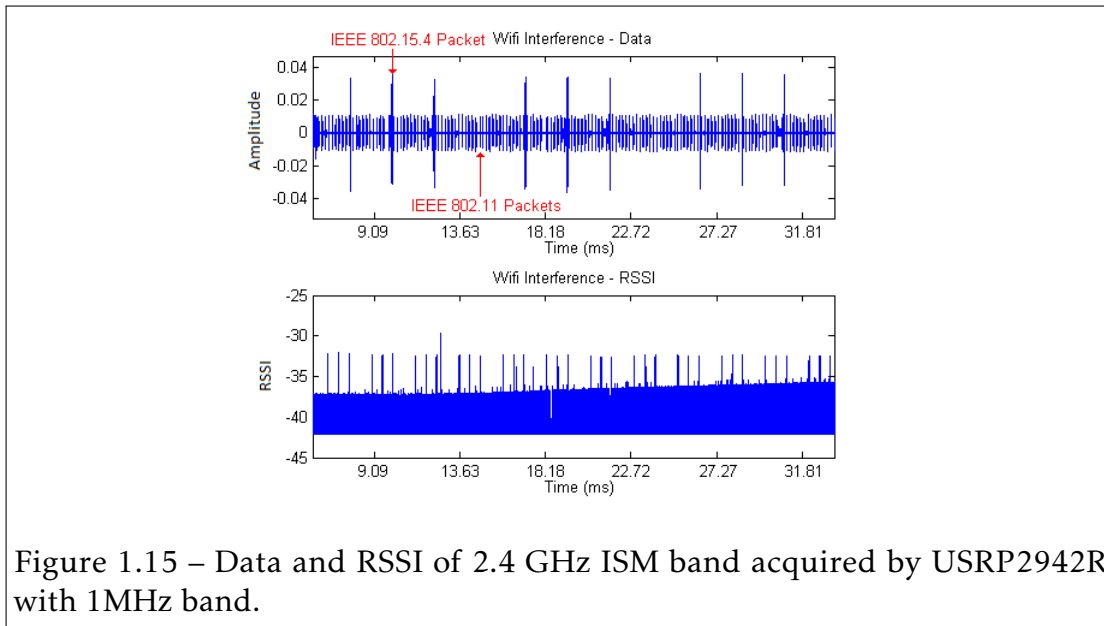
In the context of IoT and WSN, the heterogeneity of nodes and networks and the diversified requested data rates, symbol duration and packet lengths

make the set of active interferer change rapidly [Ega+17]. Analyzing the packets duration, we can evaluate the number of bits in IEEE 802.15.4 packet that will be affected by a Wifi packet. Let's denote t_z and t_w the duration of a IEEE 802.15.4 and 802.11 packets, respectively. The ratio between t_z and t_w is: $\frac{t_z}{t_w} = 30.43$, in other words, the time on-air for IEEE 802.11 is significantly shorter. A IEEE 802.11 frame occupies $\frac{40bytes}{30.43} = 1.43bytes$ of IEEE 802.15.4 frame or $1.31 \cdot 8bits = 10.51bits$, enough to corrupt a IEEE 802.15.4 packet. This dynamic interference results in a non-Gaussian interference and imposes changes on the receiver design [Mor+17].

1.7   Distribution analysis of interference

To try to determine the type of distribution of interference between IEEE 802.11 and IEEE 802.15.4 devices, a new experiment was conducted using Signal Studio software and Agilent E4438C ESG Vector Signal Generator as source of Wifi packets instead of using a notebook with D-ITG and PXA Signal Analyzer N9030A 3Hz-50GHz and Keysight Technologies VSA Software for data acquisition. The Agilent E4438C ESG Vector Signal Generator was programed using Signal Studio Software, to generate a sequence o Wifi packets on 2.4 GHz band. PXA Signal Analyzer N9030A was centered also on 2.4 GHz band as hardware interface and Keysight VSA software used to data analysis and recording. The test was repeated for the following scenarios: **(a)** Wifi only; **(b)** Wifi and Zigbee signals with 500ms between each Zigbee packet; **(c)** Wifi and Zigbee continuous signals; **(d)** Zigbee only continuous signal; **(e)** Zigbee only signal with 500 ms between each Zigbee packet; **(f)** Only background noise (no signal). For tests envoling Zigbee, were used two DIGI Xbee S1 XB24 modules programmed using XCTU (see Appendix A for details of configuration). For further details on experimental setup for this experiment, see Appendix A.

1.7.1   Discussion and results

Figure 1.18 shows the analysis of the interference between Wifi and Zigbee packets, obtained from the superposition of both packets seen on 1.17, and an

attempt of curve fitting with Gaussian model. Its distribution, when compared to Gaussian distribution, present an impulsive behavior. The non-Gaussian behavior can also be confirmed by Kolmogorov-Smirnov hypothesis test. Using parameters estimation techniques, to be discussed further, was obtained a characteristic exponent, a parameter that indicate the "thickness" of tail of distribution, $\alpha = 1.8$, instead of $\alpha = 2$, which indicates the non-Gaussian behavior.
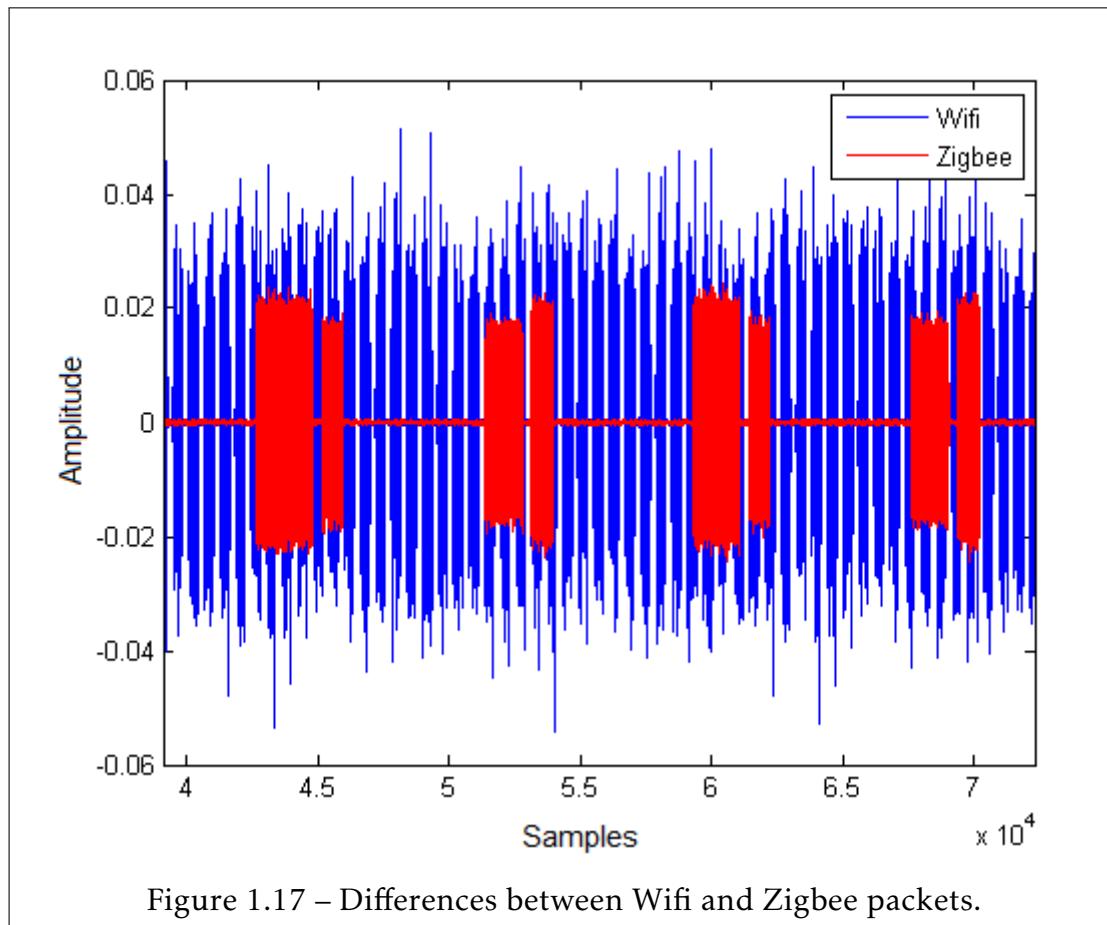
Figure 1.17 – Differences between Wifi and Zigbee packets.

Figure 1.18 – Experimental Results: the red and black curve represents a Gaussian and α-stable approximation, respectively.
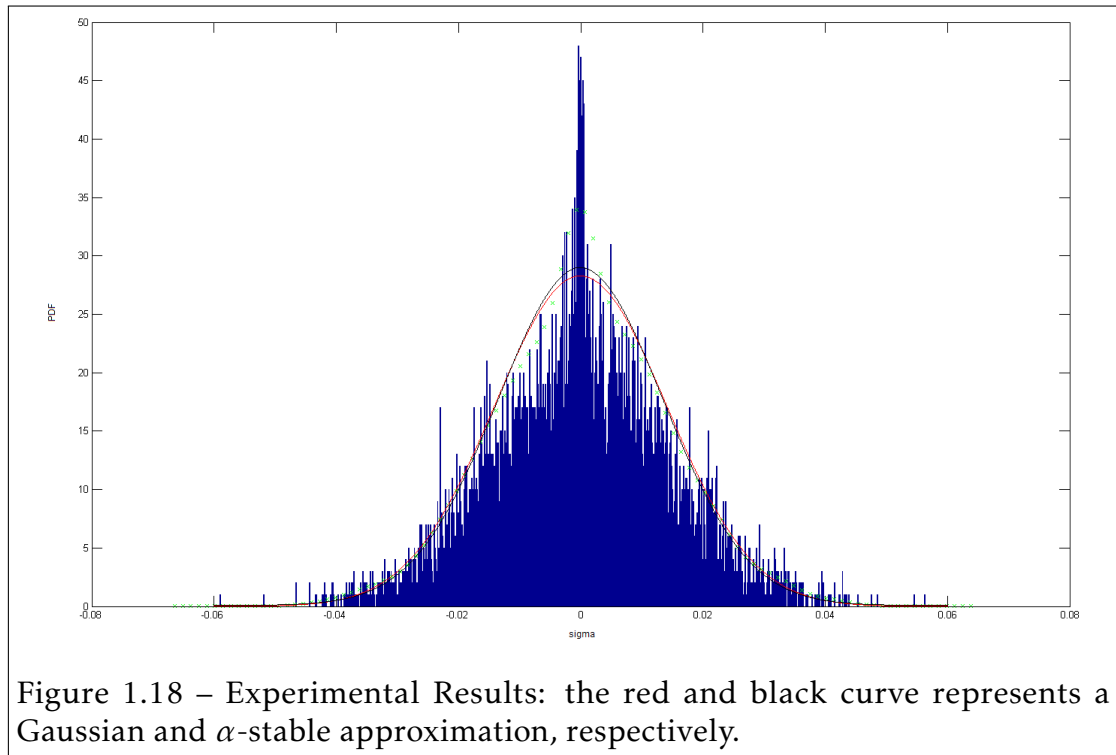
1.8   Partial conclusions

In the first part of this chapter USRP2942R and E4438C ESG Vector Signal Generator were used to verify precisely the nature of a Wifi signal and its effects over a Zigbee signal. The results obtained show that a Wifi packet is an impulsive signal and show also the duration and size of Wifi and Zigbee packets, the instant of collision of packets and how it increases RSSI. The data acquired is shown on time domain. The result obtained, mainly for RSSI, is much more accurate than using TelosB for the same measurement and shows an increase of RSSI up to 26.29% . Instead of an average over a long period that cannot show the effect of Wifi packet, USRP2942R shows the trials of sending Zigbee data and instant RSSI, giving more feasible result. These results suggest that the protocols should be modified to improve the network efficiency and the spatial reuse of the resource.

Several conclusions can be drawn from these measurements. We can identify

two important facts about interference in wireless sensor and *ad hoc* networks. (**a**) Even in a context with a small number of items but with different protocols, interference exhibits statistical properties that are different from the classical thermal noise that is encountered in all communication systems. The interference can exhibit non Gaussian properties and this impulsiveness can be critical. This result is supported by some papers [WPS09] [WA12] where this interference exhibits also an impulsive nature. This significantly impacts the performance of the receiver that needs to be adapted to keep good performance in such environments. (**b**) The link between the interference level (as measured by the Zigbee module) and the opportunity to transmit packets is not so obvious. Of course when interference is low, more packets are transmitted successfully but with a higher interference, all the cases (success at the first, the second, the third trial or no success at all) can happen. We explain this because the way the Zigbee listens to the channel is not adapted to the Wifi signal. Interference will generate long sensing periods (most of the protocols are based on Carrier Sensing), difficulties to initiate the communication and an increased number of transmissions. In particular, if we want to keep the same Quality of Service (QoS), at least in terms of packet error rate, this will significantly increase the objects consumption. So, interference heavily impacts the reliability and the consumption of the Zigbee network.

We experimentally studied in [Tol+16] interference in a Zigbee network. We showed its impact on the reliability and energy consumption of the objects. In this work we addressed the problem of interference coming from another network [Abr+14]. The useful link uses and IEEE 802.15.4 based protocol (more specifically a Zigbee link). Interference comes from an IEEE 802.11 (Wifi) network. Both standards can use the 2.4 GHz band and interact on each other. However, the physical layer characteristics are distinct - symbol duration, carrier frequencies are different, there are no time synchronization between the systems, the bandwidth and modulation schemes are different. The statistical properties of the resulting interference on the digitized useful signal are not tractable and we propose an experimental characterization.

The dinamicity of the interfering signal (its duration in comparison to a packet duration of the useful signal) and the possibly fast changing set of inter-

ferers make sensing extremely difficult. We further studied the nature of the interference. With a single interferer, the Gaussian assumption is not verified. When using a model adapted to a impulsive interference (α-stable), we estimated characteristic exponent around 1.8, instead of 2, which means the interfering signal is definitely impulsive.

From this experimental part, we can conclude that it is essential in a sensor network to design communication strategies as robust as possible, especially against interference. Then, we can also conclude that interference signal does not follow a Gaussian distribution. Such a distribution cannot account for the dynamic behavior of interference and new models are needed.

However, in our experiments, we failed to show two important aspects into account: the high number of interfering nodes and the possible mobility of same nodes. To do that, we would need some tests in real environments. That is too long to organize and it was not feasible during this PhD. To have a better understanding of these aspects, we need to rely an theoretical approach. That will be the goal of the next chapter.

Chapter 2

Statistical modelling: theoretical approach

In noise modelling for telecommunications, the Gaussian assumption has played a central role for many years. This is rather natural as long as point to point communications are considered because the main source of noise is the so-called thermal noise. Coming from the thermal agitation of the charge carriers, usually the electrons, the thermal noise is the sum of many uncorrelated contributions and, as such, a model for its distribution can be obtained from the Central Limit Theorem [LS95]:

Theorem 2.0.1 (Central Limit Theorem) *A physical phenomena is Gaussian if there are infinitely independent and identically distributed (I.I.D.) contributing factors, each of finite variance.*

Consequently, the AWGN channel assumption is obtained and it is usually a reasonable assumption. It clearly simplifies the design of receivers because the maximum likelihood detection rule when the useful signal is corrupted by Gaussian noise results in a simple linear decision rule. This will no longer be the case if noise is non Gaussian. The impulsive noise will consequently require the introduction of non-linearities [LS95] if the optimal receiver is implemented.

If we want to keep the simplicity of the linear receiver, it has been shown in many contexts that the presence of non-Gaussian noise will significantly degrade

the system performance [LS95; BY09; Cla+10]. To avoid this degradation, more
adequate models have to be proposed and used for a more appropriate receiver
design. The Probability Density Function (PDF) of Gaussian distribution is given
by:

$$f_{X,G}(x; \mu, \sigma^2) = \frac{1}{\sigma\sqrt{2\pi}} exp^{\frac{(x-\mu)^2}{2\sigma^2}}, \qquad (2.1)$$

where x denotes the Random Variable (RV), μ the mean and σ the standard devia-
tion. The important fact that we want to underline is the exponential decrease of
the distribution. Such a distribution results in the absence of events "far from the
mean". In other words, such a model is not adequate for representing suddenly
appearing large values. Because we think that such large but rare events are
highly impacting the communications, we state that other models, with heavier
tails, are needed for a better representation of the network interference in IoT.

2.1   Other non-Gaussian and impulsive models

2.1.1   Some empirical examples

Many works have identified situations where noise is not Gaussian and exhibits
some impulsive behaviour. A specifically active research domain in that case
was about Ultra Wide Band (UWB) systems in the first decade of the 21st century.
After showing that the standard Gaussian model is not accurate [DR02], non
Gaussian models were developed. The objective of the proposed models were of
two kinds:

1. increase the probability of rare events to better fit data, mainly issued form
   simulations. The way to do it is to increase the weight of the tail.

2. obtain an analytical form, rather simple to deal with, of the probability
   density function of the noise in order to design an adapted receiver, easy
   to implement.

These works have generally proposed empirical choices, justified by simulations,
observations of the estimated PDF and/or gains in BER. The main proposed
solutions include

- Gaussian-Laplace mixture [BN10], where the Laplace part increases the tail weight,

- Generalized Gaussian [FH06; BSF08; KLC09], where the exponential decay is kept but in the order of e^{-x^β} where β can be smaller than two resulting in a slower decay,

- Gaussian mixtures [HB08], where non centred components can be used to increase the tails or adding to the Gaussian representing the thermal noise another Gaussian with a smaller weight but a much larger variance that can generate the large samples,

- Cauchy-Gaussian mixture [Mei+17], where the Cauchy distribution has a polynomial decay and in the class of heavy tail distributions.

In [HB08] it is mentioned that the heavier tail of the Gaussian Mixture allows better performance than the Laplace approach. Some more details can be found in the surveys [BY09; Sha12]. We give in the following a few examples of those distributions.

Generalized Gaussian distributions Generalized Gaussian Distributions (GGD) have been proposed to model MAI in UWB systems. One of its PDF can given by [Yan15]:

$$f_{X,GG}(x; S_m, \sigma, \beta) = \frac{1}{\gamma(1 + \frac{1}{\beta}\mathcal{A}(\beta, \sigma))} exp(-|-\frac{x - S_m}{\mathcal{A}(\beta, \sigma)}|^\beta), \qquad (2.2)$$

where S_m denotes the mean, $\mathcal{A}(\beta, \sigma) = [\frac{\sigma^2 \Gamma(1/\beta)}{\Gamma(3/\beta)}]^{0.5}$ is a scaling factor and β is the shape parameter. This shape parameter is a positive real value. To represent heavier tails than the Gaussian, one needs to choose β less than 2. $\beta = 2$ is the Gaussian distribution and $\beta = 1$ gives the Laplace distribution.

Mixture of Gaussian models The mixture of Gaussian model is in general able to represent any distribution. One way to obtain heavier tail is to add some non centered components to a centered one that represents the thermal noise. In a

general form, its PDF is given by

$$f_{X,GM;\mu,\sigma}(x) = \sum_{k=1}^{K} w_k \frac{1}{\sqrt{2\pi\sigma_k^2}} \exp\left(\frac{(x-\mu_k)^2}{2\sigma_k^2}\right), \tag{2.3}$$

where μ_k denotes the mean values of the Gaussian components k and σ_k denotes its variance. The relative weights w_k verify $\sum_{k=1}^{K} w_k = 1$.

ϵ-contaminated The ϵ-contaminated (similar to the Bernouilli-Gaussian model) is a special case of the Gaussian mixtures. However, in that case if one component is still representative of the thermal noise, the other component, with a much smaller weight, is also centered but with a significantly larger variance. The impulsiveness of the model can then be adjusted by changing the weight of this second component to change the frequency if the rare events or by modifying its variance to change the amplitude that impulsive events can take. The PDF of the ϵ-contaminated is given by

$$f_{X,\epsilon}(x) = (1-\epsilon)f_G(x;0,\sigma^2) + \epsilon f_G(x;0,\nu\sigma^2), \tag{2.4}$$

where ϵ represents the level of contamination (controls the proportion of impulsive part) and ν represents the impulsive strength.

2.1.2   Middleton class A and class B

We can trace back some works on non Gaussian noise to 1960 [FI60] and 1972 [GH72] about atmospheric noise. Assuming Poisson distributed sources, the Characteristic Function (CF) of the impulsive noise can be obtained. Furthermore, appropriate assumptions on the transmission medium and source waveforms allow one to obtain the interference PDF. A similar approach based on the CF was used by Middleton [Mid77; Mid99] who obtained more general expressions based on series expansions. He classified interference in two main categories depending if the noise bandwidth is less than the useful signal (class A) or greater (class B). Class C is a sum of class A and B.

The PDF of Middleton class A model is given by

$$f_{X,M}(x;\rho) = e^{-A} \sum_{m=0}^{+\infty} \frac{A^m}{m!\sqrt{2\pi\rho_m^2}} e^{-\frac{x^2}{2\rho_m^2}}, \tag{2.5}$$

where:

$$\sigma_m^2 = (\rho_G^2 + \rho_I^2) \frac{\frac{m}{A} + \frac{\rho_G^2}{\rho_I^2}}{1 + \frac{\rho_G^2}{\rho_I^2}}, \tag{2.6}$$

with ρ_G^2 denoting the Gaussian noise power and ρ_I^2 the impulsive noise power.

Class A noise describes the type of Electromagnetic Interference (EMI) often encountered in telecommunications applications, where the noise is due to other "intelligent" communications operation and is not an α-stable process nor is reducible to such, except in the limiting Gaussian case of high noise density where the Central Limit Theorem can apply [Mid99].

In [Vas84] the locally optimum (also called threshold or weak signal) detection problem in class A noise is considered. Class B noise usually represents man-made or natural "non-intelligent" noises. It is highly impulsive [Mid99] and is also asymptotically normal. Its PDF can be given by:

$$f_{X,M}(x;\alpha,\sigma) = \frac{1}{\pi\sigma} \sum_{n=0}^{\infty} \frac{(-A)^n}{n!} \Gamma(\frac{1+\alpha n}{2}) \Phi(\frac{1+\alpha n}{2}; \frac{1}{2}; -x^2/\sigma^2) \tag{2.7}$$

where $A > 0$ denotes the intensity of the impulsive interference, while $0 < \alpha < 2$ measures the heaviness of the tail of the density function: small values indicates a more impulsive behavior (heavier tail). $\sigma > 0$ plays a similar role to the standard deviation. Φ is the confluent-hypergeometric function

$$\Phi(a;c;x) = \sum_{k=0}^{\infty} \frac{(a)_k}{(c)_k} \frac{x^k}{k!} \tag{2.8}$$

for c we have:

$$(c)_k = \begin{cases} \frac{\Gamma(c+k)}{\Gamma(c)}, & \text{if } k \geq 1, \\ 1, & \text{if } k = 0. \end{cases} \tag{2.9}$$

The PDF can also usually be approximated by a symmetric α-stable model in the case of an narrowband reception or when the PDF is symmetric and a skewed α-Stable model in broadband regime.

Figures 2.1 and Figures 2.2 shows the comparison between a Gaussian noise with $\mu = 0, \sigma = 1$ and a Middleton class A noise with $A = 5, \sigma = 0.1$, with a zoom detailing the tail of both distributions on the second figure.

Figure 2.1 – Comparison between a Gaussian noise with $\mu = 0, \sigma = 1$ and a Middleton class A noise with $A = 5, \sigma = 0.1$.

Figure 2.2 – Comparison between a Gaussian noise with $\mu = 0, \sigma = 1$ and a Middleton class A noise with $A = 5, \sigma = 0.1$ (zoom on tails).
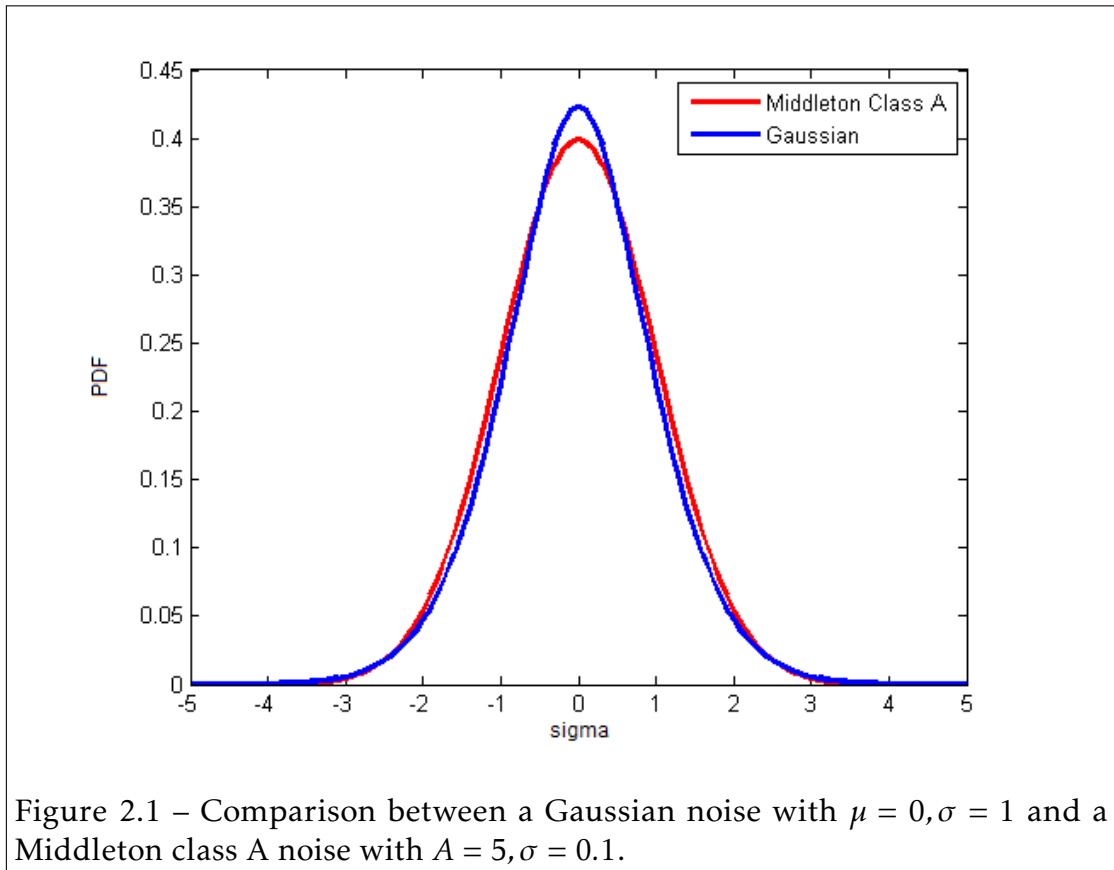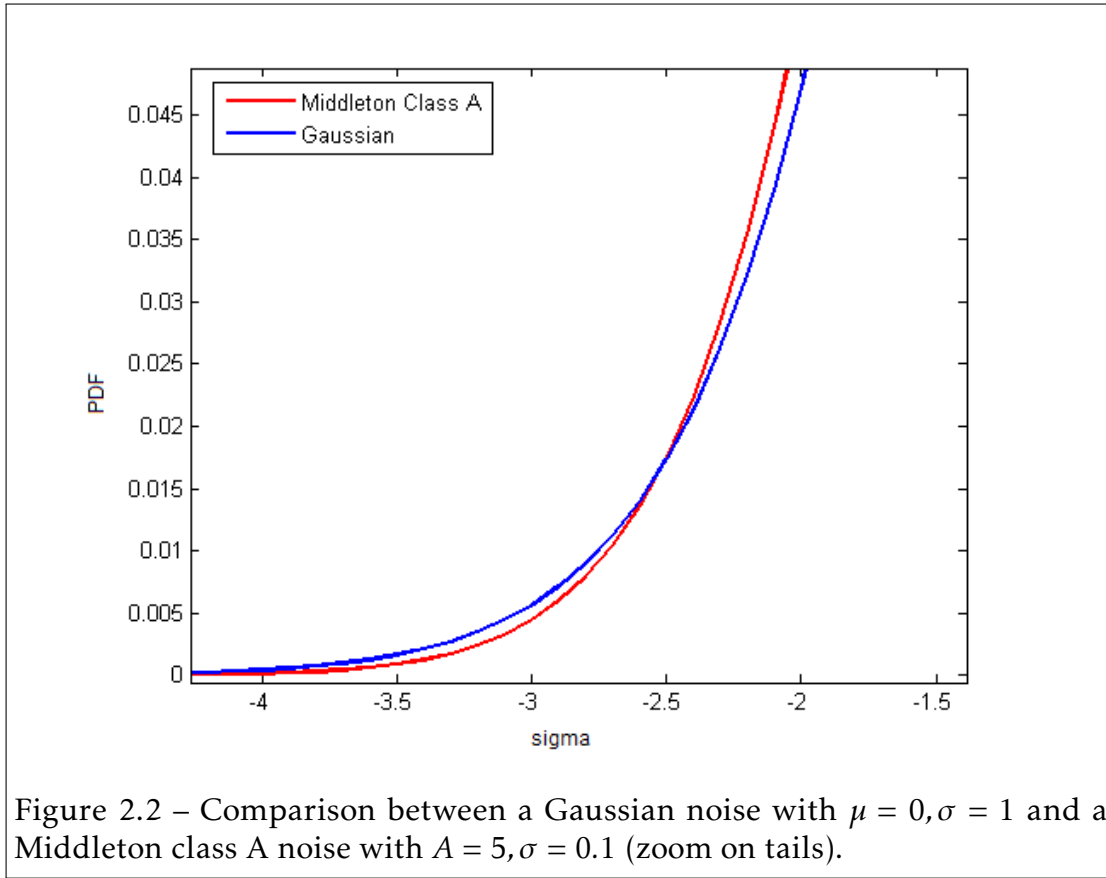
2.2   Justification

Although the first papers were published in the nineties [Sou92; TNS95; IH98], the analysis of networks has recently attracted a lot of works relying on stochastic geometry. As in Middleton's work, interferers are assumed spatially distributed according to a Poisson field. In this context, the interference can be written as

$$I = \sum_{i \in \mathcal{O}} l(d_i)\mathcal{Q}_i, \tag{2.10}$$

where $l(\cdot)$ denotes the attenuation, a function of distance d, and d_i is the distance between the i-th interferer and the destination. Usually, $l(d)$ is given by:

$$l_{h,\epsilon}(d) = d^{-h}\mathbb{I}_{r \geq \epsilon}, d \in \mathbb{R}^+, \tag{2.11}$$

where h is the channel attenuation coefficient, ϵ accounts for a minimum distance between the receiver and the transmitter for physical reasons or due to some MAC layer protocol like carrier sensing, Q_i includes diverse propagation effects such as multipath fading and shadowing as well as the physical layer of the transmitters and the receiver. $\mathcal{O}$ denotes the set of interferers.

If interferers in $\mathcal{O}$ are distributed according to an homogeneous Poisson Point Process, infinite series are obtained to describe the statistical distribution of I. In the case of an unbounded received power assumption, the interference falls in the attraction domain of a stable law. Such an assumption means that $\epsilon \to 0$. In such case, the received power $P_R \to \infty$ when $d \to 0$. This of course is not true, however the stable model appears to be rather accurate in many cases [Cla+10]. The accuracy of the approximation was questioned in [Ina+09]. However, working without the unbounded received power assumption does not allow an analytical derivation of the characteristic function [WA12], when the use of the stable distribution allows to design efficient communication solutions.

The stable approximation for the generated interference can also be seen as a consequence of the Generalized Central Limit Theorem [LS95]:

Theorem 2.2.1 (Generalized Central Limit Theorem) *The sum of i.i.d. random variables with finite or infinite variance converges to a distribution by increasing the number of variables, with a stable distribution as a limiting case.*

The proof of the result can be done considering the log-Characteristic Function of the total interference, which can be written as [Sou92; Cla+10]. Let us consider the CF $\phi_I(\omega)$:

$$\phi_I(\omega) = E\left[e^{jwI}\right], \tag{2.12}$$

where I denotes the total interference and $(\cdot)^T$ denotes the transpose. As proposed in Sousa [Sou92], we define a circle C of radius R and denote by N_I the number of interferers present in C. We compute the characteristic function of I but we first restrict the sum in (2.10) to the users included in C. We then make R tends towards infinity. We suppose that the number of active interferers follow a Poisson Point process, which means that the probability of the number of active

interferers in C is given by:

$$\mathbb{P}(N_I = k) = \frac{e^{-\lambda \pi R^2}\left(\lambda \pi R^2\right)^k}{k!} \tag{2.13}$$

λ is the expected number of interferer per unit area which is linked to the density of the network.

We can then write:

$$
\begin{aligned}
\phi_I(\omega) &= \mathbb{E}\left[e^{j\omega\left(\sum_{i=1}^{N_I} l(d_i)\mathcal{Q}_i\right)}\right] \\
&= \lim_{R \to +\infty} \sum_{k=0}^{+\infty} P(N_I = k)\,\mathbb{E}\left[e^{j\omega l(d)\mathcal{Q}}\right]^k \\
&= \lim_{R \to +\infty} \sum_{k=0}^{+\infty} \frac{e^{-\lambda \pi R^2}\left(\lambda \pi R^2\right)^k}{k!}\,\mathbb{E}\left[e^{j\omega l(d)\mathcal{Q}}\right]^k \\
&= \lim_{R \to +\infty} e^{-\lambda \pi R^2} \sum_{k=0}^{+\infty} \frac{\left(\lambda \pi R^2 \mathbb{E}\left[e^{j\omega l(d)\mathcal{Q}}\right]\right)^k}{k!} \\
&= \lim_{R \to +\infty} e^{-\lambda \pi R^2} e^{\lambda \pi R^2 \mathbb{E}\left[e^{j\omega l(d)\mathcal{Q}}\right]} \tag{2.14}
\end{aligned}
$$

We take the logarithm:

$$
\begin{aligned}
\varphi_I(\omega) &= \ln(\phi_I) \\
&= \lim_{R \to +\infty} \lambda \pi R^2 \left(\mathbb{E}\left[e^{j\omega l(d)\mathcal{Q}}\right] - 1\right) \tag{2.15}
\end{aligned}
$$

The expectation is taken over the two random variables $l(d)$ and $\mathcal{Q}$. In a first step we will calculate the expectation over $h = l(d)$ for a given R. We easily show that the PDF of $h = l(d)$ if $l(d) = d^{-a}$ and $0 \le d \le R$ is

$$f_{h_i}(x) = \frac{4x^{-\frac{4}{a}-1}}{aR^2} \text{ for } x \ge R^{-\frac{a}{2}}. \tag{2.16}$$

For $x < R^{-\frac{a}{2}}$, $f_{h_i}(x) = 0$. Then,

$$
\begin{aligned}
E\left[e^{j\omega h \mathcal{Q}}\right] &= \int_{R^{-\frac{a}{2}}}^{+\infty} E\left[e^{j\omega h\ mathcal Q}|h = x\right] f_h(x)\,dx \\
&= \int_{R^{-\frac{a}{2}}}^{+\infty} \phi_{\mathcal{Q}}(\omega x) \frac{4x^{-\frac{4}{a}-1}}{aR^2}\,dx
\end{aligned}
\tag{2.17}
$$

Integrating (2.17) by parts we obtain:

$$
\begin{aligned}
E\left[e^{j\omega\gamma\mathcal{Q}}\right] &= \left[-\frac{1}{R^2}x^{-\frac{4}{a}}\phi_{\mathcal{Q}}(\omega x)\right]_{R^{-\frac{a}{2}}}^{+\infty} + \frac{1}{R^2}\int_{R^{-\frac{a}{2}}}^{+\infty}\omega\frac{d\phi_{\mathcal{Q}}}{dx}(\omega x)x^{-\frac{4}{a}}\,dx \\
&= \phi_{\mathcal{Q}}\left(\omega R^{-\frac{a}{2}}\right) + \frac{1}{R^2}\int_{\omega R^{-\frac{a}{2}}}^{+\infty}\frac{d\phi_{\mathcal{Q}}}{du}(u)\left(\frac{u}{\omega}\right)^{-\frac{4}{a}}\,du
\end{aligned}
\tag{2.18}
$$

We can then use (2.18) in (2.15):

$$
\begin{aligned}
\varphi_I(\omega) &= \lim_{R\to+\infty}\lambda\pi R^2\left(\phi_{\mathcal{Q}}\left(\omega R^{-\frac{a}{2}}\right) + \frac{1}{R^2}\int_{\omega R^{-\frac{a}{2}}}^{+\infty}\frac{d\phi_{\mathcal{Q}}}{du}(u)\left(\frac{u}{\omega}\right)^{-\frac{4}{a}}\,du - 1\right) \\
&= \lim_{R\to+\infty}\lambda\pi R^2\left(\phi_{\mathcal{Q}}\left(\omega R^{-\frac{a}{2}}\right) - 1\right) \\
&\qquad\qquad + \lim_{R\to+\infty}\left(\lambda\pi\omega^{\frac{4}{a}}\int_{\omega R^{-\frac{a}{2}}}^{+\infty}\frac{d\phi_{\mathcal{Q}}}{du}(u)u^{-\frac{4}{a}}\,du\right) \\
&= \lim_{R\to+\infty}\lambda\pi R^2\left(\phi_{\mathcal{Q}}\left(\omega R^{-\frac{a}{2}}\right) - 1\right) + \lambda\pi\omega^{\frac{4}{a}}\int_0^{+\infty}\frac{d\phi_{\mathcal{Q}}}{du}(u)u^{-\frac{4}{a}}\,du \quad (2.19)
\end{aligned}
$$

We can show that $\lim_{R\to+\infty}\lambda\pi R^2\left(\phi_{\mathcal{Q}}\left(\omega R^{-\frac{a}{2}}\right) - 1\right) = 0$. As a consequence only the second term remains. If $\mathcal{Q}$ has a spherically symmetric probability density function, we can then write $\phi_{\mathcal{Q}}(\omega)$ as $\phi_{\mathcal{Q}_0}(\|\omega\|)$, where $\|.\|$ is the Euclidean norm. Finally we can write:

$$
\varphi_I(\omega) = \lambda\pi\|\omega\|^{\frac{4}{a}}\int_0^{+\infty}\frac{d\phi_{\mathcal{Q}_0}}{du}(u)u^{-\frac{4}{a}}\,du
\tag{2.20}
$$

In (2.20), the integral does not depend on ω and we can finally write:

$$\varphi_I(\omega) = -\sigma \|\omega\|^{\frac{4}{a}}, \tag{2.21}$$

with

$$\sigma = -\lambda \pi \int_0^{+\infty} \frac{d\phi_{Q_0}}{du}(u) u^{-\frac{4}{a}} du. \tag{2.22}$$

As we will describe in section 2.4.3, (2.21) is the log-characteristic function for the spherically symmetric stable distribution of exponent $\alpha = \frac{4}{a}$.

As it has just been shown, the unbounded path-loss model allows to derive the characteristic function in an elegant way and, moreover, to end on the α-stable family of distributions, and the special symmetric case. This allows to have a statistical distribution for intereference which is parametrized by only two parameters:

- the characteristic exponent $\alpha = \frac{4}{a}$. It defines the heaviness of the tail or, in other words, the probability that (rare) large events appear. It only depends on the attenuation coefficient a. If a increases, α decreases meaning a heavier tail: the presence of close interferers impacts "more" when the attenuation coefficient is large.

- the dispersion σ in (2.22) which can be related to the strength of the intereference. It depends on λ, the density of interferer and on the different system and environment parameters that are included in Q (small scale fading, possible shadowing, waveform and signal processing at the PHY layer).

This is one reason why the α-stable model is very attractive to model impulsive noises, even if we do not have in the general case an analytical expression of the PDF.

Another elegant way to obtain this result is to use the Lepages Series representation of an α-stable random variable [IH98; Ega+17].

2.3 Related works

Stable distributions often give a very good fit to empirical data and have been applied to different areas: physics, hydrology, biology, electrical engineering [LS95]. We can give some example here and a more detailed reference has been given in [Nol97] and further information on applications can also be found in [Kas88].

- **Natural phenomena**: Random variations of gravitational fields of stars in space under certain natural conditions follows a stable law with $\alpha = 1.5$ [LS95]. Some natural catastrophes also present non-Gaussian behavior [Nol97]. Thunderstorms and lightning discharges behave as independent sources in space while modeling the low-frequency atmospheric noise. Considering a large number of this atmospheric phenomena and applying the Generalized Central Limit Theorem may yield to a impulsive model [Ibu66; WM57; Cri+60; HH56; FI61; Bec64; GH72].

- **Man-made noises**: Some man-made noises and interferences exhibit an impulsive behavior, like automobile ignition spark plugs [Vas84; Mid77], microwave ovens [KMM], neon lights [Vas84] and radar data [Nol01] and others [Sko78; Mid72; Mid73; Mid77; Mid79; SM77a]. The α-stable models have also been successfully used for noise reduction to suppress the "cracks" when digitizing slightly damaged vinyl records.

- **Economics** In economics[Han10] α stable have often been used and many phenomena present non-Gaussian behavior, like market dynamics, econophysics, price behavior, common stock price changes and data, fluctuations in speculative prices, foreign exchange rate, interest rates and risk measures [Man63; LS95; Cis07; BHW05; Nol01]. It has been observed for instance that asset returns are not normally distributed: empirical observations have shown that they exhibit heavy tails. This characteristic, also named leptokurtic character of the distribution, of price changes has been observed in various markets and extreme financial events like market crashes [Nol97; Man63; SK14; Rac03].

- **Electronics** Measured EMI generated by the clocks and buses in laptop and desktop environments or theEMI from household appliances on digital subscriber loop systems are shown to be well modeled by SαS distribution [Nas+09].

- **Communications** Urban indoor, underwater acoustic communications, channels and signals are not well modeled by Gaussian models [Vas84; SM77a; Mid99; Gu12]. Ocean wave energy, submarine communications and sonar systems on Artic regions may present some impulsive noise due to ice cracking [Nol01; LS95; TR95; Vas84]. Studies on aquatic animals such as snapping shrimp in Singapore show that it produces acoustic shockwaves with ($\alpha \in [1.6, 1.9]$) [Vas84; PSK11]. We can also notice that the α-stable process is used in queuing theory when the traffic is modeled with Poisson process.

- **Biology** Molecular communication systems and molecular timing channels [Ega+16] also exhibits strong impulsive behavior where the α-stable distribution can be an accurate modelling tool.

In the study of communication networks, the principle that have lead to the use of stable distributions can be found in stochastic geometry and for instance in [WPS09; WA12]. When users are spatially distributed according to a Poisson point process, it has been shown that interference exhibits statistical properties that are different from classical thermal noise and an impulsive nature. The complex baseband noise derived from passband additive white symmetric α-stable noise was studied and analyzed by [MCA12]. The paper proves that: (1) all baseband noise samples are i.i.d.; (2) any given noise sample is shown to be SαS and (3) under the condition $f_s/f_c = 4$, where f_c and f_s denote respectively the carrier and passband sampling frequencies, respectively, the real and imaginary components are independent for any given sample.

Figure 2.3 shows the comparison between a Gaussian noise with $\mu = 0, \sigma = 1$ and a SαS noise with $\alpha = 0.8, h = 1, \beta = \delta = 0$.

Figure 2.3 – Comparison between a Gaussian noise with $\mu = 0, \sigma = 1$ and a SαS noise with $\alpha = 0.8, \gamma = 1, \beta = \delta = 0$.
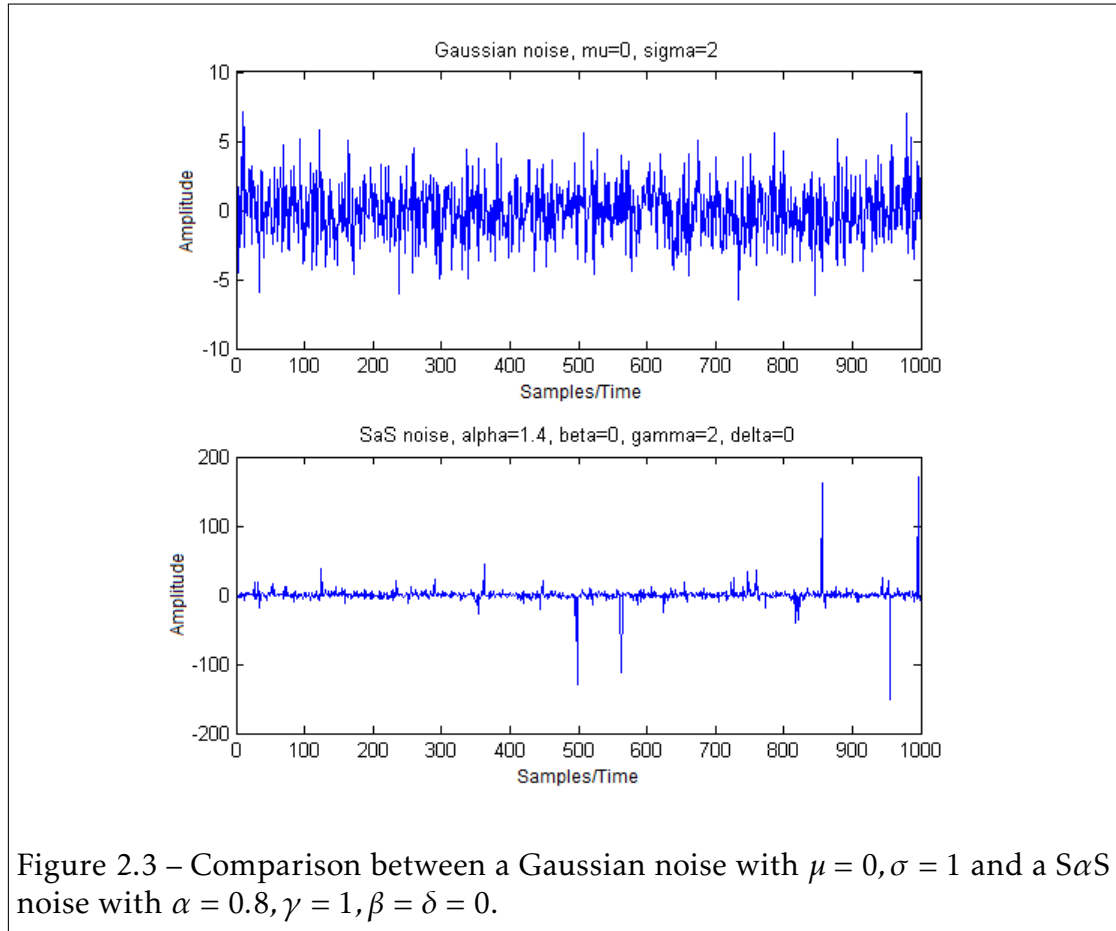
One specific property that makes α-stable laws attractive for modelling impulsive noises is their tail behavior. The probability density function of a stable model when $\alpha \neq 2$ decays in the tails less rapidly than the Gaussian density, or in other words, their tails are heavier, what makes the stable model more adequate for modelling impulsive noises [LS95]. In probability theory, heavy-tailed distributions are probability distributions whose tails are not exponentially bounded. So, stable model is characterized by a higher probability of large amplitude value [Ega+16].

When $\alpha < 2$, it can be shown that:

$$\begin{cases} \lim_{x \to \infty} x^\alpha \mathbb{P}(X > x) = C_\alpha (1 + \beta) \sigma^\alpha \\ \lim_{x \to \infty} x^\alpha \mathbb{P}(X < -x) = C_\alpha (1 + \beta) \sigma^\alpha \end{cases} \tag{2.23}$$

where:

$$C_\alpha = \left(2\int_0^\infty x^{-\alpha} sin(x)dx\right)^{-1} = \frac{1}{\pi}\Gamma(\alpha)sin\frac{\pi\alpha}{2}. \tag{2.24}$$

We can say that a stable RV, for $\alpha < 2$, has an algebric tail meaning there exist $c, \alpha > 0$ such that $\lim_{x\to\infty} x^\alpha \mathbb{P}(|X| > x) = c$.

Many works about modern communications networks have used the α-stable model. Interferences that exhibits impulsive behavior are also observed in Ultra-Wide Band (UWB) impulse radios [BY09], environments where narrowband and wide-band systems coexist, they are present in cognitive networks and are also used for modeling accurately Multiple Access Interference (MAI) in *ad hoc* or cellular networks [Sou92; Hug00; YP03; Hae+09; WPS09; PW10; Gul+10; Cla+10; Car10; CKP12; Yan15; Ega+17].

[Cla+10] studies the MAI based on Time Hopping (TH)- Pulse Position Modulation PPM-UWB, applying the α-stable model Impulse Radio (IR) based physical layer up-converted to 60 GHz band and purposes the use of Cauchy receiver for this scenario. [Sha12] investigates the impact of MAI on the performance of UWB systems: it approximates PDF by the Laplacian, Generalized Gaussian and Symmetric α-stable distributions. The results show that SαS distribution gives the best approximation to the PDF of the MAI. The Gaussian underestimates the accurate Bit Error Rate (BER) for medium and large SNR values even when there is a moderately large number of interferers in the UWB system. The Laplacian approximation underestimates the accurate BER for large SNR values and Generalized Gaussian gives much better approximation than Gaussian and Laplacian approximations.

Wireless cellular networks modeled via Poisson Point Process (PPP) and also in mollecular timing channels can also be described using α-stable models [IH98; Far+]. As stated before, with such kind of interference, that is badly captured by a Gaussian model, the classical linear receiver is no longer robust [Yan15].

In [Ega+16], the authors provide an example where AIαSN channels arise in the context of wireless cellular communications and studied more precisely the complex case. The authors considers a network, where base stations are located according to an homogeneous Poisson Point Process with rate ν and

assumes that the base band emission x_k of each interfering base station k is a circularly symmetric complex Gaussian random variable $\mathcal{CN}(0, P)$. For a typical user in this network, the interference can be expressed, very similarly as what we previously presented in (2.10), by

$$I = \sum_{k=1}^{\infty} r_k^{-\eta/2} h_k x_k, \tag{2.25}$$

where η is the path loss exponent and $h_k \sim \mathcal{CN}(0, 1)$ is Rayleigh fading. Let $z_k = h_k x_k = \mathcal{R}(z_k) + i\mathcal{I}(z_k)$, where $\mathcal{R}(z_k)$ and $\mathcal{I}(z_k)$ denotes respectively the real and imaginary parts of z_k. Applying the LePage series representation for α-stable RV, it follows that I converges almost surely to

$$I = I_r + iI_i, \tag{2.26}$$

where I_r, I_i are symmetric $2/\eta$-stable RVs. We can observe that h_k, x_k are isotropic circularly symmetric Gaussian RVs, which implies that I is an isotropic α-stable RV, also described as a sub-Gaussian RV.

2.4   Some properties of Stable distributions

2.4.1   Definition

One way to define an α-stable RV is through the stability property. A RV X has a stable distribution if and only if for any independent samples X_1 and X_2, with same distribution as X, and for any arbitrary constants a_1 and a_2, there are constants a and b such that [ST94; LS95]:

$$aX + b \stackrel{\mathrm{d}}{=} a_1 X_1 + a_2 X_2, \tag{2.27}$$

where $X \stackrel{\mathrm{d}}{=} Y$ denotes equality in distribution. In other words, the sum of two independent stable random variables with same characteristic exponent is again stable with the same characteristic exponent. Stable distributions are the only distribution that have this property. In the case where X has a finite variance, the

resulting distribution is the Gaussian and the characteristic exponent is $\alpha = 2$.

This property can be easily generalized for n independent stable RVs X_i with same α, β, where all the linear combinations $\sum_{i=1}^{n} a_i X_i$ are also stable with characteristic exponent and symmetry parameters α and β, respectively.

2.4.2 Generalized Central Limit theorem

As a consequence of stability property is that the sum of n I.I.D. RVs $X_i, i = 1, 2, ..., n$, with or without finite variance, converges to a distribution by increasing the number of variables ($n \to \infty$) and the limit distribution X is a stable distribution (see Theorem 2.2.1). The Central Limit Theorem discussed in Theorem 2.0.1 for Gaussian RVs is a particular case of the Generalized Central Limit Theorem where $X_{i's}$ have finite variance.

2.4.3 Characteristic function and parameterization

Another way to describe a stable distribution is to use its characteristic function, given by [LS95]

$$\phi(t) = \exp\{j\delta t - \gamma |t|^{\alpha} [1 + j\beta sign(t)\omega(t,\alpha)]\}, \tag{2.28}$$

where

$$\omega(t,\alpha) = \begin{cases} \tan(\frac{\alpha\pi}{2}) & \text{if } \alpha \neq 1 \\ \frac{2}{\pi}\log|t| & \text{if } \alpha = 1 \end{cases}$$

$$sign(t) = \begin{cases} 1 & \text{if } t > 0 \\ 0 & \text{if } t = 0 \\ -1 & \text{if } t < 0 \end{cases},$$

and $a \in \mathbb{R}, \gamma \in \mathbb{R}_*^+, \alpha \in (0,2], \beta \in [-1,1]$. For a RV distributed according to the CF described in (2.28), we use the notation $X \sim S_\alpha(\sigma, \beta, \mu)$ [JW94].

Four parameters describe the α-stable distribution:

- Parameter $\alpha \in]0,2]$ is called characteristic exponent and measures the "thickness" of the tails. Small values of α indicates high impulsiveness, while values close to 2 indicates a more Gaussian behavior. When $\alpha = 2$, the RV is Gaussian.

- Parameter γ (strictly positive) is called dispersion and plays a similar role to variance for Gaussian distribution. In the case $\alpha = 2$, it is equal to half of the variance.

- Parameter $\beta \in]-1,1]$ is a symmetry parameter. $\beta = 0$ corresponds to a symmetric variable, when $\beta = 1$ (respectively -1) corresponds to a variable totally skewed to the right (respectively to the left).

- Parameter δ is the location parameter. When $1 < \alpha \leq 2$ it represents the mean and for $0 < \alpha < 1$ it represents the median [LS95].

2.4.4 Some difficulties

Stable distributions present two important drawbacks: the first one is that there is no closed-form expression for the probability density function except for three specific cases: the Gaussian ($\alpha = 2$), Cauchy ($\alpha = 1, \beta = 0$) and Levy cases ($\alpha = 0.5, \beta = 1$) [LS95]. On the other hand there exists efficient techniques to generate stable RV so that Monte-Carlo based schemes can be used to make calculations.

A second difficulty is that for $\alpha < 2$, the p-th moments of a stable RV with characteristic exponent α exist and are finite only for $p < \alpha$. In particular, the variance (second order moment) of a stable distribution with $\alpha < 2$ does no exist. This can be seen as the price to pay to allow abrupt changes and rare events in the interference signal.

2.4.5   The probability density function and its approximations

The PDF of the standard stable ($\beta = \delta = 0$) density function can be obtained by taking the inverse Fourier transform of the CF:

$$f(x; \alpha, \beta) = \frac{1}{\pi} \int_0^\infty \exp(-t^\alpha) \cos[xt + \beta t^\alpha \omega(t, \alpha)] dt, \qquad (2.29)$$

Observe that $f(x; \alpha, \beta) = f(-x; \alpha, -\beta)$. The PDFs of stable distributions are bounded and have derivatives of arbitrary orders. The PDF can also represented by power series [LS95]. The Standard stable density function is given by the following absolutely convergent series, for $x > 0$:

$$f(x; \alpha, \beta) = \begin{cases} \frac{1}{\pi x} \sum_{k=1}^\infty \frac{(-1)^{k-1}}{k!} \Gamma(\alpha k + 1)(\frac{x}{r})^{\alpha k} sin[\frac{k\pi}{2}(\alpha + \xi)] & \text{if } 0 < \alpha < 1 \\ \frac{1}{\pi x} \sum_{k=1}^\infty \frac{(-1)^{k-1}}{k!} \Gamma(\frac{k}{\alpha} + 1)(\frac{x}{r})^{k} sin[\frac{k\pi}{2}(\alpha + \xi)] & \text{if } 1 < \alpha \leq 2 \end{cases}, \qquad (2.30)$$

where $r = (1 + \eta^2)^{-1/(2\alpha)}$ and $\xi = -(2/\pi) \arctan \eta$, with $\eta = \beta \tan(\pi \alpha / 2)$ and Γ is the Gamma function, given by:

$$\Gamma(x) = \int_0^\infty t^{x-1} e^{-t} dt, \qquad (2.31)$$

The maximum likelihood approach for estimation of PDF demands a relevant computational effort due to numerical approximations used. Usually, two approaches are used for calculating the PDF: apply Fast Fourier Transform (FFT) to the characteristic function or direct integration. For data points between the equally spaced FFT grid nodes an interpolation technique has to be used. Taking a larger number of grid point increases the accuracy but, in the other hand, demands a higher computational effort. The FFT based approach is faster for large samples. In addition, the FFT-based approach is efficient only for large values of α and only for PDF calculations. The direct integration method presents best performance for small data set, since it can be computed at any arbitrarily chosen point, but in some cases the integrand becomes very peaky and numerical algorithms can miss the spike and underestimate the integral, being interesting to calculate it as the sum of two integrals for different intervals

[BHW05].

In [Bel05] different methods for the evaluation of PDF of stable distributions are discussed: direct numerical integration methods, FFT and method of two quadratures. [SK14] propose several methods of approximation of stable distributions by some discrete distributions. Further information can also be found [Nol97]. Figure 2.4 compares a Gaussian distribution with $\mu = 0, \sigma = 1$ and a SαS distribution with $\alpha = 0.8, \gamma = 1, \beta = \delta = 0$.
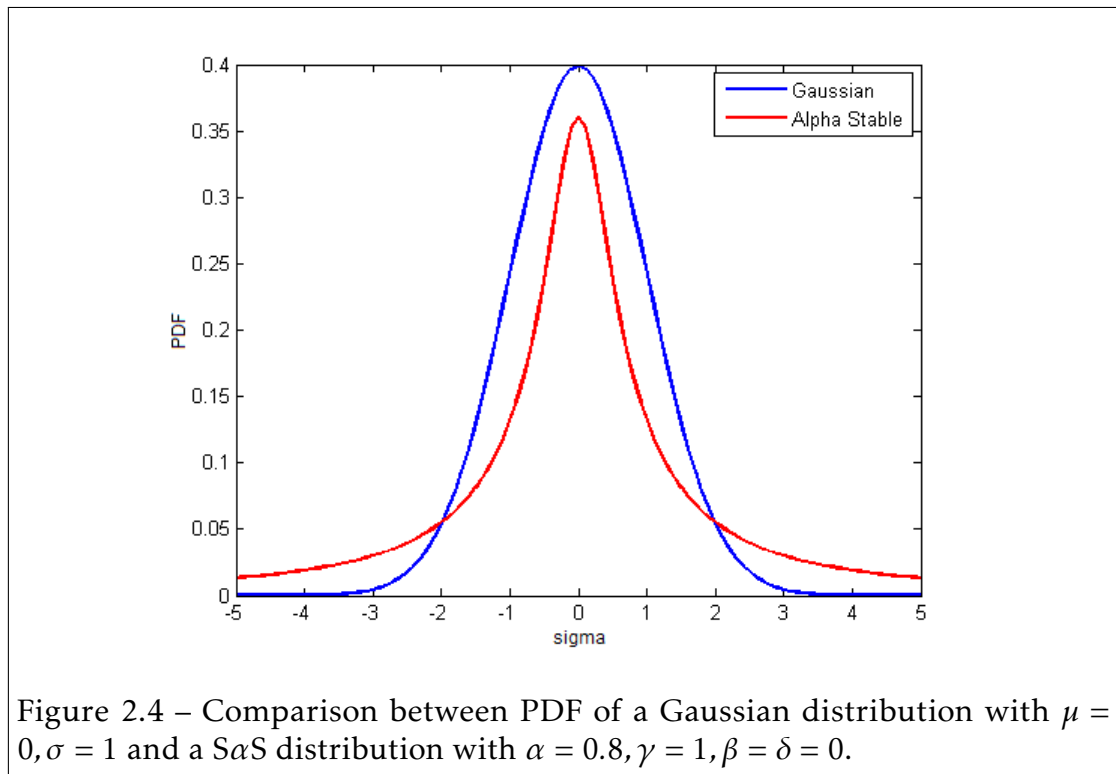
Figure 2.4 – Comparison between PDF of a Gaussian distribution with $\mu = 0, \sigma = 1$ and a SαS distribution with $\alpha = 0.8, \gamma = 1, \beta = \delta = 0$.

2.4.6   Moments

As stated on 2.4.4, for an α-stable RV X, if $0 < \alpha < 2$, then:

$$\mathbb{E}|X|^p = \infty, p \geq \alpha, \tag{2.32}$$

If $\alpha = 2$:

$$\mathbb{E}|X|^p < \infty, \ \forall p \geq 0, \tag{2.33}$$

what means that, except for the limiting case $\alpha = 2$, where all moments exist, there is no second-order moment for stable distributions and more generally for $0 < \alpha \leq 1$, α-stable distributions have no finite first or higher order moments. We can however define Fractional Lower-Order Moments (FLOMs) of order $p < \alpha$.

2.4.7 Fractional Lower Order Moments

Let X be a SαS random variable with $\delta = 0$ and dispersion γ, then

$$\mathbb{E}(|X|^p) = C(p, \alpha)\gamma^{p/\alpha}, 0 < p < \alpha, \tag{2.34}$$

where

$$C(p, \alpha) = \frac{2^{p+1}\Gamma(\frac{p+1}{2})\Gamma(-p/\alpha)}{\alpha\sqrt{\pi}\Gamma(-p/2)}. \tag{2.35}$$

2.4.8 Covariation

The covariation for SαS RVs plays a similar role to covariance for Gaussian RVs: given two jointly SαS RVs X and Y with $1 < \alpha \leq 2$, the covariation of X with Y is defined by

$$[X, Y]_\alpha = \int_S xy^{<\alpha-1>}\mu(d\mathbf{s}), \tag{2.36}$$

where S is the unit circle and $\mu(\cdot)$ is the spectral measure of the SαS random vector (X, Y) and

$$z^{<a>} = |z|^a sign(z), \tag{2.37}$$

for any given $z \in \mathbb{R}$ and $a \geq 0$. The covariation coefficient of X with Y is given by [LS95]:

$$\lambda = \frac{[X, Y]_\alpha}{[Y, Y]_\alpha}. \tag{2.38}$$

We note that the covariation $[X, Y]_\alpha$ is linear in X ($[aX_1 + bX_2, Y]_\alpha = a[X_1, Y]_\alpha + b[X_2, Y]_\alpha$) but not with respect to Y. Consequently, X and Y play asymmetric roles according to the definition given above. Denoting now γ_y as the dispersion of Y, we have

$$[Y, Y]_\alpha = \|Y\|_\alpha^\alpha = \gamma_y, \tag{2.39}$$

$$\lambda_{XY} = \frac{\mathbb{E}(XY^{<p-1>})}{\mathbb{E}(|Y|^p)}, 1 \le p < \alpha, \tag{2.40}$$

$$[X, Y]_\alpha = \frac{\mathbb{E}(XY^{p-1})}{\mathbb{E}(|Y|^p)}, 1 \le p < \alpha, \tag{2.41}$$

It is interesting to note that the covariation can allow to define a norm and a distance for α-stable RV. Besides, this norm can be estimated using the p-norm as described by the following equations:

$$\|X - Y\|_\alpha = [X - Y, X - Y]_\alpha = \begin{cases} [\mathbb{E}|X - Y|^p / C(\alpha, p)]^{1/p}, & 1 \le \alpha \le 2, \\ [\mathbb{E}|X - Y|^p / C(\alpha, p)]^{\alpha/p}, & 0 < \alpha < 1, \end{cases} \tag{2.42}$$

where $C(\alpha, p) = \frac{2^{p+1}\Gamma((p+1)/2)\Gamma(-p/\alpha)}{\alpha\sqrt{\pi}\Gamma(-p/2)}$, and $\Gamma(.)$ is the gamma function.

2.4.9   Generation and simulation of α stable models

[LS95] presents an accurate and inexpensive algorithm for generating stable RVs for arbitrary characteristic exponent α and skewness parameter β developed by J.M. Chambers, C.L. Mallows and B.W. Stuck. The algorithm does a nonlinear transformation of two independent uniform RVs into one stable random variable. Let's suppose that we want to generate a random sample X from the standard stable distribution. The algorithm is shown in Algorithm 1. More details on simulation of α-stable RV can be found in [JW94] and further information on generation of α-stable RV can be found in [Yan15; Wei12].

Algorithm 1 Simulation of α stable random variables. Source: [LS95].

---

  begin SimulationSaS(α,β)

  if $\alpha = 1$ **then**

    Define:

    $\beta_A \leftarrow \beta$;

    $\gamma_A \leftarrow \pi/2$;

    $\beta' = \beta_A$.

    $\varphi_X(t) = \exp(-|t|(1 + \frac{2}{\pi} j \beta' log|t| sign(t)))$.

  else

    Define:

    $k(\alpha) \leftarrow 1 - |1 - \alpha|$;

    $\beta_A \leftarrow 2 \arctan(\beta/cot(\pi\alpha/2))/(\pi(\alpha))$;

    $\gamma_B \leftarrow cos(\pi\beta_A k(\alpha)/2)$;

    $\Xi_0 \leftarrow -0.5\pi\beta_A(k(\alpha)/\alpha)$;

    $\beta' \leftarrow -\tan(0.5\pi(1-\alpha))tan(\alpha\Xi_0)$;

    $\varphi_X(t) \leftarrow exp(-|t|^\alpha - jt(1 - |t|^{\alpha-1})\beta'tan(0.5\pi\alpha))$.

  end if

  Generate two independent samples Ξ and W, where Ξ is uniform on $(-0.5\pi, 0.5\pi)$ and W is exponentially distributed with unit mean;

  $\epsilon \leftarrow 1 - \alpha$

  $\tau \leftarrow \epsilon \tan(\alpha\Xi_0)$;

  $a \leftarrow \tan(0.5\Xi)$;

  $B \leftarrow \tan(0.5\epsilon\Xi)/(0.5\epsilon\Xi)$;

  $b \leftarrow \tan(0.5\epsilon\Xi)$;

  $z \leftarrow \frac{\cos(\epsilon\Xi) - \tan(\alpha\Xi_0 \sin(\epsilon\Xi)}{W\cos(\Xi)}$;

  $d \leftarrow \frac{z^{\epsilon/\alpha} - 1}{\epsilon}$;

  $X \leftarrow \frac{2(a-b)(1+ab) - \Xi\tau B(b(1-a^2) - 2a)}{((1-a^2)(1-b^2))}(1 + \epsilon d) + \tau d$.

  return X

  end

2.4.10   Complex symmetric stable variables and Isotropic stable variables

A complex RV $X = X_1 + jX_2$ is SαS if the random vector (X_1, X_2) is SαS in $\mathbb{R}^2$ [LS95; ST94].

A complex SαS RV $X = X_1 + iX_2$ is called isotropic (or rotationally invariant) if $X = X_1 + iX_2$ where $X_1, X_2 \in \mathbb{R}$ and $\mathbf{X} = (X_1, X_2)^T$ is symmetric in $\mathbb{R}^2$, i.e., $\mathbb{P}(-\mathbf{X} \in A) = \mathbb{P}(\mathbf{X} \in A)$ for all Borel sets in $\mathbb{R}$ [ST94; Ega+16], i.e.:

$$e^{i\phi}X \stackrel{\mathrm{d}}{=} X, \tag{2.43}$$

for any $\phi \in [0, 2\pi)$.

2.5   Parameter estimation

One last important point we discuss in this chapter is the parameter estimation. The classical literature presents three main approaches: Maximum Likelihood (ML), used on this work, quantiles method and regression-type method. [DK] solves the general problem of stable parameter estimation analitically by proposing three solutions: weighted sums of independent α-stable variates, FLOM methods and logarithmic moments. For this thesis, we will introduce the regression type method, FLOM methods and logarithmic moments. Further information on quantiles method can be found in [Yan15; SN93] and on weighted sums of independent α-stable variates in [DK].

2.5.1   Tail exponent estimation

According to [BHW05], the simplest way of estimating α is to plot the right tail of the empirical CDF on a double logarithmic plot. The slope of the linear regression for large values of x yields the estimate of the tail index $\alpha = -slope$. This method is very sensitive to the size of the sample and to the choice of the number of regression observations [BHW05]. An estimator for stable index based on the linear relation between U-statistics and V-statistics can be found in [Pan14]. Further information can be found in [SN93; BHW05].

2.5.2   Method of Sample Characteristic Function / Regression-type method

Denoting $c = \gamma^{1/\alpha}$ and let [SN93]:

$$\hat{\phi}(t) = \frac{1}{N} \sum_{k=1} N \exp(jtx_k), \tag{2.44}$$

be the sample characteristic function, where N is the sample size and $x_1, x_2, ..., x_N$ are the observations. So [SN93]:

$$\log(-\log|\phi(t)|^2) = \log(2c^\alpha) + \alpha \log|t| \tag{2.45}$$

and

$$\frac{\mathcal{I}\phi(t)}{\mathcal{R}\phi(t)} = \tan(at), \tag{2.46}$$

the parameters α and c can be estimated from the linear regression [SN93]:

$$r_k = \mu + \alpha w_k + \epsilon_k, k = 1, 2, ..., K, \tag{2.47}$$

where $r_k = \log(-log|\phi(t)|^2)$, $\mu = \log(2c^\alpha)$, $w_k = \log|t_k|$. $\epsilon_k, k = 1, 2, ..., K$ denotes the error terms which are assumed to be i.i.d. with mean zero and $t_1, t_2, ..., t_k$ are an appropriate set of real numbers. The location parameter a can be estimated in a similar way [SN93]:

$$z_k = au_k + \epsilon_k, l = 1, 2, ..., L, \tag{2.48}$$

where

$$z_k = \arctan(\mathcal{I}(\hat{\phi}(u_k))/\mathcal{R}(\hat{\phi}(u_k))), \tag{2.49}$$

and $u_1, ..., u_L$ is an appropriate set of real numbers [SN93].

2.5.3   FLOM methods

- **Estimator for** α Let $X \sim S_\alpha(\beta, \gamma, 0)$ for $\alpha \neq 1$, the estimate of α is the solution to [DK]:

$$sinc(\frac{p\pi}{\alpha}) = [a(\frac{A_p A_{-p}}{\tan q} + S_p S_{-p} \tan q)]^{-1}, \tag{2.50}$$

where $q = \frac{p\pi}{2}$, $A_p = \mathbb{E}[|X|^p]$, $S_p = [X^{<p>}]$, and:

$$\mathbb{E}[X^{<p>}] = \frac{\gamma(1 - \frac{p}{\alpha})}{\gamma(1 - p)}|\frac{\gamma}{\cos\theta}|^{p/\alpha}\frac{\sin(\frac{p\theta}{\alpha})}{\sin(\frac{p\pi}{2})} \text{ for } p \in (-2, -1) \cup (-1, \alpha), \tag{2.51}$$

$$\mathbb{E}[|X|^p] = \frac{\gamma(1 - \frac{p}{\alpha})}{\gamma(1 - p)}|\frac{\gamma}{\cos\theta}|^{p/\alpha}\frac{\sin(\frac{p\theta}{\alpha})}{\sin(\frac{p\pi}{2})} \text{ for } p \in (-1, \alpha), \tag{2.52}$$

where $\theta = arctan(\beta\tan\alpha\pi2)$ and $x^{<p>} = sign(x)|x|^p$.

- **Estimator for β** Given an estimate of α, estimate θ can be found by solving

$$S_p/A_p = \tan(\frac{p\theta}{\alpha})/tan(\frac{p\pi}{2}). \tag{2.53}$$

Given this estimate of of θ, the estimate of β is given by:

$$\hat{\beta} = \frac{\tan(\theta)}{\tan(\frac{\alpha\pi}{2})}. \tag{2.54}$$

- **Estimator for γ** Given an estimate for α and θ, the estimate of γ is given by [DK]:

$$\hat{\gamma} = |\cos\theta|(\frac{\Gamma(1 - p)}{\Gamma(1 - p/\alpha)}\frac{\cos p\pi/2}{\cos p\theta/\alpha}A_p)^{\alpha/p}. \tag{2.55}$$

2.5.4   Logarithmic moments

Let $X \sim S_\alpha(\beta, \gamma, 0)$ [DK]:

$$\mathbb{E}[(log|X|)^n] = \lim_{p \to 0}\frac{d^n}{dp^n}\mathbb{E}[|X|^p], n = 1, 2, 3... \tag{2.56}$$

$$L_1 = \mathbb{E}[log|X|] = \psi_0(1 - \frac{1}{\alpha}) + \frac{1}{\alpha}\log\left|\frac{\gamma}{\cos\theta}\right|, \tag{2.57}$$

$$L_2 = \mathbb{E}[(\log|X| - \mathbb{E}[\log|X|])^2] = \psi_1(\frac{1}{2} + \frac{1}{\alpha^2}) - \frac{\theta^2}{\alpha^2}, \tag{2.58}$$

$$L_3 = \mathbb{E}[(\log|X| - \mathbb{E}[\log|X|])^3] = \psi_2(1 - \frac{1}{\alpha^3}), \tag{2.59}$$

with $\psi_{k-1} = \frac{d^k}{dx^k}\log\Gamma(x)|_{x=1}$

- **Estimator for** α Parameter α can be estimated by

$$\hat{\alpha} = (\frac{L_2}{\psi_1} - 0.5)^{-1/2}. \tag{2.60}$$

- **Estimator for** β Assuming that an estimate for α is available and $\delta = 0$, then

$$|\theta| = ((\frac{\psi_1}{2} - L_2)\alpha^2 - \psi_1)^{1/2}, \tag{2.61}$$

the estimate of β then, can be obtained by

$$S_p/A_p = \tan(\frac{p\theta}{\alpha})/tan(\frac{p\pi}{2}). \tag{2.62}$$

If centering was applied is necessary to transform the resulting b by $\frac{2+2^\alpha}{2-2^\alpha}$

- **Estimator for** γ Assuming again $\delta = 0$, then

$$\hat{\gamma} = \cos(\theta)\exp((L_1 - \psi_0)\alpha + 1), \tag{2.63}$$

Again, if centering was applied, is necessary to transform the resulting γ by multiplying it by $\frac{1}{2+2^\alpha}$.

2.6 Conclusion

The fist part of this thesis presented an statistical analysis of interference on heterogeneous sensor networks. Initially was discussed the importance of robustness of communication on IoT, being followed by experimental studies on the nature of interference between Zigbee and Wifi devices. These studies showed the non-Gaussian behavior of this scenario. The theoretical analysis based on

PPP assumption presented on this chapter led to the conclusion that this scenario can be modelled by the α-stable model. An overview of main properties of this model is presented to conclude the characterization and modelling of interference based on experimental and theoretical approaches. The next chapter present a robust receiver design using spacial diversity to deal with impulsive interferneces.

Chapter 3

Robust receiver design using space diversity

Before coping with non Gaussian interference, it is important to keep in mind that the first reliability issue in wireless communication is the radio channel. If we can expect that the planning of the networks is done according to the possible range of the communication, large and small scale fading give an uncertainty on the link quality that can not be compensated by a higher transmission power, which would reduce the life time of the nodes. In this chapter we will first introduce the main aspects of the radio channel that impact the received signal and the link quality. To face the channel variability, we propose to introduce space diversity, slightly at the transmitter side, using 2 antennas, and more significantly at the receiver side which will be considered as the gateway, connected to a power source and with more computation capabilities. This scheme does not hold for multihop communication but space diversity can then be achieved by multiple relays and path for information transfer.

3.1 Wireless propagation channel

The propagation channel transforms the transmitted signal into the received signal through electromagnetic waves. Propagation involves several physical phenomena [Cho+10; Hon10; Mas12]:

- **Reflection** occurs when electromagnetic waves are reflected on an obstacle instead of passing through. The reflection occurs when obstacles are present on the path of wave and their dimension are bigger than wavelength. When the surface is not irregular, we have a specular reflexion and the direction and amplitude of reflected wave are described by Snell-Descartes and Fresnel laws, otherwise, when random and non-negligible irregularities on the surface are present, we can have a diffuse reflection.

- **Transmission** occurs when a non radio-opaque environment is encountered. In that case, the electromagnetic wave goes through the obstacle.

- **Diffraction** occurs when the radio path between transmitter and receiver is obstructed by a high dimension obstacle in front of the electromagnetic wavelength with sharp irregularities or small openings and happens on the edges of this obstacle.

- **Diffusion** corresponds to the superposition of a non-negligible number of random diffractions. Usually it is supposed that the wave is redirected to all directions with variable attenuations.

- **Waveguiding** corresponds to the successive reflections over two parallel obstacles leading to the transmission of the electromagnetic wave according to the guidance direction.

- **Scattering** occurs when an electromagnetic wave is deviated from a straight path by one or more obstacles with small dimensions compared to the wavelength.

The main consequences of these physical phenomena are: attenuation, shadowing and multipath propagation.

3.1.1   Narrow-band analysis

Many IoT applications are low data rate and, consequently, can use a rather narrow bandwidth for the transmission, the extreme case being represented by SigFox, which uses a 100 Hz band. In that case the whole transmitted signal $x(t)$

is attenuated by a single coefficient $a(t)$, that can change in time and the received signal (without interference nor thermal noise) is given by $y(t) = a(t)x(t)$. The variations in $a(t)$ can be due to several factors: distance (pathloss), shadowing from obstacles (large scale fading) or multipath propagation (small scale fading).

Free space propagation model and attenuation (path loss)

The strength of the signal attenuates as it goes through the environment. It becomes weaker as the propagation distance increases [Hon10]. The attenuation, or path loss, corresponds to the energy loss during this propagation and depends on the frequency of the signal.

The attenuation is given by the ratio between the output and the input powers of the signal, usually expressed in dB. In non homogeneous environment, the pathloss refers to the mean received power at a given distance. Let P_t and P_r be the transmitted and received power respectively, so:

$$\eta_{dB} = 10 \log_{10} \frac{P_t}{P_r}.$$
(3.1)

This ratio depends on the geographical characteristics of the environment. In free space, no obstacle are present and the propagation environment can be considered homogeneous in every directions. The propagation model then allows to predict the exact received signal power according to the distance between transmitter and receiver. This model also ignores atmospheric losses.

Let's define G_t, G_r and d, respectively, the transmitter antenna gain, the receiver antenna gain and the distance between transmitter and receiver. In free space, the receiver power P_r for long distances (far field) is given by the Friss law:

$$P_r = P_t G_t G_r \frac{\mathcal{L}^2}{(4\pi d)^2}$$
(3.2)

where $\mathcal{L}$ is the wavelength of the electromagnetic wave. Denoting the carrier frequency by f_c, $\mathcal{L}$ is given by:

$$\mathcal{L} = \frac{\mathcal{C}}{f_c}$$
(3.3)

where $\mathcal{C}$ denotes the light speed ($3 \cdot 10^8 ms^{-1}$). The path loss is a positive value

measured in dB and defines the difference between the transmitted and received powers:

$$A_{dB} = -10\log_{10}\left(G_t G_r \frac{\lambda^2}{(4\pi d)^2}\right) \tag{3.4}$$

The Friss model is not applicable when obstacles are present and the propagation

environment is not homogeneous, i.e. the same in all directions. Consequently we express an average received power as a function of the distance between the transmitter and the receiver:

$$\overline{A}_{dB} = \overline{A}_{0dB} + 10h\log_{10}\left(\frac{d}{d_0}\right), \tag{3.5}$$

where $\overline{A}_{0dB}$ is the mean path loss at distance d_0. The main difference with the Friss law is given by the attenuation coefficient h. This coefficient h indicates the attenuation speed according to the distance and depends on the environment. For free space, $h = 2$. In outdoor environments, e.g. GSM, usually $2 < h < 5$. However, in indoor situations, as corridors with behavior similar to wave guides, h can be slightly below 2.

Shadowing

As stated before, the obstacles that appear along the transmission path may absorb part of the signal energy of the electromagnetic wave, resulting in signal strength degradation. This power variation is called shadowing effect and is considered as large scale fading [Hon10] due to the size of the obstacles as compared to the wavelength. For general statistical purpose, we can add the shadowing to the path loss and obtain the following path loss plus shadowing model:

$$\overline{A_{Sh}}_{dB} = \overline{A}_{dB} + \chi_\sigma = \overline{A}_{0dB} + 10h\log_{10}\left(\frac{d}{d_0}\right) + \chi_\sigma \tag{3.6}$$

where χ_σ is a Gaussian random variable centered (in dB) and with standard deviation σ (in dB) and describes the random effects of environment (shadowing).

Multipath fading

The signal arriving at the receiver is most of the time the superposition of signals from multiple propagation paths that add constructively or destructively. It can create rapid fluctuations over time, space and frequency of the signal strength. This is called multipath fading or small scale fading. To illustrate this in the narrowband case we consider a source S which transmits a signal $x(t) = \cos(2\pi f_c t)$ to a destination D and two possible paths: one direct and the other resulting from a reflection with a delay t_1. The received signal is then given by:

$$r(t) = a_0 x(t) + a_1 x(t - t_1) = a_0 \cos(2\pi f_c t) + a_1 \cos(2\pi f_c(t - t_1)). \quad (3.7)$$

The resulting mean received power is given by

$$P_r = \frac{1}{2}(a_0^2 + a_1^2) + a_0 a_1 \cos(2\pi f_c t_1). \quad (3.8)$$

This means that P_c varies between $0.5(a_0 + a_1)^2$ and $0.5(a_0 - a_1)^2$.

The narrowband transmission can also be described as "flat-fading", referring to frequency-non-selective fading [Cho+10; Hon10]. In that case, all paths contribute to a single channel coefficient whose statistical properties have been largely studied. The two most well-known distribution are the Rayleigh and the Rice ones. Let's consider now N paths, then:

$$r(t) = \sum_{i=1}^{N} a_i \cos(2\pi f_c(t - t_i)) = \sum_{i=1}^{N} a_i \cos(2\pi f_c t - \phi_i)$$

$$= \left(\sum_{i=1}^{N} a_i \cos(\phi_i) \right) \cos(2\pi f_c t) + \left(\sum_{i=1}^{N} a_i \sin(\phi_i) \right) \sin(2\pi f_c t). \quad (3.9)$$

In the equivalent baseband representation, the received signal amplitude can be described as a complex random variable. So, each of its components, real and imaginary ones, are the sum of a possibly large number of contributions. If there is no more significant than others contribution, we can apply the central

limit theorem and this amplitude will be a centered complex Gaussian random
variable and its module will obey the Rayleigh law:

$$f_X(x) = \frac{x}{\sigma^2} exp\left\{\frac{x}{2\sigma^2}\right\}. \tag{3.10}$$

So, we have the so-called Rayleigh channel, the absence of dominant contribution
being equivalent to no direct path. If there is a direct path, the amplitude will
obey a non-centered Gaussian complex law and its module will obey the Rice
law:

$$f(x) = \frac{x}{\sigma^2} \exp\left(\frac{-(x^2 + a^2)}{2\sigma^2}\right) K_0\left(\frac{ax}{\sigma^2}\right), \tag{3.11}$$

where $K_0(z)$ denotes the zero-order first kind modified Bessel function. In this
case, we have the so-called Rice channel, resulting from the presence of a fixed,
possibly line-of-sight (LoS), component.

Slow and fast fading

The radio channel evolution during the transmission of a packet depends on
the length of the packet and the mobility speed of the transmitter, receiver and
environment. We consider that the coherence time is the period of time during
which we can consider that the communication channel remains unchanged. If
the packet duration is shorter than this coherence time, we have a slow fading
channel, otherwise, we have a fast fading channel. In the rest of this chapter we
are going to consider slow fading (or equivalently called block fading). This is
representative of many wireless sensor networks applications where nodes are
attached to static things. This should however be further analyzed, especially
for LPWAN, where the time on, air of a packet can be very long, more than one
second in some specific situations in LoRa or Sigfox.

3.1.2   The MIMO Channel

As we will detail in the next section, the MIMO channel is represented by a
$(N_T \times N_R)$ matrix where N_T is the number of transmitting antennas and N_R the
number of receiving antennas. Each coefficient of the matrix represents a Single

Input Single Output (SISO) narrowband channel. They are commonly modeled as a Rayleigh random variable, so zero-mean circularly symmetric complex Gaussian random variables. In fact this Rayleigh assumption is the best case in MIMO situations, giving a maximum diversity between each channel.

The degree of correlation between the individual $N_T \times N_R$ channel gains is a function of the scattering in the environment and the antenna spacing at the transmitter and the receiver. If we consider the extreme event where all antenna elements at the transmitter are collocated and likewise at the receiver, all elements of **H** will be fully correlated (in fact identical) and the spatial diversity order of the channel is one. The typical antenna spacing required for decorrelation is approximately $\lambda/2$, where λ denotes the wavelength corresponding to the frequency of operation [Big+07].

The wideband situation is more complex to analyze because a third dimension (time) has to be added to channel matrix. In this work we will consider a narrowband situation. This is relevant in IoT applications where the expected data rate is very low so that transmission can be done on narrow bandwidth. This is also relevant when techniques like Orthogonal Frequency Division Multiplexing are used and when we can consider the transmission on a sub-band which is narrow by construction of the system.

3.2   MIMO technology

This thesis aims to design a reliable and low power communication scheme for IoT. We want to take advantage of spatial diversity in order to reduce or even eliminate the effects of small scale fading. However we do not want to significantly increase the complexity and the cost at the transmitter side. This implies that (*a*) we are going to use only two transmit antenna and (*b*) we do not assume any knowledge of the channel state information at the transmitter. On another hand we assume that complexity can be increased at the receiver side, especially when the receiver is the gateway or sink. The MIMO technology represents in the last decade one of the most significant advance in wireless communications, in order to increase the rates and/or the number of transmitting devices. It is possible to list four main advantages of the MIMO technology:

array gain, spatial diversity gain, spatial multiplexing gain and interference reduction and avoidance [Big+07]:

- Array gain improves resistance to noise, thereby improving the coverage and the range of a wireless network;

- The spatial diversity gain improves robustness against radio channel fading [BFC05];

- The spatial multiplexing gain increases the capacity of a wireless network;

- Interference may be mitigated in MIMO systems by exploiting the spatial dimension to increase the separation between users. Interference reduction and avoidance improve the coverage (range) in a wireless network.

Coding and signal processing are important elements of a successful implementation of a MIMO system and the communication channel represents a major component that determines the system performance [GS05]. In the following we will discuss these two important elements and see what advantages of MIMO can be exploited in massive machine type communications.

3.2.1 System model

In a MIMO transmitter, the information bits to be transmitted are encoded and mapped to data symbols. These data symbols are sent to space-time encoder. The outputs are called spatial data streams: they are transmitted, propagate through the channel and arrive to the receiver antenna array. The different signals received at each antenna are then decoded through the receiver space-time processing, symbol demapping and decoding [Big+07], as described in Fig. 3.1.
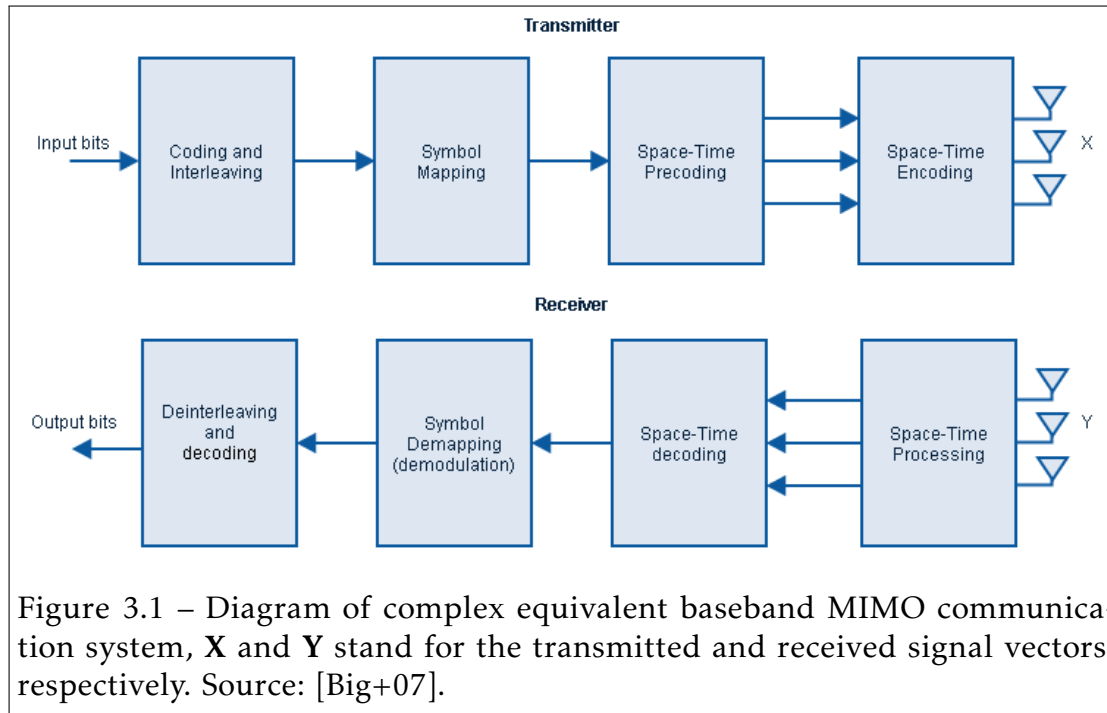
Figure 3.1 – Diagram of complex equivalent baseband MIMO communication system, **X** and **Y** stand for the transmitted and received signal vectors, respectively. Source: [Big+07].

We use the following notations: $\mathbf{A}_{M,N} \in \mathbb{C}^{M \times N}$ is a $M \times N$ complex matrix, s is a symbol taken from the set of possible symbols $\mathcal{S} = \{s_k\}$. Let us consider the following communication system model:

- N_s is the number of transmitted symbols (different times), N_t is the number of transmit antennas and N_r the number of receive antennas.

- All possible transmitted symbols that are equiprobable, i.e. $\mathbb{P}(s = s_i) = \mathbb{P}(s = s_j)$, $\forall \{i, j\}$, $i \neq j$.

- $\mathbf{X}_{N_s,N_t} \in \mathbb{C}^{N_s \times N_t}$ denotes the matrix of all transmitted symbols in a given packet, where the column $\mathbf{X}_{N_s,1}^{(i)}$, $i = 1, 2, ..., N_t$ represents the signals transmitted over the ith transmitting antenna.

- The channel is represented by $\mathbf{H}_{N_t,N_r}$, with $\mathbf{H}_{N_t,N_r} \in \mathbb{C}^{N_t \times N_r}$, where the matrix element $h_{i,m} \in \mathbf{H}_{N_t,N_r}$ is the complex gain and represents the fading channel coefficient between the ith transmit antenna and the mth receive antenna, with $i = 1, 2, ..., N_t$ and $m = 1, .., N_r$. The nth column of **H** is often

referred to as the spatial signature of the nth transmit antenna across the receive antenna array [Big+07].

- We denote $\mathbf{N}_{N_s,N_r} \in \mathbb{C}^{N_s \times N_r}$ the matrix of the noise which all elements $n_{i,m} \in \mathbf{N}_{N_s,N_r}$ are assumed i.i.d.

We can then write the received signal as

$$\mathbf{Y}_{N_s,N_r} = \mathbf{X}_{N_s,N_t}\mathbf{H}_{N_t,N_r} + \mathbf{N}_{N_s,N_r}. \tag{3.12}$$

The vector $\mathbf{Y}_{N_s,1}^{(m)}$ denotes a column of $\mathbf{Y}_{N_s,N_r}$ and represents the signal received on the mth receive antenna. Due to a question of simplicity, except if necessary, we will suppress the indexes.

3.2.2   Channel estimation

The received signal is distorted by the channel. In order to recover the transmitted bits, the channel effect must be estimated and compensated at the receiver [Cho+10]. A traditional way to achieve channel estimation is to use a preamble (training sequence) or pilot symbols known to both transmitter and receiver. Various estimation or interpolation techniques can then be employed to estimate the channel response. In our situation, we have a single narrow band transmission. Our goal is then to estimate the channel matrix $\mathbf{H}_{N_t,N_r}$.

Denoting the known training sequence by $\mathbf{T}$ and assuming Gaussian noise, the Maximum Likelihood (ML) estimate of the channel matrix is given by [BW03]:

$$\hat{\mathbf{H}}_{ML} = \underset{\mathbf{H}}{argmin}\|\mathbf{Y} - \sqrt{\frac{\rho}{N}}\mathbf{H}\mathbf{T}\|^2 = \sqrt{\frac{\rho}{N}}\mathbf{Y}\mathbf{T}^H(\mathbf{T}\mathbf{T}^H)^{-1}. \tag{3.13}$$

Where $(\cdot)^H$ denotes the Hermitian operator. The optimal training symbol sequence $\mathbf{T}$ that minimizes the channel estimation error should satisfy:

$$\mathbf{T}\mathbf{T}^H = T\mathbf{I}_{N_T}. \tag{3.14}$$

One way to generate such optimal training sequence is to use Hadamard matrices.

To solve the estimation problem in a tractable way, two main approaches can be used: the Least-Squares (LS) and Minimum-Mean-Square-Error (MMSE). Both techniques are widely used [Cho+10].

Least Squares Estimation

The Least Squares (LS) method gives the channel matrix estimate $\hat{\mathbf{H}}_{LS}$ that minimizes the Euclidean distance $\left\| \mathbf{TH} - \mathbf{Y}^{(m)'} \right\|_2$ [Hei+04]. Let us take the example of one receive antenna, two transmit antenna and one symbol. Then $\hat{\mathbf{H}}_{LS} \in \mathbb{C}^{2 \times 1}$. We have

$$\hat{\mathbf{H}}_{LS} = \underset{\mathbf{H}}{argmin} \left\| \mathbf{TH} - \mathbf{Y}^{(m)'} \right\|_2. \tag{3.15}$$

This problem can be solved taking the partial derivatives and finding the solution of the following system of equations:

$$\frac{\partial}{\partial \hat{\mathbf{H}}_{LS}} \left\| (\mathbf{T}\hat{\mathbf{H}}_{LS} - \mathbf{Y}^{(m)'}) \right\|_2 = 0. \tag{3.16}$$

This equation can be solved:

$$-2\mathbf{T}^H \mathbf{Y}^{(m)} + 2\mathbf{T}^H \mathbf{T}\hat{\mathbf{H}}_{LS} = 0 \Leftrightarrow 2\mathbf{T}^H \mathbf{T}\hat{\mathbf{H}}_{LS} = 2\mathbf{T}^H \mathbf{Y}^{(m)}, \tag{3.17}$$

which give the following solution:

$$\hat{\mathbf{H}}_{LS} = (\mathbf{T}^H \mathbf{T})^\dagger \mathbf{T}^H \mathbf{Y}^{(m)}. \tag{3.18}$$

where $(\cdot)^\dagger$ denotes the pseudo inverse.

3.2.3   Space-Time Coding and Diversity

Data to be transmitted can be considered as Space-Time Blocks. The benefit of MIMO can be dealt at the transmitter side, using precoding techniques or at the receiver side using some combining schemes. We present in the following some important techniques.

BLAST

Bell-Labs Layered Space Time (BLAST, see Fig. 3.2) is a high speed wireless communication scheme employing multiple antennas at both the transmitter and the receiver. The transmitted data are split equally into N_T transmitting antennas and then simultaneously sent to a channel overlapping in time and frequency. The signals are received by N_R receive antennas and signal processor at the receiver attempts to separate the received signals and recover the transmitted data [BW03].

BLAST may use two detection algorithms: Maximum Likelihood (ML) and Zero-Forcing (ZF). Its main drawbacks are: (1) it requires $N_T \leq N_R$; (2) the performance of the suboptimal BLAST decoding algorithms is limited by error propagation[BW03].
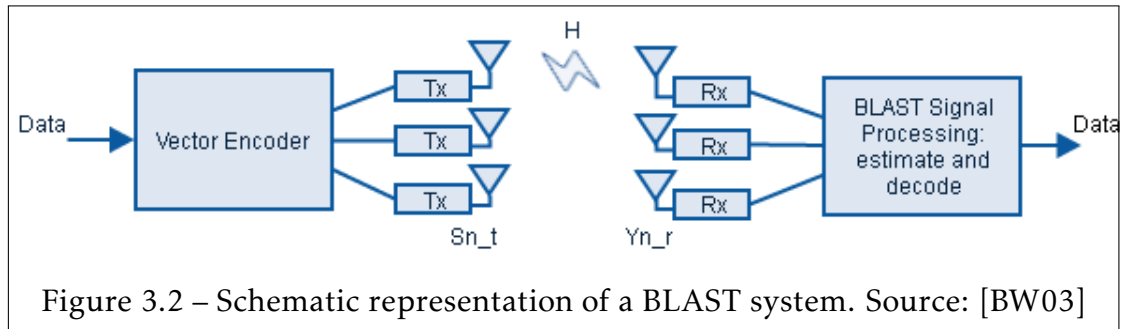
Figure 3.2 – Schematic representation of a BLAST system. Source: [BW03]

Maximal Ratio Combining

The technique was invented by American engineer Leonard R. Kahn in 1954. Maximum-Ratio Combining (MRC) is a method of diversity combining in which the signals from each channel are added together, the gain of each channel is made proportional to the square root of the received signal to noise power ratio. MRC is the optimum combiner for independent Additive White Gaussian Noise (AWGN) channels. The output Signal-to-Noise Ratio (SNR) of the linear combiner is given by:

$$z[n] = \sum_{k=1}^{N_R} \alpha_k y_k[n], \tag{3.19}$$

is maximize with the set of coefficients

$$\alpha_k = ch_k^*/\sigma_k^2, k = 1,..,N_R, \tag{3.20}$$

where c is an arbitrary constant.

Space-Time Block Codes

Instead of transmitting independent data streams as in BLAST, the idea of Space-Time Block Code (STBC) is to transmit the same information simultaneously from different transmit antennas to obtain diversity. Comparing with BLAST, STBC transmits less symbols [BW03] but reliability is increased. Because in IoT, rate is not a crucial parameter, STBC can make sense. A STBC is defined by a code matrix with orthogonal columns. Two main objectives of orthogonal space-time code design are to achieve the diversity order of $N_T N_R$ and to implement computationally efficient per-symbol detection at the receiver that achieves the ML performance [Cho+10; BFC05; Big+07; Hon10; OC07]. The output of the space-time block encoder is a codeword matrix $\mathcal{X}$ with dimension of $N_T \times N_s$ where N_s is the number of symbols of each block. Let $\mathbf{x}_i$ denote the ith row of the codeword matrix. Then $\mathbf{x}_i$ will be transmitted by the ith antenna over N_s symbols duration. The following property is required:

$$\mathbf{X}\mathbf{X}^H = c\|\mathbf{x}_i\|^2\mathbf{I}_{N_T}, \tag{3.21}$$

where c is constant. The above property implies that the row vectors of the codeword matrix $\mathcal{X}$ are orthogonal:

$$\mathbf{x}_i\mathbf{x}_j^H = \sum_{t=1}^{T} x_i^t(x_j^t)^* = 0, i \neq j, i, \in \{1, 2, N_s\}. \tag{3.22}$$

STBCs are a generalization of the Alamouti transmission scheme that will be detailed in section 3.4. We will use this specific scheme which is easy to implement at the transmitter side, allowing a robustness increase with only two transmit antennas and without the need of channel state information (at the

transmitter side).

Space-Time Trellis Codes

The main advantage of STBCs is that a maximum diversity gain can be achieved with a relatively simple linear-processing receiver. In general, however, the coding gain can be further improved with another type of Space Time Codes (STC), known as a Space-Time Trellis Code (STTC). The STTC encoder can be considered as a convolutional encoder with the memory size of v_k delay units for the kth branch for each output symbol. The Viterbi algorithm can be used for decoding the space-time trellis-coded systems [Cho+10; BFC05; Big+07; Hon10; OC07]. It provides full diversity and coding gain, but has high decoding complexity which grows exponentially with the number of antennas [BW03].

3.3   Receiver design

The linear detector is optimal in the presence of Gaussian noise. However it is no longer adequate under the presence of impulsive noise, presenting a significant loss of performance [LS95; LJL09]. This section gives an overview on receiver design, especially for environments with impulsive interference.

3.3.1   Optimal receiver

In communication, an optimal receiver can be seen as the one minimizing the BER $\mathbb{P}_e$ or, equivalently, to maximize the probability of successful transmission $\mathbb{P}_s$. Let:

- $\mathcal{X} = \{x_i\}_{i=1,\dots,N_s}$ be the set of symbols that can be transmitted,

- π_i be the probability that x_i was transmitted,

- N_s the number of source symbols,

- $\mathbb{P}_{e|i}$ is the probability that x_i was transmitted but not decoded

- $f(y|x_i)$ is the probability density function of the received signal y if x_i was transmitted

- Ω_i is the decision region associated to x_i and $\bar{\Omega}_i$ its complementary region. It means that if $y \in \Omega_i$ then the decision is $\hat{x} = x_i$.

The error probability can be written as

$$
\begin{aligned}
\mathbb{P}_e &= \sum_{i=1}^{N_s} \pi_i \mathbb{P}_{e|i} \\
&= \sum_{i=1}^{N_s} \pi_i \int_{\bar{\Omega}_i} f(y|x_i)\,dy
\end{aligned}
\tag{3.23}
$$

and the probability of success is

$$
\begin{aligned}
\mathbb{P}_s &= \sum_{i=1}^{N_s} \pi_i \mathbb{P}_{s|i} \\
&= \sum_{i=1}^{N_s} \pi_i \int_{\Omega_i} f(y|x_i)\,dy
\end{aligned}
\tag{3.24}
$$

The optimal receiver will consist in designing the decision regions Ω_i that minimize $\mathbb{P}_e$ or maximize $\mathbb{P}_s$. So we need to maximize $\sum_{i=1}^{N_s} \pi_i \int_{\Omega_i} f(y|x_i)$. We know that $\pi_i \int_{\Omega_i} f(y|x_i)\,dy \geq 0$ and that a point only belongs to one region. Consequently, the decision regions can be defined as

$$
\Omega_i = \left\{ y \,\middle|\, \pi_i f(y|x_i) > \pi_j f(y|x_j),\ \forall j \neq i \right\}
\tag{3.25}
$$

Finally, we can write the optimal decision, in terms of maximum success rate or minimum bit error rate

$$
\hat{x} = \operatorname*{argmax}_{x_i} \left\{ \pi_i f(y|x_i) \right\}
\tag{3.26}
$$

Maximum A Posteriori

This can be seen as the Maximum A Posteriori (MAP) receiver. Indeed, the *a posteriori* probability is given by

$$\mathbb{P}\left(x_i \middle| y\right) = \frac{\pi_i f\left(y \middle| x_i\right)}{f\left(y\right)}. \tag{3.27}$$

The MAP is given by (3.26)

Maximum Likelihood

The Maximum Likelihood (ML) receiver consists in maximizing the *a priori* probability $\mathbb{P}(y|x_i)$. It is clearly equivalent to the MAP approach if the transmitted symbols have the same probabilities ($\pi_i = \pi_j$, $\forall(i,j)$). The ML receiver is given by

$$\hat{x} = \underset{x_i}{\mathrm{argmax}}\left\{f\left(y \middle| x_i\right)\right\} \tag{3.28}$$

Receiver design

In most of the communication schemes, source symbols are equiprobable and the optimal receiver is then given by the ML detector. In the following we also assume that the channel is known. When y is a multidimensionnal vector (for instance the different replicas received on different antennas) and if we assume the noise realization to be uncorrelated in the different dimensions, the decoding rule is given by the solution to the following optimization problem:

$$\begin{aligned}
\widehat{x} &= \underset{x_i \in \mathcal{X}}{\mathrm{argmax}}\, f\left(y \middle| x_i; h\right) \\
&= \underset{x_i \in \mathcal{X}}{\mathrm{argmax}} \prod_{k=1}^{K} f\left(y_k \middle| x_i; h_k\right) \\
&= \underset{x_i \in \mathcal{X}}{\mathrm{argmax}} \sum_{k=1}^{K} \log\left(f\left(y_k \middle| x_i; h_k\right)\right),
\end{aligned} \tag{3.29}$$

where K is the number of dimensions of the received vector and the second equality assumes independent noise samples.

Calculating (3.29) requires the evaluation of the measure $f(y_k|x_i;h_k)$, where $y_k = h_k x_i + i_k + n_k$:

1. We first need to specify the representation of the interference, either by its characteristic function (CF) or its probability density function (PDF) when it exists in closed form. If the interference is known through its CF $\varphi_{i_k}(\omega) := \mathbb{E}\left[e^{i i_k \omega}\right]$, we have to evaluate its PDF

$$f_{i_k}(\zeta) = \frac{1}{2\pi} \int_{-\infty}^{\infty} \varphi_{i_k}(t) e^{-i\zeta t} dt, \ \ \forall k \in \{1, \dots, K\}. \tag{3.30}$$

2. We then need to calculate the PDF of the interference plus thermal noise $i_k + n_k$, via the convolution

$$f_{i_k+n_k}(\zeta) = \frac{1}{2\pi} \int_{-\infty}^{\infty} f_{n_k}(\tau) \int_{-\infty}^{\infty} \varphi_{i_k}(t) e^{-i(\zeta-\tau)t} dt d\tau,$$
$$\forall k \in \{1, \dots, K\}. \tag{3.31}$$

3. Finally, conditional on the channel state information, we need to find the likelihood as a function of s denoted by $f(y|x_i;h)$.

The description of the different steps allows to highlight the difficulties one can encounter when designing a receiver. Firstly, specifying the PDF of the interference can simply be *a priori* impossible because the transmission environment is not predictable. Besides, it is in some cases complex, especially for the popular heavy tailed interference models such as α-stable distributions. The following two points introduce some numerical complexity that can be prohibitive for real time implementation. All these steps challenge how one approaches receiver design.

3.3.2 Gaussian case

The Gaussian receiver is derived by assuming that $i_k + n_k$ is accurately modeled by a Gaussian random variable. In that case the PDF of $y_k = h_k x_i + i_k + n_k$, given x_i and h_k, is complex Gaussian, centred with mean $h_k x_i$ and variance σ_k^2:

$$f(y_k | x_i; h_k) = \frac{1}{\sqrt{2\pi\sigma_k^2}} \exp\left(-\frac{|y_k - h_k x_i|^2}{2\sigma_k^2}\right). \tag{3.32}$$

Taking the log, we have

$$\log(f(y_k | x_i; h_k)) = \log\left(\frac{1}{\sqrt{2\pi\sigma_k^2}}\right) - \left(\frac{|y_k - h_k x_i|^2}{2\sigma_k^2}\right). \tag{3.33}$$

The decision rule in (3.29) can consequently be expressed as

$$\widehat{x} = \underset{x_i \in \mathcal{X}}{\operatorname{argmax}} \sum_{k=1}^{K} \left(\log\left(\frac{1}{\sqrt{2\pi\sigma_k^2}}\right) - \left(\frac{|y_k - h_k x_i|^2}{2\sigma_k^2}\right)\right) = \underset{x_i \in \mathcal{X}}{\operatorname{argmin}} \sum_{k=1}^{K} \left(\frac{|y_k - h_k x_i|^2}{2\sigma_k^2}\right).$$

In the case where $i_k + n_k$ is identically distributed in the different dimensions of the received vector, we have $\sigma_k = \sigma$, $\forall k \in \{1, ..., K\}$ and the final decision can be summarized by

$$\widehat{x} = \underset{x_i \in \mathcal{X}}{\operatorname{argmin}} \sum_{k=1}^{K} |y_k - h_k x_i|^2 = \underset{x_i \in \mathcal{X}}{\operatorname{argmin}} \|y - h x_i\|_2^2,$$

where $\|.\|_2$ denotes the Euclidean distance.

The first thing to be noticed is that the ML receiver is equivalent to minimizing the Euclidean distance between the received symbol and the possible transmitted ones (after crossing the channel). Then we can further develop

(3.34):

$$\widehat{x} = \underset{x_i \in \mathcal{X}}{\operatorname{argmin}} \sum_{k=1}^{K} |y_k - h_k x_i|^2 = \underset{x_i \in \mathcal{X}}{\operatorname{argmin}} \sum_{k=1}^{K} \left(|y_k|^2 - h_k^* x_i^* y_k - h_k x_i y_k^* + |h_k x_i|^2 \right)$$

$$= \underset{x_i \in \mathcal{X}}{\operatorname{argmin}} \left(-2 \sum_{k=1}^{K} \mathcal{R} \left(h_k^* x_i^* y_k \right) + \sum_{k=1}^{K} |h_k x_i|^2 \right),$$

where $\mathcal{R}(.)$ denotes the real part. What is important to notice in (3.34) is that the operation to be executed on the received signal y is a linear function. The optimal receiver in Gaussian noise is linear which makes it simple to implement and so attractive.

Finally, if the x_i have the same energy ($|x_i|^2 = E_x$, $\forall x_i \in \mathcal{X}$), the decision rule can be further simplified:

$$\widehat{x} = \underset{x_i \in \mathcal{X}}{\operatorname{argmin}} \left(-2 \sum_{k=1}^{K} \mathcal{R} \left(h_k^* x_i^* y_k \right) + E_x \sum_{k=1}^{K} |h_k|^2 \right) = \underset{x_i \in \mathcal{X}}{\operatorname{argmax}} \left(\mathcal{R} \left(x_i^* \sum_{k=1}^{K} h_k^* y_k \right) \right),$$

This last operation $\sum_{k=1}^{K} h_k^* y_k$ is called Maximum Ratio Combining MRC. It is shown that this operation is the way to combine the received symbols that maximizes the signal to noise ratio before the decision step.

3.3.3 Impulsive case

It has been shown that the Gaussian detector gives poor performance compared to the optimal one when noise is impulsive [Yan15; LS95; Cla+10]. The second observation is the difficulty in developing an optimal receiver. One reason is the variety of proposed interference models: which model should I design my receiver for and how will it perform if my environment changes? If empirical models, chosen to offer analytic solutions, are attractive, their ability to adapt to different contexts is to be proven. Another reason is that implementing a receiver can be complex for some specific interference distributions, for instance with the infinite series from Middleton's model, stochastic geometry or the absence of closed-form α-stable PDF. Consequently several sub-optimal receiving strategies

Figure 3.3 – Realization examples for different noise processes. The following parameters were used in each case: Gaussian case ($\mu = 0$ and $\sigma^2 = 0.2$); α-stable ($\alpha = 1.5$, $\gamma = 0.1$); ϵ-contaminated case ($\epsilon = 0.01$, $N_s = 100$, $\sigma^2 = 0.2$); sum of Gaussian and α-stable in a moderately impulsive case ($\alpha = 1.5$, $\gamma = 0.1$ and $\sigma^2 = 0.2$ ($NIR = 0$)).
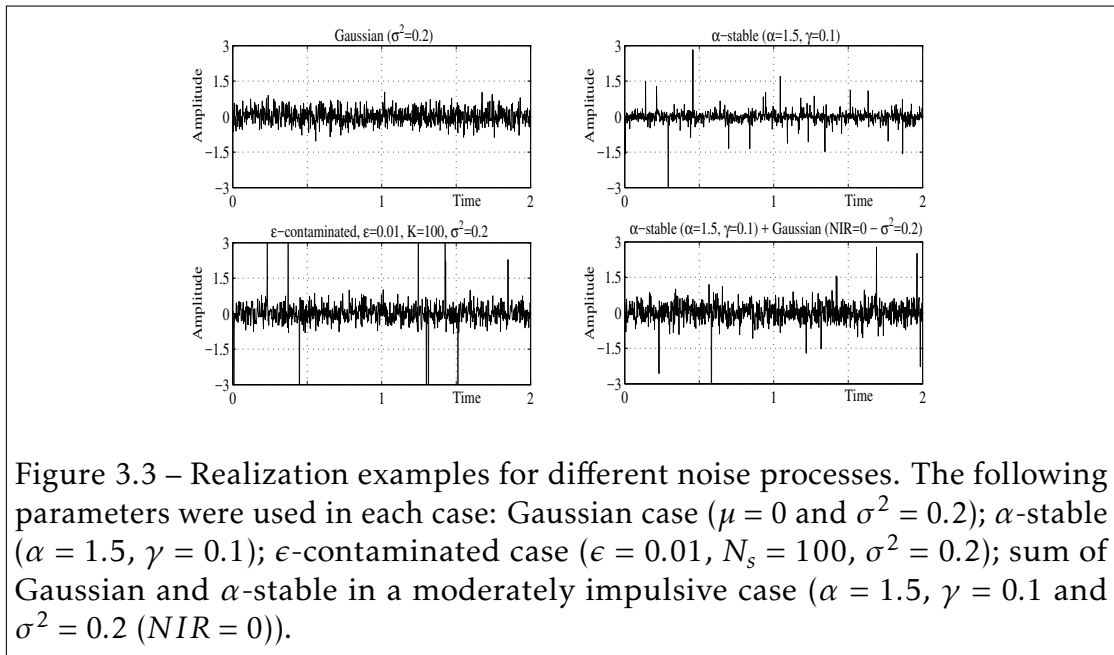
have been developed to improve performance in non Gaussian situations.

Impact of impulsiveness on the optimal decision

An efficient way to characterize and understand the influence of impulsive noise is to visualize the impact of the non linearities by representing the decision regions. This was proposed by Saaifan and Henkel [SH12] for the Middleton class A case and by Shehat *et al.* [SME10] and by Saleh *et al.* [SME12] for the α-stable case.

We represent in Fig. 3.3 four different examples of noise realizations. Then we show in Fig. 3.4 the decision regions that the optimal receiver must produce in a binary case under each of the different models, i.e., the regions that maximize the probability of having transmitted s when $y = (y_1, y_2)$ is received.

It is well known that the optimal decision regions are linearly separated under interference with exponential tail decay, such as the Gaussian case shown in Fig. 3.4. However, the optimal decision regions under heavy tailed interference produce non-linear frontiers and disjoint regions, as seen with the α-stable noise. We can identify two operating regions: for small received values y_1, y_2, boundaries are linear. However, when at least one value becomes larger, linear

Figure 3.4 – Optimal decision regions for the different noise processes. We follow the framework proposed in [SME12] and use the same parameters defined in Fig. 3.3: the received vector $\mathbf{Y}$ is composed of two received samples (two dimensions, $\mathbf{Y} = [y_1 \ y_2]$), the wireless channel is set to $\mathbf{h} = [1 \ 1]$, and we consider two possible transmitted values (ie. $\Omega = \{-1, 1\}$). The areas in black correspond to a decision $\hat{s} = +1$, the areas in white to $\hat{s} = -1$.

boundaries completely fail to recover the most likely transmitted symbol. In the ϵ-contaminated case, we see that for large values, the exponential tails makes the decision boundary become linear again. However, the impulses generated by the rare but large variance Gaussian component in the noise distribution create a non linear area; very similar to the α-stable case. Finally, in the α-stable and Gaussian mixture, the heavy-tailed interference noise dominates the light tailed Gaussian thermal noise in extremes and dictates the extent of the non linearity in the decision boundaries, considerably increasing the complexity of the optimal receiver design.

Receivers

In the following we do not try to be exhaustive about the existing receiver strategies but we propose to classify the different receiver design approaches into three categories, see Table 3.1. We will then describe some of them.

Receiver Strategies	
Type of receiver	*Examples*
Linear	Linear combiner [Joh96; NB09; NB10; CE13]
Noise distribution approximation	Gaussian mixture [ECD08], ϵ-contaminated [Nam+06], Generalized Gaussian [FH06], mixture of Laplacian and Gaussian [BN10], Cauchy [Cla+10], Myriad [GA01; NB08; SME12], NIG[Gu+12]
LLR inspired	Soft limiter and Hole puncher [LS95; AIH94; TNS95; SME12; Maa+13], p-norm [GC12], LLR approximation [Dim+14], approximation of $f'_{I+N}(.)/f_{I+N}(.)$ [SM77a; SM77b; ZBA06]

Table 3.1 – Receiver strategies discussed in this paper.

Linear approaches : if the MRC is optimal in Gaussian noise, it is known to perform poorly in impulsive situations [Yan15; LS95; Cla+10]. Johnson [Joh96] proposes a general study of linear optimal receivers in non Gaussian noise and takes the specific example of α-stable noise. This is further studied for a rake receiver in [NB09; NB10] and for diversity combining schemes in a multi-antenna receiver in [CE13] in presence of symmetric α-stable interference. A

linear combiner can in general be written as

$$z = \sum_{k=1}^{K} w_k y_k \tag{3.34}$$

where $\mathbf{w} = \{w_k\}_{k=1}^{K} \in \mathbb{R}^K$ are the combiner weights. The conventional MRC leads to $w_k = h_k^*$ and is optimal for independent Gaussian channels. When SαS noise is present, the optimal weights are given by

$$\begin{cases} w_k = \text{sign}(y_k)|y_k|^{\frac{1}{\alpha-1}} & \text{if } 1 < \alpha \leq 2 \\ w_j = \text{sign}(y_j) \text{ and } w_k = 0 \ \forall k \neq j \text{ and } j = \underset{k}{\text{argmax}}|h_k| & \text{if } 0 < \alpha \leq 1 \end{cases} \tag{3.35}$$

Noise distribution approximation : When the optimal receiver is complex to design, a solution is to find a distribution that approximates well the true noise plus interference PDF $f_{i_k+n_k}(.)$ (whatever the dominant noise term), having an analytical expression and parameters that can be simply estimated. Erseghe *et al.* used a Gaussian mixture for UWB communications [ECD08]. In [Nam+06], the ϵ-contaminated is used to study the impact of impulsive noise on Parity Check Codes. The importance to take the real noise model into account during the decoding is underlined. A review in the UWB case can be found in [BY09]. For instance Fiorina [FH06] proposed a receiver based on a generalized Gaussian distribution approximation. Beaulieu and Niranjayan [BN10] considered a mixture of Laplacian and Gaussian noise. The Cauchy model is proposed in [Cla+10]. Each solution is shown to significantly improve the performance in their specific context. We can wonder how robust they will be in case of a model mismatch. We can give a few solutions that use such an approach:

- **Generalized Gaussian Model (GGM)**: a Generalized Gaussian is used to model the noise plus interference. In that case the likelihood can be given in closed form. In the binary case, the log likelihood ratio is given by [NB08]:

$$\Lambda = \sum_{i=1}^{N_s} |\gamma_{i,b} + s|^\alpha / \varsigma^\alpha - \sum_{i=1}^{N_s} |\gamma_{i,b} - s|^\alpha / \varsigma^\alpha \tag{3.36}$$

and its sign gives the transmitted bit.

- **Normal Inverse Gaussian (NIG) approximation**: The NIG distributions have analytical expressions for the PDF and their parameters can be estimated by the Method of Moments using four moments. Gaussian and Cauchy distributions are special limiting cases. This solution was proposed in [Gu12; Gu+12; GC12]. The density function is given by

$$f_{NIG}(y; \alpha, \beta, \mu, \delta) = \frac{\alpha \delta}{\pi} \frac{\exp[g(y)]}{h(y)} K_1[\alpha(y)] \qquad (3.37)$$

where $g(y) = \delta\sqrt{\alpha^2 - \beta^2} + \beta(y - \mu)$ and $h(y) = [(y - \mu)^2 + \delta^2]^{1/2}$, $K_1(\cdot)$ is a modified second kind Bessel function with index 1. The parameter α is inversely related to the heaviness, i.e., where small values of α corresponds to heavy tails, the skewness is controlled by β ($0 \leq |\beta| \leq \alpha$)and $\beta = 0$ indicates the skewness. μ ($\mu \in \mathbb{R}$) and δ ($\delta > 0$) represents, respectively, the location and scale parameters. Considering a symmetric case ($\beta = 0$), the mean, variance, skewness and kurtosis of NIG model are given, respectively, by

$$\mathbb{E}[y_k] = \mu \qquad (3.38)$$

$$\mathbb{V}ar[y_k] = \frac{\delta}{\alpha} \qquad (3.39)$$

$$\mathbb{S}kew[y_k] = 0 \qquad (3.40)$$

$$\mathbb{K}[y_k] = \frac{3}{\delta\alpha} \qquad (3.41)$$

These equations allow to estimate the model parameters and the receiver can be implemented.

- **Cauchy and Myriad Detector** In general, α-stable random variables do not have a closed form PDF. However, such a closed form exist for $\alpha = 1$, which corresponds to a Cauchy distribution,

$$f(y) = \frac{\gamma}{\pi} \frac{1}{\gamma^2 + (y)^2} \qquad (3.42)$$

If we make this assumption, we can design the Cauchy detector [SME12;

Gu+12; GC12; Gu12]:

$$\prod_{k=1}^{K}[\xi^2 + (\gamma_{i,b} + s)^2] - \prod_{i=1}^{N_s}[\xi^2 + (\gamma_{i,b} - s)^2] \tag{3.43}$$

In the binary case and taking the log, we can express the Log-Likelihood Ratio (LLR):

$$\Lambda_{Cauchy} = \sum_{k=1}^{N} log\left\{\frac{\gamma^2 + [y_k + h_k]^2}{\gamma^2 + [y(k) - h_k]^2}\right\} \tag{3.44}$$

Several works have proposed to improve the Cauchy receiver to the case of $1 < \alpha \le 2$ or to the sum of an α-stable noise and a Gaussian noise. Instead of using γ, a term κ is used to adapt the Myriad filter to get near-optimal performance [SME12].

The Myriad detector is given by [NB08]:

$$\prod_{i=1}^{N_s}[K^2 + (\gamma_{i,b} + s)^2] - \prod_{i=1}^{N_s}[K^2 + (\gamma_{i,b} - s)^2] \tag{3.45}$$

And in the binary case:

$$\Lambda_{Myriad} = \sum_{k=1}^{N} log\left\{\frac{\kappa^2 + [y(k) + s_1(k)]^2}{\kappa^2 + [y(k) - s_0(k)]^2}\right\} \tag{3.46}$$

The choice of κ depends on the noise conditions. When $\alpha = 2$ the Myriad reaches optimal efficiency for $\kappa = \infty$. For $\alpha = 1$, the optmality is obtained for $\kappa = \gamma$ and for $\alpha \to 0$, the optimality is reached when $\kappa = 0$. Let α, γ the characteristic exponent and dispersion parameter, respectively, of a SαS distribution. An optimal tuning value of κ, $\kappa_0(\alpha, \gamma)$ that minimizes a performance criterion (usually variance) is given by [GA01]:

$$\kappa_0(\alpha, \gamma) = \kappa_0(\alpha, 1)\gamma^{1/\alpha} \tag{3.47}$$

Another choice for κ_0 can be given also by the following empirical formula

[GA01; NB08]:

$$\kappa(\alpha) = \sqrt{\frac{\alpha}{2-\alpha}} \gamma^{1/\alpha} \qquad (3.48)$$

For a detailed discussion on the optimality of the Myriad filter in the α-stable model see [GA01; Nas+12; ND07].

- It is also possible to use approximation of the PDF. In the α-stable case for instance, [ND07] suggests the use of an approximation proposed by Kuruoglu:

$$f_{\alpha,0,\gamma,\mu}(z) = \frac{\sum_{i=1}^{N} 2e^{-\frac{(z-\mu)^2}{2\gamma v_i^2}} f_Y(v_i^2)}{\sum_{i=1}^{N} f_Y(v_i^2)} \qquad (3.49)$$

- **Algebraic-tailed Zero-Memory Non Linearity (AZMNL)** Another possible approximation can be obtained using the properties of the α-stable PDF [LJL09]. The standard SαS density function can be represented by series expansion:

$$f_\alpha(x) = \frac{1}{\pi\alpha} \sum_{k=0}^{\infty} \frac{(-1)^k}{2k!} \Gamma\left(\frac{2k+1}{\alpha}\right) x^{2k}. \qquad (3.50)$$

For $1 < \alpha < 2$, we have, near $x = 0$:

$$f_\alpha(x) \approx \frac{1}{\pi\alpha}\left(\Gamma(1/\alpha) - \frac{\Gamma\left(\frac{3}{\alpha}\right)}{2} x^2\right) \qquad (3.51)$$

and the derivative is given by

$$f'_\alpha(x) \approx \frac{\Gamma(3/\alpha)x}{\pi\alpha}. \qquad (3.52)$$

Then, the PDF in the vicinity of $x = 0$ can be approximated by

$$g(x;\alpha) \approx \frac{\Gamma(3/\alpha)}{\Gamma(1/\alpha)} x \qquad (3.53)$$

i.e., a linear function with slope $\frac{\Gamma(3/\alpha)}{\Gamma(1/\alpha)}$. For large values, we consider the

tail property

$$\mathbb{P}(x > \lambda) \approx \sigma^\alpha \frac{C_\alpha}{2} \lambda^{-\alpha} \tag{3.54}$$

as $\lambda \to \infty$ and $1 < \alpha < 2$, where

$$C_\alpha = \frac{1 - \alpha}{\Gamma(2 - \alpha)\cos(\pi\alpha/2)}. \tag{3.55}$$

The approximation for large values of x can then be

$$g(x|x \to \infty, \alpha) = \frac{\alpha + 1}{x}. \tag{3.56}$$

This indicates that the α-stable distribution has an algebraic tail as $(\alpha+1)/x$. The AZMNL is finally

$$g(x) = \begin{cases} \frac{K(\alpha)}{x} & \text{if } |x| > \tau \\ kx & \text{if } |x| \le \tau \end{cases} \tag{3.57}$$

where $k = \Gamma(3/\alpha)/\Gamma(1/\alpha), \tau = \sqrt{K(\alpha)/k}$ and $K(\alpha)$ is a polynomial expression on α, which near-optimum value can be obtained through the Mean Square Error (MSE) criterion

$$MSE(K(\alpha)) = \int_{\mathbb{R}} \left(\frac{-f'_{\alpha,\sigma}(x)}{f_{\alpha,\sigma}(x)} - g(x) \right) f_{\alpha,\sigma}(x) dx \tag{3.58}$$

LLR inspired solutions   When we consider the binary case and when noise is impulsive, the optimal LLR, $\Lambda = \log \frac{f(y|x_i=1,h)}{f(y|x_i=-1,h)}$, tends to reduce the weight of large values in the decision, when in the Gaussian case the resulting linear function always increases whan the received value increases. It means that we should not trust large positive or negative received values, contrary to the decision weight that the linear receiver would attribute. This is illustrated in Fig. 3.5, which represents the LLR as a function of the received value for the four previously described noise settings. Except for the Gaussian noise whose LLR is a linear function, the three other cases reaches a maximum and then decrease and tends towards 0. We notice the strong resemblance between the
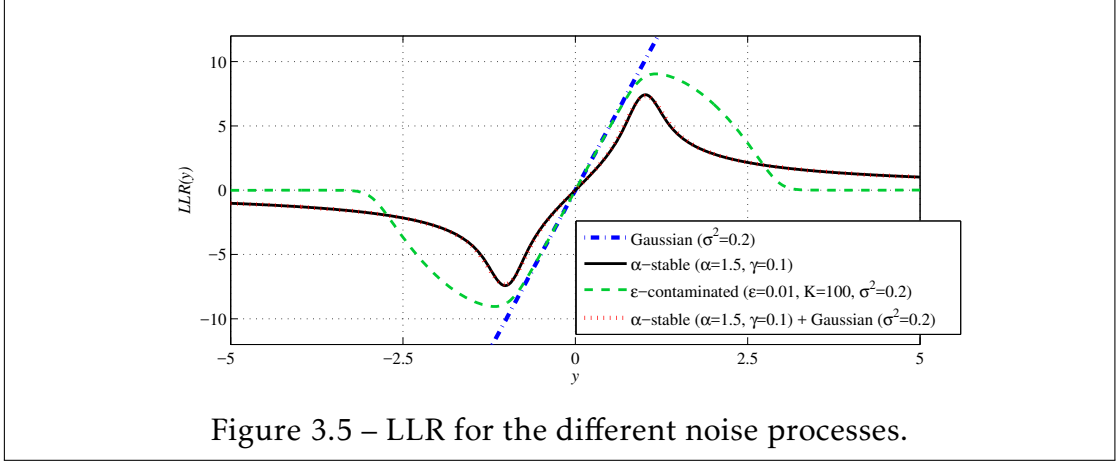
Figure 3.5 – LLR for the different noise processes.

pure α-stable and the mixture with the Gaussian noise, curves being nearly superposed.

This idea leads to a modification of the LLR function. The received signal is modified by this function and the decision is made through a classical linear approach. Classical examples are the soft limiter and the hole puncher [LS95; AIH94; TNS95; SME12; Maa+13].

- **Soft Limiter** Small values are transformed through a linear operation and larger values are clipped:

$$g(y_k) = \begin{cases} -b & \text{if } y_k < -b \\ ay_k & \text{if } |y_k| \le \frac{b}{a} \\ b & \text{if } y_k > b \end{cases} \tag{3.59}$$

- **Hole Puncher** Similarly to the soft limiter, small values are transformed through a linear operation but larger values are set to 0 [ND07; Gu+12]:

$$g(y_k) = \begin{cases} 0 & \text{if } |y_k| > b \\ ay_k & \text{if } |y_k| \le \frac{b}{a} \end{cases} \tag{3.60}$$

- Another approximation is given by:

$$f(y_k) = \text{sign}(y_k) \min\left(a|y_k|, \frac{b}{|y_k|}\right) \tag{3.61}$$

where $\text{sign}(x)$ is the sign of x. It was proposed in [Dim+14] for Low Density Parity Check codes. The model fits the linear part of the LLR for small values of x and the $1/x$ approximation is inspired from the limit of the likelihood ratio for high values of x in the α-stable case. Parameters a and b are estimated with different methods. Good results are obtained in α-stable and Middleton class A interference. This can be further improved using $f(y_k) = \text{sign}(y_k) \min\left(a|y_k|, \frac{b}{|y_k|}, c\right)$ which however gives one further parameter to estimate.

- Some more solutions exist, always giving a linear approximation for small values and a $1/x$ approximation for larger values. For instance:

$$f(y_k) = \frac{y_k}{a + by_k^2} \tag{3.62}$$

3.3.4   Comparison Between the Receivers

It as been shown, for instance in [GC12; Gu+12; Gu12; ND07], that the linear receiver and MRC has good performance only when the Gaussian noise is dominant.

The Hole-Puncher and Soft-Limiter are good choices if the thresholds are well configured but they are still far from optimality under strong impulsive noise. This is for instance shown in [SME12] and a better non-linearity is obtained by approximating the PDF by a finite Gaussian mixture, at the expanse of an increased complexity.

The Cauchy detector is optimum for $\alpha = 1$ and can be used as a suboptimal detector for any value of α, outperforming the Gaussian detector as soon as some impulsiveness is present, but remains however more complex to implement. The Myriad filter has similar complexity but improved performance when α gets closer to 2 or when a non negligible thermal noise is present [SME12]. The NIG

approximation presents very good performance in most of the environments and is generally very close to the optimal receiver when impulsiveness increases.

[ND07] also investigates methods to mitigate α-stable interference. We did not discuss in this section the p-norm receiver. This approach could be introduced by approximating the noise density with a Generalized Gaussian distribution. It could also be seen as an approximation of the LLR function with $g(x) = \|x\|_p$. As we will see, it can also be seen as a modified version of distance calculation. We selected this approach because it is efficient in both impulsive and Gaussian situations and also because it is reduced to a single parameter p that can be efficiently estimated.

3.4   A MIMO transceiver robust against SαS noise.

We now propose a transmission scheme with spatial diversity and a receiver strategy adapted to impulsive noise but also able to well behave in traditional Gaussian noise. For the transmission, we add a second antenna. If it slightly increases the cost of the end device it will also allow a significant increase in robustness. We choose an Alamouti scheme for transmission because it does not require any channel state information at the transmitter side but allows to benefit from the spatial diversity. At the receiver side, we can either have two antennas or more if the receiver is the gateway, less constraint both in cost and energy. To face impulsive noise we adapt the channel estimation and the decision strategy.

3.4.1   System model

The proposed system is shown in Fig. 3.6. It is composed by

- a Quadrature Phase Shift Keying (QPSK) modulator,

- an Alamouti encoder,

- 2 transmitting antennas

- N_r receiving antennas,

- QPSK demodulator,

- a channel estimator and

- a decision block, including a parameter estimation step.
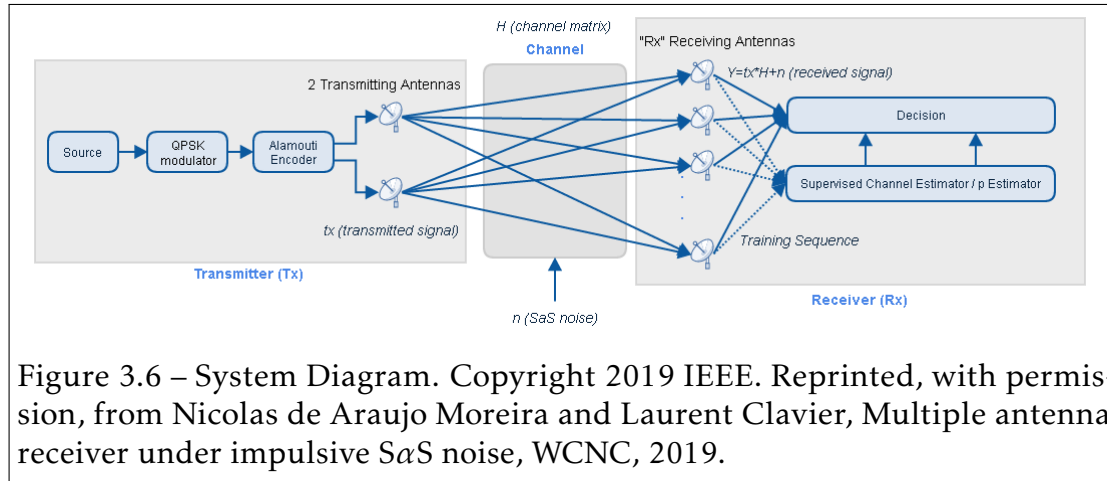
Figure 3.6 – System Diagram. Copyright 2019 IEEE. Reprinted, with permission, from Nicolas de Araujo Moreira and Laurent Clavier, Multiple antenna receiver under impulsive SαS noise, WCNC, 2019.

The general model was presented in section 3.2.1, but we now consider the Alamouti coding. It means that we have two transmitting antennas ($N_t = 2$) and N_r receiver antennas. Let's recall that we denote by s a symbol defined on the discrete support $\mathcal{S} = \{s_k\}_{k \in \{1,2,3,4\}}$. All possible transmitted symbols that are equiprobable, i.e. $\mathbb{P}_{s_i} = \mathbb{P}_{s_j}$, $\forall (i,j) \in \{1,2,3,4\}^2$, $i \neq j$.

$\mathbf{X}_{N_s,2} \in \mathbb{C}^{N_s \times 2}$ denotes the matrix of all transmitted symbols in a given packet. The channel is represented by $\mathbf{H}_{2,N_r}$, with $\mathbf{H}_{2,N_r} \in \mathbb{C}^{2 \times N_r}$. Finally, denoting $\mathbf{N}_{N_s,N_r} \in \mathbb{C}^{N_s \times N_r}$ the matrix of symmetric α-stable noise, which all elements $n_{i,m} \in \mathbf{N}_{N_s,N_r}$ are assumed I.I.D., then, the received signal is given by:

$$\mathbf{Y}_{N_s,N_r} = \mathbf{X}_{N_s,2}\mathbf{H}_{2,N_r} + \mathbf{N}_{N_s,N_r} \tag{3.63}$$

We consider the case where $\mathbf{N}_{N_s,N_r}$ is an I.I.D. random vector. Each marginal is a complex symetric α-stable random variable with independant real and imaginary part.

3.4.2 Alamouti coding

The Alamouti coding is a particular STBC. It is a simple two-branch diversity transmit scheme that uses $N_T = 2$ transmitting antennas and N_R receiving antennas [M A98; BW03; Big+07]. The Alamouti coding is effective in all of the applications where the system capacity is limited by the multipath fading [M A98].

The Alamouti Scheme is defined by three functions:

1. encoding and transmission sequence of symbols at transmitter,

2. combining scheme and

3. the decision rule for (ML) detection.

Advantages

The Alamouti scheme improves the signal quality at the receiver by processing the signal across the two transmitting antennas, improving the error performance. It does not require bandwidth expansion nor any feedback from the receiver to the transmitter, including channel state knowledge [OC07]. The Alamouti coding is cost-effective and presents quality and efficiency without a complete redesign of existing systems.

Transmission sequence and encoding

The Alamouti coding requires two transmitting antennas, which simultaneously transmit two different symbols. We denote by T a symbol period, $s_i \in \mathbb{C}$ the complex symbol transmitted from antenna 0 and $s_j \in \mathbb{C}$ the complex symbol transmitted from antenna 1 during a given symbol period $[t, t + T]$. During the next symbol period starting at $t + T$, antenna 0 transmits $-s_j^*$ and antenna 1 transmits s_i^*, where $(\cdot)^*$ denotes the complex conjugate operation. So, during a time interval $2T$, the transmission sequence is given by the codeword matrix $\mathbf{C}_{Ala} \in \mathcal{C}$, where $\mathcal{C}$ is the set of all possibilities for the codeword matrix:

$$\mathbf{C}_{Ala} = \begin{bmatrix} s_i & -s_j^* \\ s_j & s_i^* \end{bmatrix} \tag{3.64}$$

where the first and second column represent times starting at t and at $t + T$, respectively and the first and second rows represent the symbols transmitted over antennas 0 and 1, respectively, with $s_k \in S$.

Is important to observe that Alamouti codeword $\mathbf{C}_{Ala}$ is a complex orthogonal matrix [Cho+10; Hon10]:

$$\mathbf{C}_{Ala}\mathbf{C}_{Ala}^H = \begin{bmatrix} |s_i|^2 + |s_j|^2 & 0 \\ 0 & |s_i|^2 + |s_j|^2 \end{bmatrix} = (|s_i|^2 + |s_j|^2)\mathbf{I}_2 \qquad (3.65)$$

where $\mathbf{I}_2$ denotes the 2×2 identity matrix.

Fig. 3.7 shows a schematic of Alamouti coding from the point of view of transmitter.
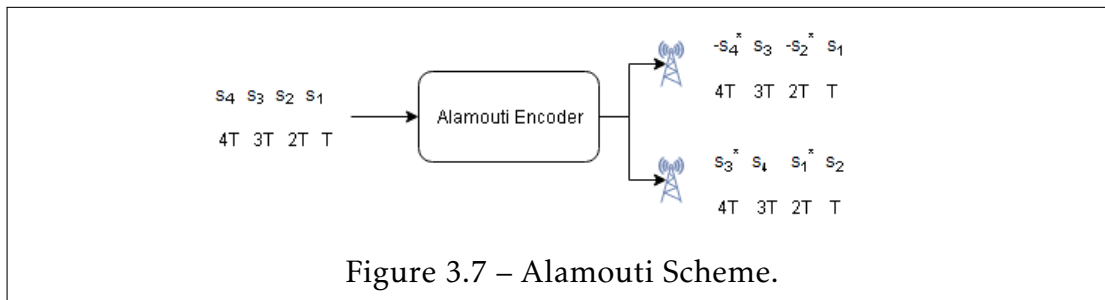
Figure 3.7 – Alamouti Scheme.

Additional information

Further basic information on Alamouti coding can be found also in [GS05; Hon10; Gui06]. [KZ10] presents also the application of Alamouti coding for UWB systems. [Hut+05] studies the perfomance of Alamouti-based space-frequency coding for OFDM systems. [SPV13] discusses the design of Alamouti scheme for MIMO receiver embedded on a Field Programmable Gate Array (FPGA).

3.4.3 Channel estimation algorithms

Let's denote $\mathbf{T}_{L,2}$ a training sequence, known at the receiver, where L denotes its length and which is transmitted through the unknown channel $\mathbf{H}_{2,N_r}$ under the

presence of a complex symmetric α-stable noise $\mathbf{N}_{L,N_r}$ as previously described. The received signal at the m-th antenna is denoted by the column-vector $\mathbf{Y}_{L,1}^m$. From now on, we will omit the dimensions of matrices for a question of simplicity. The objective of the estimator is to find the estimated channel matrix $\hat{\mathbf{H}} \approx \mathbf{H}$.

Channel estimation under SαS noise

Although it is very suitable under Gaussian assumption, LS is no longer appropriate under the presence of impulsive noise due to its lack of robustness against outliers in the data set. In other words, it means that for extreme events, its performance deteriorates significantly [LS95].

The authors in [PC13] study the channel estimation in environments that exhibit sparse, time-varying impulse responses and impulsive noise with SαS statistics. They design online adaptive algorithms that exploit channel sparseness and achieve robust performance:

- Recursive Least-Squares (RLS) type algorithms based on differentiable cost function that combines robust nonlinear methods with sparse-prompting L_0 norm regularization;

- Natural Gradient (NG) incorporating nonlinear methods for channel prediction error as well the L_0 norm of the channel taps.

The performance of both approaches are compared with conventional robust algorithms, such as Recursive Least M-Estimate (RLM) and Recursive Least p-norm algorithm (RLP). The paper shows that RLM is not robust under specific SαS noise conditions and demonstrates the superiority of the NG-type algorithms over the RLS-type ones, once NG-type filters use the Riemannian distance [1] to modify the gradient search direction for faster adaptation.

Least Absolute Deviation

The Least Absolute Deviation (LAD) estimation tries to find $\hat{\mathbf{H}}_{LAD} \in \mathbb{C}^{2\times 1}$ that minimizes the L1-norm loss function below [LA04] which can be solved using

---

[1]the length of a curve in the riemmanian manifold between two points having the minimum length (geodesic)

classical linear programming techniques:

$$\hat{\mathbf{H}}_{LAD} = \underset{\mathbf{H}}{\operatorname{argmin}} \sum_{i=1}^{N_s} \left| y_i - \sum_{r=1}^{2} t_{ir} h_{rj} \right|$$
(3.66)

$\forall i, j, 1 \le i \le L, 1 \le j \le M$, with $y_i \in \mathbf{Y}^{(\mathbf{m})'}, t_{ir} \in \mathbf{T}$.

The algorithm for finding $\hat{\mathbf{H}}_{LAD}$ is shown in Algorithm 2. Its a recursive algorithm, where $\mathbf{H}_{old}$ denotes the channel matrix found on previous iteration and starts with a null matrix and $\mathbf{H}_{old}$ denotes the channel matrix found on the current iteration and is initialized with a N_r by N_t matrix with all entries equal to 0.5. The stop criteria is based on an arbitrary threshold for the different between previous and current channel matrix and an arbitrary number of iterations. Obviously, the criteria for choosing them is based on time for computing and precision. These procedures of finding $\hat{\mathbf{H}}$ are repeated for each receiving antenna for both estimators.

Algorithm 2 Optimization algorithm for LAD Estimation.

  begin EstimationLAD($\mathbf{Y}, \mathbf{X}, N_r, N_t, L$)

  $\mathbf{H} \leftarrow 0.5 \mathbf{1}_{N_r N_t}$;

  $\mathbf{H}_{old} \leftarrow \mathbf{0}_{N_r N_t}$;

  $\mathbf{H}_{new} \leftarrow \mathbf{H}$;

  $\mathbf{W} \leftarrow \mathbf{X}$;

  $i \leftarrow 0$;

  while $max|h_{new} - h_{old}| > threshold$ and $i < max\_iterations$ **do**

    $\mathbf{H}_{old} \leftarrow \mathbf{H}_{new}$

    $\mathbf{H}_{new} \leftarrow [(\mathbf{W}^H \mathbf{X})(\mathbf{W}^H \mathbf{Y})]^\dagger$

    $\mathbf{W} \leftarrow \text{MATDIV}(\mathbf{X}, |\mathbf{Y} - \mathbf{X}\mathbf{H}_{new}|^p)$

    $i \leftarrow i + 1$;

  end while

  return $\mathbf{H}_{new}$

3.4.4 Decision strategy.

Classical approach

Assuming block fading channel, i.e., the channel remains constant over a packet and more specifically over two successive symbol periods from t to $t + 2T$, i.e., we denote $h_{i,m}(t) = h_{i,m}(t + T) = |h_{i,m}|e^{j\theta_{i,m}}$, where $\theta_{i,m}$ denotes the phase rotation with $i = 1, 2$ and $m = 1, 2, ..., N_R$. Assuming $N_T = 2$ transmitting antennas and N_R receiving antennas, the received signals for the m-th receiver antenna is given by

$$\begin{cases} r_m = h_{0,m}s_i + h_{1,m}s_j + n_{0,m} & \text{at } [t, t + T] \\ r_m = -h_{0,m}s_j^* + h_{1,m}s_i^* + n_{1,m} & \text{at } [t + T, t + 2T]. \end{cases} \tag{3.67}$$

The Alamouti receiver is composed by a combining scheme and a decision rule. For (ML) detection, the combiner generates the following signals:

$$\begin{aligned} \tilde{s}_i &= h_{0,m}^* r_0 + h_{1,m} r_1^* \\ \tilde{s}_j &= h_{1,m}^* r_0 - h_{0,m} r_1^*. \end{aligned} \tag{3.68}$$

Applying (3.67) in (3.68) we have

$$\begin{aligned} \tilde{s}_i &= (|h_{0,m}|^2 + |h_{1,m}|^2)s_i + h_{0,m}^* n_{0,m} + h_{1,m} n_{1,m}^* \\ \tilde{s}_j &= (|h_{0,m}|^2 + |h_{1,m}|^2)s_j + h_{0,m}^* n_{0,m} + h_{1,m} n_{1,m}^*. \end{aligned} \tag{3.69}$$

The combined signals are then used for the decision: choose s_k if and only if

$$d^2(\tilde{s}_i, s_k) \leq d^2(\tilde{s}_i, s_l), \; \forall k \neq l \tag{3.70}$$

Fig. 3.8 shows the full block diagram of the Alamouti scheme for the cases $N_R = 1$ (left) and $N_R = 2$ (right).

(a) Alamouti Scheme for $N_R = 1$

(b) Alamouti Scheme for $N_R = 2$.

Figure 3.8 – Alamouti coding for the cases $N_R = 1$ (left) and $N_R = 2$ (right).
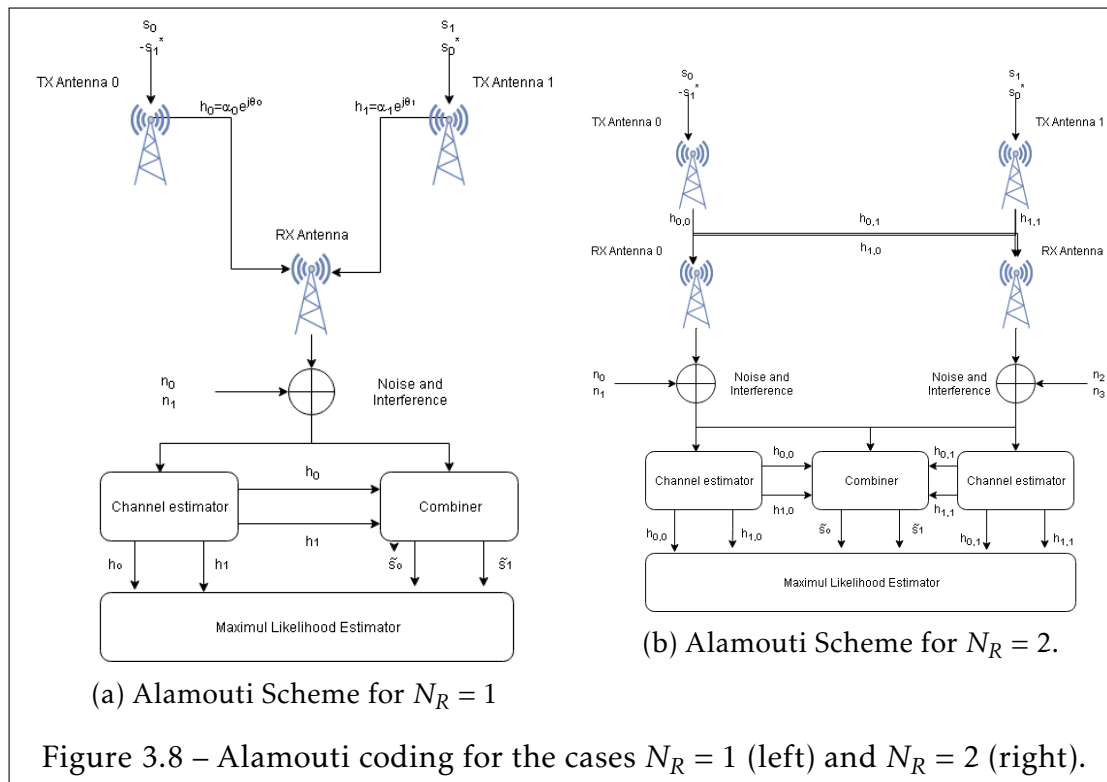
The Alamouti scheme under α-stable noise

Few works have studied the effects of SαS noise over STBC. Receiver and code designs issues (gain and diversity) are discussed in [GT07; LT11]. The performance of a Genie-Aided Receiver (GAR), Minimum-Distance Receiver (MDR) and MAP receivers in the first paper and GAR , MDR, ML and Asymptotically Optimal Receiver (AOR) in the second are compared. The MAP or ML presents the best performance but the AOR is very close but necessitates the knowledge of the noise parameters. Besides, both works assume that the channel is perfectly known at the receiver and does not perform any channel estimation. Papers on impulsive noise usually focus on channel estimation or decision algorithms but not both. The present thesis aims to fill this gap on research on dynamic interference and impulsive noises.

p-**norm receiver**

The classical Euclidean distance based receivers present poor performance under non-Gaussian noise. Thus, it is important to develop new sub-optimal receivers. The design and implementation of optimal receivers is a complex task, especially with α-stable noise because we do not dispose of any analytical expression of the density. One way to adress the question is to find a metric better suited to α-stable random variables. As discussed in B.3, we can not rely on second order moments, which do not exist for α-stable RV with $0 < \alpha < 2$. On another hand, the covariation allows to define a norm for α-stable vectors: given an α-stable random vector Y and an α with $1 < \alpha < 2$, then:

$$\|Y\|_\alpha = ([Y, Y]_\alpha)^{1/\alpha} \tag{3.71}$$

This α-norm can be used for distance estimation between the received symbol and the possible transmitted ones. One imprtant property is then that we can estilate this α-norm using the *p*-norm. The link for $1 < \alpha < 2$, $p < \alpha$ is given by [GC12; Gu+12; Gu12]

$$\|X - Y\|_\alpha = \left(\frac{|\mathbf{X} - \mathbf{Y}|^p}{C(\alpha, p)}\right)^{1/p}, \tag{3.72}$$

where $C_{\alpha, p}$ was defined in B.1. Using the *p*-norm metric, the decision statistic can be expressed as [GC12; Gu+12; Gu12]

$$\hat{X} = \min_{X \in \mathcal{X}} \left(\left\|Y - \hat{H}X\right\|_p\right). \tag{3.73}$$

The *p*-norm receiver has robust performance in impulsive but also in Gaussian noise. A simulated comparison between the *p*-norm and Euclidean metric is shown in [Gu12].

Estimation of *p*

To estimate *p* we use the same approach that is used to estimate the shape parameter β of a generalized Gaussian distribution. Indeed, in Generalized Gaussian noise, the optimal receiver is also given by the *p*-norm. The maximum

likelihood can be used with the Newton-Raphson method.

Let m_1 and m_2 denote the first and second statistical moments of the absolute values:

$$m_1 = \frac{1}{N}\sum_{i=1}^{N}|x_i|, m_2 = \frac{1}{N}\sum_{i=1}^{N}|x_i|^2, \tag{3.74}$$

And $g'(\beta)$ denotes the derivative of $g(\beta)$, defined on on Algorithm 3, and $\psi^m(\cdot)$ denotes the polygamma function, which is given by:

$$\psi^{(m)}(z) = \frac{\mathrm{d}^{m+1}}{\mathrm{d}z^{m+1}}ln\Gamma(z), \text{ with } \psi^{(0)}(z) = \frac{\Gamma'(z)}{\Gamma(z)} \tag{3.75}$$

The estimation procedure for p is shown on Algorithm 3.

Algorithm 3 Estimation algorithm for p. Source: [Yan15].

---

begin EstimateOfBeta(X,N)

Set $\beta_0 = \frac{m_1}{\sqrt{m_2}}$

Set initial value for β: $\beta \leftarrow \beta_0$

repeat

$g(\beta) \leftarrow 1 + \frac{\psi^{(0)}(1/\beta)}{\beta} - \frac{\sum_{i=1}^{N}|x_i|^\beta log|x_i|}{\sum_{i=1}^{N}|x_i|^\beta} + \frac{log(\frac{\beta}{N}\sum_{i=1}^{N}|x_i|^\beta)}{\beta}$

$\beta_{i+1} \leftarrow \beta_i - \frac{g(\beta_i)}{g'(\beta_i)}$

until get the estimated β

$p \leftarrow \beta$

return p

end

3.4.5   Results and discussions

A Matlab™ script was developed for simulating different situations and environments which includes the number of receiving antennas, the modulation type, the channel estimation approach, the type of noise and different receiver designs for simulation. Its pseudo-code is shown on Algorithm 4. a Graphical User Interface (GUI), shown on Figure 3.9 was created using Matlab™ GUIDE application.

Algorithm 4 Simulation Algorithm

Define data to be transmitted $\mathbf{X}_{N_s} \in \mathbb{C}^{N_s}$;

$\mathbf{X}_{N_s,2} = \text{AlamoutiCoding}(\mathbf{X}_{N_s})$;

Generate random SαS noise matrix $\mathbf{N}_{N_s,M} \in \mathbb{C}^{N_s \times M}$

Generate complex channel coefficients matrix $\mathbf{H}_{2,M} \in \mathbb{C}^{2 \times M}$

Received signal $\mathbf{Y}_{N_s,M} = \mathbf{X}_{N_s,2}\mathbf{H}_{2,M} + \mathbf{N}_{N_s,M}$

Estimate channel coefficients matrix:

Generate (previously known) training sequence $\mathbf{T}_{N_s} \in \mathbb{C}^{N_s}$;

$\mathbf{T}_{N_s,2} = \text{AlamoutiCoding}(\mathbf{T}_{N_s})$;

Calculate expected received signal $\mathbf{Y}'_{N_s,M} = \mathbf{T}_{N_s,2}\mathbf{H}_{2,M} + \mathbf{N}_{N_s,M}$

$\hat{\mathbf{H}}_{LAD_{2,M}} = LAD(\mathbf{Y}'_{N_s,M}, \mathbf{T}_{N_s})$;

$\hat{\mathbf{H}}_{LS_{2,M}} = LS(\mathbf{Y}'_{N_s,M}, \mathbf{T}_{N_s})$;

Estimate p value

Decision: D=$p$normDetector($\mathbf{Y}'$,$\hat{\mathbf{H}}_{2,M}$,p)
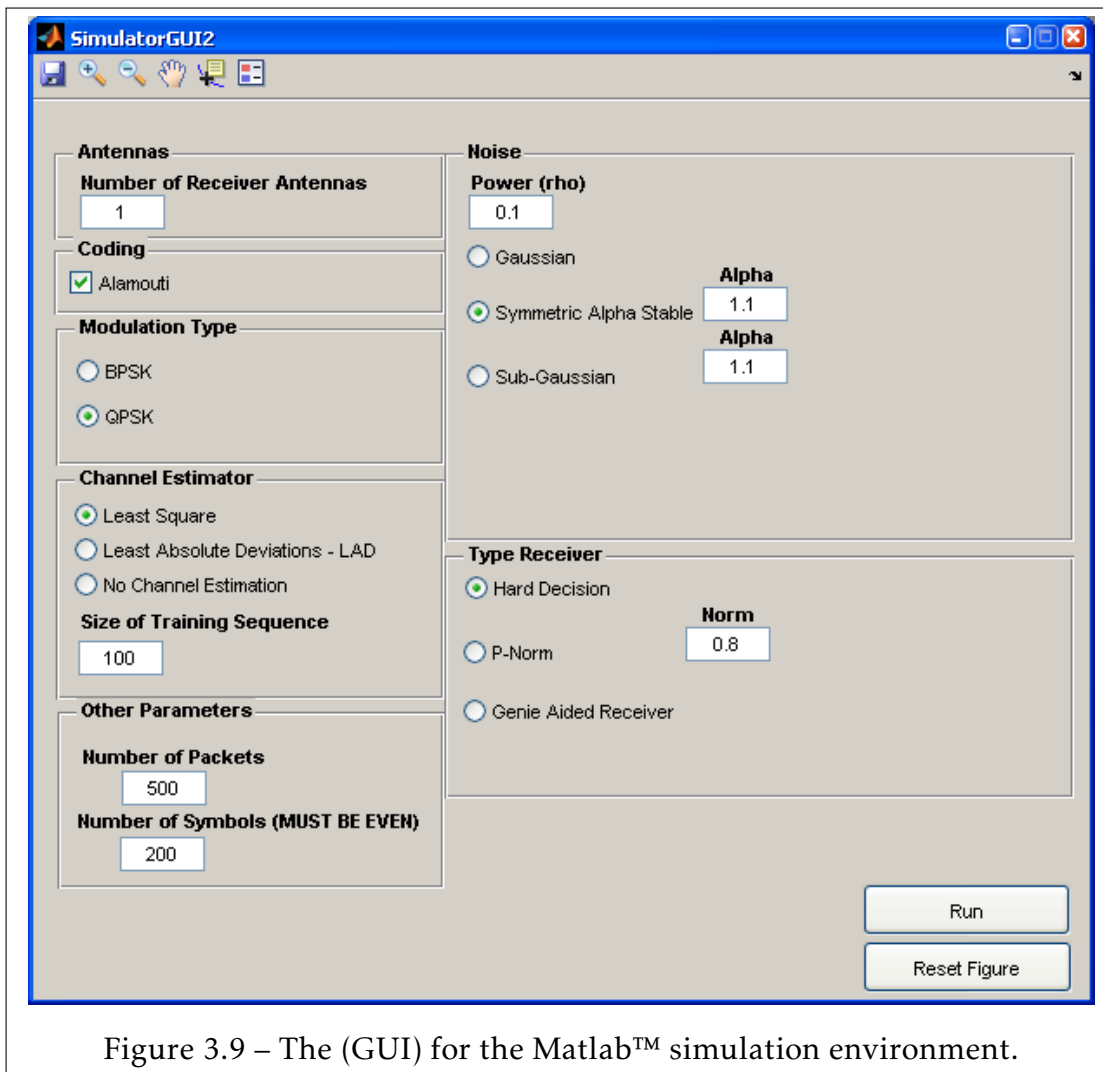
Figure 3.9 – The (GUI) for the Matlab™ simulation environment.

Value of p

A preliminary analysis focuses on the estimated p-value for the p-norm receiver. It compares it with the value that minimizes the BER, obtained with exhaustive search and Monte-Carlo simulations [Sob09]. Examples of results are shown in Table 3.2. The estimated p are always close to the optimum value and the impact on the BER is small, validating our proposal. The simulations showed also that optimal p changes according to γ and α values (Fig. 3.10).

	Optimal	Estimated	Optimal	Estimated
	$\alpha = 0.8$		$\alpha = 1.4$	
P	$4.00 \cdot 10^{-1}$	$2.43 \cdot 10^{-1}$	$7.00 \cdot 10^{-1}$	$6.11 \cdot 10^{-1}$
BER	$1.65 \cdot 10^{-2}$	$1.68 \cdot 10^{-2}$	$3.96 \cdot 10^{-3}$	$4.10 \cdot 10^{-3}$
	$\alpha = 1.9$		$\alpha = 2.0$	
P	1.10	1.38	2.00	1.98
BER	$8.44 \cdot 10^{-4}$	$1.07 \cdot 10^{-3}$	$3.75 \cdot 10^{-4}$	$4.00 \cdot 10^{-4}$

Table 3.2 – Comparison between simulated optimal p and estimated p for $\gamma = 0.9$

Figure 3.10 – BER behavior and estimated p according to value of α. Copyright 2019 IEEE. Reprinted, with permission, from Nicolas de Araujo Moreira and Laurent Clavier, Multiple antenna receiver under impulsive SαS noise, WCNC, 2019.
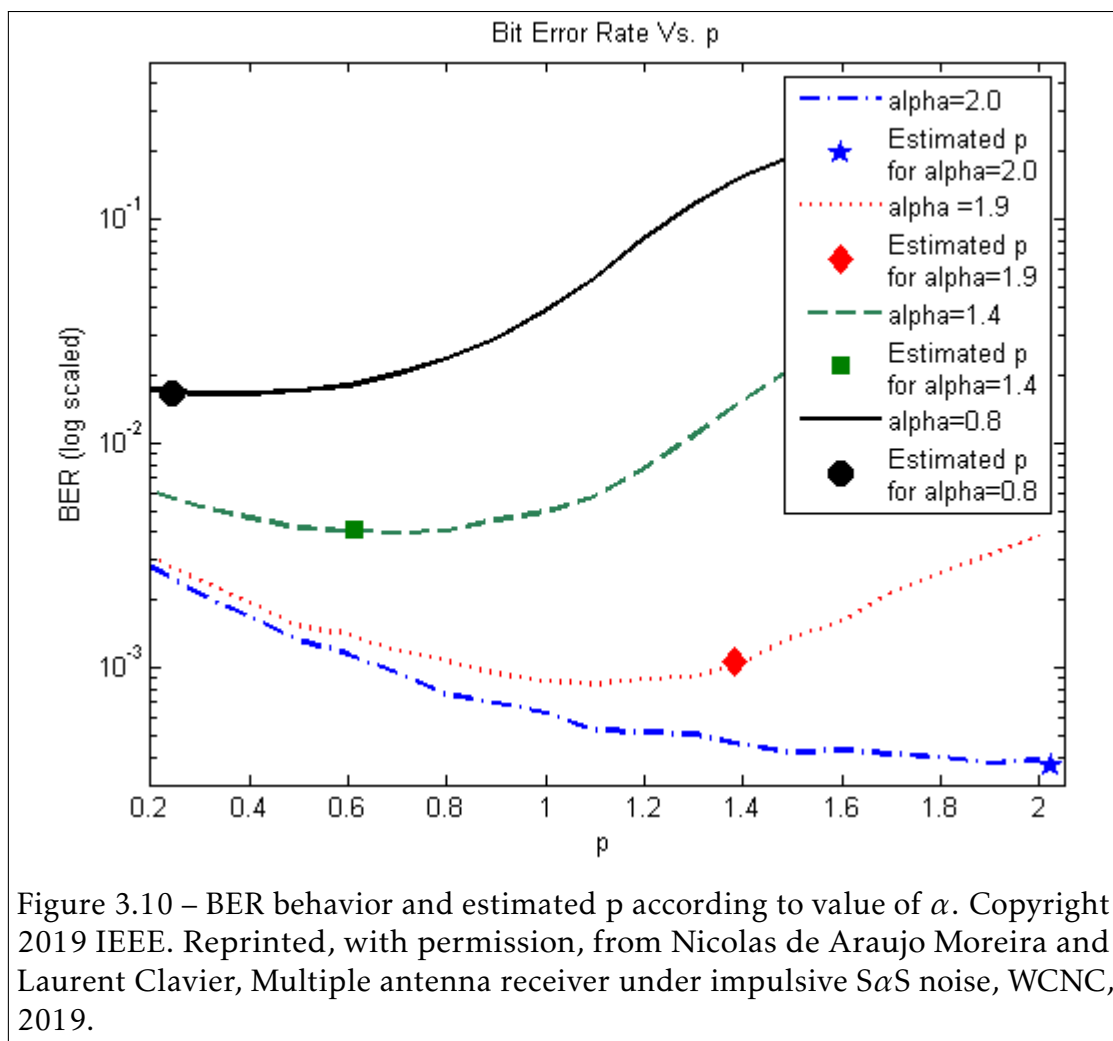
Receiver performance

In a second step, we analyzed the performance of receiver under the following scenarios:

- 10.000 packets were sent for evaluating the BER,

- $N_s = 100$ per packet,

- $N_r = 6$ received antennas,

- the noise is a symmetric ($\beta = 0, \mu = 0$) α-stable noise with $\alpha = 1.4$ and $\gamma_{dB} \in [-1.5, 1.5]$,

- for both channel estimation scheme (LS and LAD), a training sequence of length $L = 500$ is used.

The performance is compared with a GAR, with the channel state perfectly known, but with the estimation of the value of p. We also use the original $L2$-norm and the LS channel estimation to evaluate the gain of our proposal over this usual approach. Results are shown in Fig. 3.11. The BER for $\gamma_{dB} \in \{-1.5, 0, 1.5\}$ are also shown in Table 3.3.

The results show that LAD estimator when combined with p-norm receiver presents a performance close to the case of perfectly known channel. Similar results were obtained for $\alpha = 0.8, 1.1, 1.43, 1.9, 2.0$, different γ intervals. The LAD is in any case outperforming the other systems, except for $\alpha = 2$, where LS presents a small advantage. The simulation was repeated for two different sizes of training sequence, $L = 200$ and $L = 500$, giving similar results. The simulation was also repeated for different number of receiving antenna, $N_r = 1, 2, 4, 6$, with more significant gains when N_r increases. Fig. 3.12, 3.13 and 3.14 show the case for $N_R = 2$ and $\alpha = 1.4$, $N_R = 6$ and $\alpha = 0.8$, $N_R = 6$ and $\alpha = 2.0$. It is important to observe and emphasize that the purposed system does not degrade its performance when the impulsive interference is not present and noise reduces to the thermal Gaussian noise. This gives robustness against changes in transmission conditions.

The purposed approach outperforms the traditional method and presents a performance close to the optimal receiver assuming the perfect knowledge of channel behavior and the noise distribution.

$\gamma_d B$	Ideal Case	LAD	LS	LS,p=2
-1.5	-1.47	**-1.46**	-1.24	-0.82
0	-2.14	**-2.12**	-1.81	-1.09
1.5	-3.03	**-3.01**	-2.58	-1.30

Table 3.3 – $log_{10}(BER)$ for $\gamma_{dB} \in \{-1.5, 0, 1.5\}$

Figure 3.11 – Results for a 2x6 MIMO system, with 10.000 sent packets, $N_s = 100$ under Sα-stable noise with $\alpha = 1.4$, $\gamma_{dB} \in [-1.5, 1.5]$. Obs: PN indicates the p-norm receiver.

Figure 3.12 – Results for a 2x2 MIMO system, with 10.000 sent packets, $N_s = 100$ under Sα-stable noise with $\alpha = 1.4, \gamma_{dB} \in [-1.5, 1.5]$. Obs: PN indicates the p-norm receiver. Copyright 2019 IEEE. Reprinted, with permission, from Nicolas de Araujo Moreira and Laurent Clavier, Multiple antenna receiver under impulsive SαS noise, WCNC, 2019.

Figure 3.13 – Results for a 2x6 MIMO system, with 10.000 sent packets, $N_s = 100$ under Sα-stable noise with $\alpha = 0.8, \gamma_{dB} \in [-1.5, 1.5]$. Obs: PN indicates the p-norm receiver. Copyright 2019 IEEE. Reprinted, with permission, from Nicolas de Araujo Moreira and Laurent Clavier, Multiple antenna receiver under impulsive SαS noise, WCNC, 2019.

Figure 3.14 – Results for a 2x6 MIMO system, with 10.000 sent packets, $N_s = 100$ under Sα-stable noise with $\alpha = 2.0, \gamma_{dB} \in [-1.5, 1.5]$. Obs: PN indicates the p-norm receiver. Copyright 2019 IEEE. Reprinted, with permission, from Nicolas de Araujo Moreira and Laurent Clavier, Multiple antenna receiver under impulsive SαS noise, WCNC, 2019.

Conclusion

In this work, we studied the coexistence of different networks in the same frequency bands. More specifically, we started with an experimental evaluation of the effect of WIFI interferers on a Zigbee network. We showed the significant impact of such a coexistence on both reliability and energy consumption. We also noticed the non Gaussian behaviour of the interfering signal. To comfort this observation, we did a theoretical analysis of this interference. Many works have addressed the problem and the α-stable assumption seems to be a good one, allowing some interesting analytical studies.

Based on those results, we presented a MIMO communication system robust against SαS noise. The proposed system is composed by a QPSK modulation and an Alamouti coder. Two transmitting antennas and M receiving antennas are used. To increase robustness against the impulsive noise, a p-norm receiver is used. To complete the receiver architecture, we proposed an estimator for the value of p, a supervised channel estimator and a decoder on receiver side. For the channel, two different estimators were tested: LS and LAD. Their performance were compared with the ideal case when the channel state is perfectly known. Monte-Carlo simulations showed that the estimation of p gives a near-optimal value. The optimal p changes according to γ and α. For different scenarios with $\alpha \neq 2$, LAD outperforms LS. For $\alpha = 2$, both estimators present results close to the perfect channel knowledge. The simulations were executed for different values of N_R (receiving antennas), α, γ and L.

Our proposal is a relevant design of flexible communication architecture that outperforms the conventional Gaussian-based approaches under the presence of SαS noise. Besides, the performance are still very close to the traditional scheme

under the presence of purely Gaussian noise.

Future Works

Experimental works with higher number of mobile interfering nodes under a real environment are necessary to approach to a more dynamic realistic scenario. We assume however that our proposal will adapt to any type of noise, impulsive with statistics that differs from the α-stable case or to the more traditional Gaussian context.

Low complexity alternatives for the algorithm for finding the optimal value of p could improve the performance of the receiver. Especially, we can notice that the performance is not so sensitive to this estimation step, the performance remaining equal for a rather large set of p values.

An implementation of the proposed architecture would be interesting to evaluate the impact on energy saving while under the presence of high level of impulsive noises. Further studies are also necessary to take into account the dependency in space and/or in time of the interference. This dependence structure with α-stable noise is not trivial and on-going works propose the use of copula-based techniques.

Bibliography

[Abr+14]   Danilo M. Abrignani et al. "Testing the impact of Wi-Fi interference on Zigbee Networks". In: *2014 Euro Med Telco Conference (EMTC)*. Naples, Italy, Nov. 2014.

[Ada06]   John T. Adams. "An introduction to IEEE std 802.15.4". In: *2006 IEEE Aerospace Conference*. Big Sky, MT, USA, Mar. 2006.

[AIH94]   S. Ambike, J. Ilow, and D. Hatzinakos. "Detection for binary transmission in a mixture of Gaussian noise and impulsive noise modeled as an alpha-stable process". In: *IEEE Signal Processing Letters* 1.3 (Mar. 1994), pp. 55–57.

[BSF08]   N. C. Beaulieu, H. Shao, and J. Fiorina. "P-order metric UWB receiver structures with superior performance". In: *IEEE Trans. Commun.* 56 (Oct. 2008), pp. 1666–1676.

[BN10]   N.C. Beaulieu and S. Niranjayan. "UWB receiver designs based on a Gaussian-Laplacian noise-plus-MAI model". In: *IEEE Trans. Wireless Commun.* 58.3 (Mar. 2010), pp. 997–1006.

[BY09]   N.C. Beaulieu and David J. Young. "Designing Time-Hopping Ultrawide Bandwidth Receivers for Multiuser Interference Environments". In: *Proceedings of the IEEE* 97.2 (Feb. 2009), pp. 255–284.

[Bec64]   P. Beckmann. "Amplitude-probability distribution of atmospheric radio noise". In: *J. Res. NBS* 68D (1964), pp. 723–736.

[Bel05]   I.A. Belov. "On the computation of the probability density function of α-stable distributions". In: *Proceedings of the 10th International Conference MMA2005 CMAM2*. Trakai, 2005, pp. 333–341.

[BW03]   Inaki Berenguer and Xiaodong Wang. *Coding and signal processing for MIMO communications - a primer*. July 2003.

[Big+07]   Ezio Biglieri et al. *MIMO Wireless Communications*. Cambridge, 2007.

[BFC05]   Daniel W. Bliss, Keith W. Forsythe, and Amanda M. Chan. "MIMO wireless communication". In: *Licoln laboratory journal* 15.1 (2005), pp. 97–126.

[BHW05]   Szymon Borak, Wolfgang Härdle, and Rafał Weron. "Stable Distributions". In: *Statistical Tools for Finance and Insurance*. Berlin, Heidelberg: Springer Berlin Heidelberg, 2005, pp. 21–44.

[BDP12]   Alessio Botta, Alberto Dainotti, and Antonio Pescapé. "A tool for the generation of realistic network workload for emerging networking scenarios". In: *Computer Networks* (2012), pp. 3531–3547.

[Car10]   P. Cardieri. "Modeling Interference in Wireless Ad Hoc Networks". In: *IEEE Communications Surveys Tutorials* 12.4 (2010), pp. 551–572.

[CS04]   Jean Carle and David Simplot-Ryl. "Energy-efficient area monitoring sensor networks". In: *Computer* (2004), pp. 40–46.

[Cav+14]   Riccardo Cavallari et al. "A survey on wireless body area networks: technologies and design challenges". In: *IEEE communications surveys and tutorials* 16.3 (Third quarter 2014), pp. 1635–1657.

[CKP12]   M. Chitre, S. Kuselan, and V. Pallayil. "Ambient noise imaging in warm shallow waters; robust statistical algorithms and range estimation". In: *The Journal of the Acoustical Society of America* 132.2 (2012), pp. 838–847.

[Cho+10]   Yong Soo Cho et al. *MIMO-OFDM wireless communications with MATLAB*. Singapore: John Wiley and Sons, 2010.

[CE13]   A. Chopra and B.L. Evans. "Outage Probability for Diversity Combining in Interference-Limited Channels". In: 12.2 (Feb. 2013), pp. 550–560.

[Cis07]   Enrica Vera Cisana. "Non-Gaussian stochastic models and their applications in Econophysics". PhD thesis. Pavia, Italia: Università degli Studi di Pavia, 2007.

[Cla+10]   Laurent Claiver et al. "α-stable interfernece modeling and Cauchy receiver for an IR-UWB ad hoc network". In: *IEEE Transactions on Communications* 58.6 (June 2010), pp. 1748–1757.

[Cla05]   Cory L Clark. *LabVIEW digital signal processing and digital communications*. InTech, 2005. ISBN: 978 953 307 650 8.

[CD09]   Giulio Cottone and Mario Di Paola. "On the use of fractional calculus for the probabilistic characterization of random variables". In: *Probabilistic Engineering Mechanics* 24 (3 2009), pp. 321–330.

[Cri+60]   W. Q. Crichlow et al. "Determination of the amplitude-probability distribution of atmospheric radio noise from statistical moments". In: *J. Res. NBS* 65D (1960), pp. 49–56.

[DK]   Christopher R. Dance and Ercan E. Kuruoglu. *Estimation of the parameters of Skewed α-stable distribution.*

[DP12]   Mario Di Paola and Francesco Paolo Pinnola. "Riesz fractional integrals and complex fractional moments for the probabilistic characterization of random variables". In: *Probabilistic Engineering Mechanics* 29 (2012), pp. 149–156.

[Dim+14]   V. Dimanche et al. "On Detection Method for Soft Iterative Decoding in the Presence of Impulsive Interference". In: *IEEE Communication Letters* 18.6 (June 2014), pp. 945–948.

[DR02]   G. Durisi and G. Romano. "On the Validity of Gaussian Approximation to Characterize the Multiuser Capacity of UWB TH-PPM". In: *IEEE Conf. on Ultra Wideband Systems and Technologies* (May 2002), pp. 20–23.

[Ega+16]   Malcolm Egan et al. "Achievable rates for additive isotropic α-stable noise channels". In: *2016 IEEE International Symposium on Information Theory*. 2016, pp. 1874–1878.

[Ega+17]   Malcom Egan et al. "Wireless communications in dynamic interference". In: *Proceedings of IEEE Global Communications Conference (Globecom)*. Dec. 2017, pp. 1–6.

[Erg04]   Coleri Sinem Ergen. *ZigBee/IEEE 802.15.4 Summary*. Sept. 2004.

[ECD08]   T. Erseghe, V. Cellini, and G. Dona. "On UWB Impulse Radio Receivers Derived by Modeling MAI as a Gaussian Mixture Process". In: *IEEE Trans. Wireless Commun.* 7.6 (June 2008), pp. 2388–2396.

[Far+]   N. Farsad et al. "Stable distributions as noise models for molecular communication". In: *Proc. IEEE Global Communications Conference*. (2015), p. 383.

[Fic+13]   Anthony Fiche et al. "Features modeling with an α-stable distribution: application to pattern recognition based on continuous belief functions". In: *Information fusion* 14 (2013), pp. 504–520.

[FH06]   J. Fiorina and W. Hachem. "On the asymptotic distribution of the correlation receiver output for time-hopped UWB signals". In: *IEEE Trans. Signal Processing* 54.7 (July 2006), pp. 2529–2545.

[Fol11]   Silviu Folea. *Practical applications and solutions using LabVIEW software*. McGraw-Hill, 2011.

[FI60]   K. Furutsu and T. Ishida. "On the theory of amlitude distribution of impulsive random noise and its application to the atmospheric noise". In: *Journal of the radio research laboratories (Japan)* 7.32 (1960).

[FI61]   K. Furutsu and T. Ishida. "On the theory of amplitude distribution of impulsive random noise". In: *J. Appl. Phys.* 32 (1961), pp. 1206–1221.

[GT07]   Ping Gao and Cihan Tepedelenlioglu. "Space-time coding over fading channels with impulsive noise". In: *IEEE Transactions on Vehicular Technology* 6.1 (Jan. 2007), pp. 220–229.

[GS05]   A. B. Gershman and N. D. Sidiropoulos. *Space-time processing for MIMO communications*. John Wiley and Sons, 2005.

[GH72]   A. A. Giordano and F. Haber. "Modeling of,atmospheric noise". In: *Radio Sci.* 7 (1972), pp. 1101–1123.

[Gio+02]   Carlos L. Giovaneli et al. "Application of spacetime diversity/coding for power line channels". In: *Proceedings IEEE ISPLC*. Apr. 2002, pp. 101–105.

[GA01]   Juan G. Gonzalez and Gonzalo R. Arce. "Optimality of the Myriad filter in practical impuslive-noise environments". In: *IEEE Transactions on Signal Processing* 49.2 (Feb. 2001).

[GA02]   Juan G. Gonzalez and Gonzalo R. Arce. "Statistically-efficient filtering in impulsive environments: weighted myriad filters". In: *EURASIP Journal on Applied Signal Processing* (2002), pp. 5–19.

[GPA06]   Juan G. Gonzalez, José L. Peredes, and Gonzalo R. Arce. "Zero-order statistics: a mathematical framework for the processing and characterization of very impulsive signals". In: *IEEE Transactions on Signal Processing* 54.10 (Oct. 2006), pp. 3839–3851.

[Gu12]   Wei Gu. "Robustness against interference in internet of things". PhD thesis. Université de Lille 1, 2012.

[GC12]   Wei Gu and Laurent Clavier. "Decoding metric study for turbo codes in very impuslive environment". In: *IEEE communications letters* 16.2 (Feb. 2012).

[Gu+12]   Wei Gu et al. "Receiver study for cooperative communications in convolved additive α-stable interference plus Gaussian thermal noise". In: *9th International Symposium on Wireless Communication Systems*. Paris, France, Aug. 2012.

[Gui06]   Ferre Guillaume. "Codage spatio-temporel et techniques de dé-codage itératives pour systèmes multi-antennas". PhD thesis. Université de Limoges, 2006.

[Gul+10]   K. Gulati et al. "Statistics of Co-Channel Interference in a Field of Poisson and Poisson-Poisson Clustered Interferers". In: *IEEE Transactions on Signal Processing* 58.12 (Dec. 2010), pp. 6207–6222.

[GDK06]   Nazli Güney, Hakan Deliç, and Mutlu Koca. "Robust detection of Ultra-Wideband signals in non-Gaussian noise". In: *IEEE Transactions on Microwave Theory and Techniques* 54.4 (Apr. 2006).

[Hae+09]   M. Haenggi et al. "Stochastic geometry and random graphs for the analysis and design of wireless networks". In: *IEEE J. Sel. Areas Commun.* 27.7 (Sept. 2009), pp. 1029–1046.

[Han10]   Greg Hannsgen. *Infinite-variance, Alpha-stable Shocks in Monetary SVAR*. Annandale on Hudson, NY, USA, May 2010.

[Hei+04]   Christiaan Heij et al. *Econometric methods with applications in business and economics*. Oxford University Press, 2004.

[HSD14]   Anwar Hithnawi, Hossein Shafagh, and Simon Duquennoy. "Understanding the Impact of Cross Technology Interference on IEEE 802.15.4". In: *Proceedings of the 9th ACM International Workshop on Wireless Network Testbeds, Experimental Evaluation and Characterization*. WiNTECH '14. Maui, Hawaii, USA: ACM, 2014, pp. 49–56. ISBN: 978-1-4503-3072-5. DOI: 10.1145/2643230.2643235. URL: http://doi.acm.org/10.1145/2643230.2643235.

[Hol01]   Bengt Holter. "On the capacity if the MIMO channel -a tutorial introduction". In: *Proc. IEEE Norwegian Symposium on Signal Processing*. 2001, pp. 167–172.

[Hon10]   Y.-W. Peter et al. Hong. *Cooperative communications and networking*. Springer Science, 2010.

[HH56]   F. Horrier and J. Harwood. "An investigation of atmospheric radio noise at very low frequencies". In: *Proc. Inst. Elec. Eng.* 103 (1956), pp. 743–751.

[HB08]   B. Hu and N. C. Beaulieu. "On characterizing multiple access interference in TH UWB systems with impulsive noise models". In: *Proc. IEEE Radio Wireless Symp.* Orlando, FL, Jan. 2008, pp. 879–882.

[Hug00]   B. Hughes. "Alpha-stable models of multiuser interference". In: *Proc. IEEE ISIT'00*. June 2000, p. 383.

[Hut+05]   Andreas A Hutter et al. "Alamouti-based space-frequency cod-
            ing for OFDM". In: *Wireless personal communications, Volume 35,
            N°1-2, October 2005* (Oct. 2005). DOI: http://dx.doi.org/10.
            1007/s11277-005-8747-5. URL: http://www.eurecom.fr/
            publication/1879.

[Ibu66]   0. Ibukun. "Structural aspects of atmospheric radio noise in the
            tropics". In: *Proc. IEEE* 54 (1966), pp. 361–367.

[IH98]   J. Ilow and D. Hatzinakos. "Analytic alpha-stable noise modeling in
            a poisson field of interfers or scatterers". In: *IEEE Transactions on
            Signal Processing* 46.6 (1998), pp. 1601–1611.

[Ina+09]   H. Inaltekin et al. "On unbounded path-loss models: effects of sin-
            gularity on wireless network performance". In: *IEEE J. Sel. Areas
            Commun.* 27.7 (Sept. 2009), pp. 1078–1092.

[Ins14a]   National Instruments. *Device Specifications NI USRP-2942R*. 2014.

[Ins15a]   National Instruments. *Getting Started Guide NI USRP-2940R/2942R/2943R*.
            2015.

[Ins15b]   National Instruments. *NI USRP RIO Datasheet*. Aug. 2015.

[Ins14b]   National Instruments. *NI USRP-29xx Getting Started Guide*. 2014.

[Ins13]   National Instruments. *Une introduction à la radio définie par logiciel
            avec NI LabVIEW et NI USRP*. 2013.

[JW94]   Aleksander Janicki and Aleksander Weron. *Simulation and chaotic
            behavior of α-stable stochastic processes*. New York, United States of
            America: Marcel Dekker Inc., 1994.

[Jes15]   Thomas Kolbaek Jespersen. *Software Defined Radio - Getting started
            with USRP N200 and LabVIEW (Student Report)*. 2015.

[Joh96]   D.H. Johnson. "Optimal Linear Detectors for Additive Noise Chan-
            nels". In: *IEEE Trans. Signal Processing* 44.12 (Dec. 1996), pp. 3079–
            3084.

[KZ10]   Thomas Kaiser and Feng Zheng. *Ultra wideband systems with MIMO*.
            John Willey and Sons, 2010. ISBN: 978 0 470 71224 5.

[KMM]   H. Kanemoto, S. Miyamoto, and N. Morinaga. "Statistical model
            of microwave oven interference and optimum reception". In: *Proc.
            IEEE ICC'98*. (Oct. 1998), pp. 1660–1664.

[Kas88]   Saleem A. Kassam. *Signal detection in non-Gaussian noise*. Springer-
            Verlag, 1988.

[KMD08]   D. G. Khairnar, S. N. Merchant, and U. B. Desai. "Radar signal detection in non-Gaussian noise using RBF neual network". In: *Journal of Computers* 3.1 (Jan. 2008).

[KLC09]   F. Kharrat Kammoun, C.J. Le Martret, and P. Ciblat. "Performance analysis of IR UWB in a multi-user environment". In: *IEEE Transactions on Wireless Comunications* 8.11 (Nov. 2009), pp. 5552–5563.

[Kid00]   Preben Kidmose. "Alpha-stable distributions in signal processing of audio signals". In: *41st Conference on Simulation and Modelling*. Australia, 2000, pp. 87–94.

[LS95]   Chrysostomos L. Nikias and Min Shao. *Signal processing with Alpha-Stable distributions and applications*. United States of America: John Wiley and Sons, 1995.

[Lau+17]   M. Lauridsen et al. "Interference Measurements in the European 868 MHz ISM Band with Focus on LoRa and SigFox". In: *IEEE Wireless Communications and Networking Conference (WCNC)*. San Francisco, CA, 2017, pp. 1–6.

[LT11]   Junghoon Lee and Chian Tepedelenlioglu. "Space-time coding over fading channels with stable noise". In: *IEEE Transactions on Vehicular Technology* 60.7 (Sept. 2011), pp. 3169–3177.

[LJL09]   Xutao Li, Yongquan Jiang, and Miao Liu. "A near optimum detection in alpha-stable impulsive noise". In: *IEEE ICASSP 2009*. 2009, pp. 3305–3308.

[LA04]   Y. Li and G.R. Arce. "A maximum likelihood approach to Least Absolute Deviation Regression". In: *EURASIP Journal on Applied Signal Processing* 12 (2004), pp. 1762–1769.

[M A98]   Siavash M. Alamouti. "A simple transmit diversity technique for wireless communications". In: *IEEE Jounral on Selected Areas in Communications* 16.8 (Oct. 1998), pp. 1451–1458.

[Maa+13]   H.B. Maad et al. "Clipping Demapper for LDPC Decoding in Impulsive Channel". In: 17.5 (May 2013), pp. 968–971.

[MCA12]   A. Mahmood, M. Chitre, and M.A. Armand. "PSK communication with passband additive symmetric α-stable noise". In: *IEEE Transactions on Communications* 60.10 (Oct. 2012), pp. 2990–3000.

[Man63]   Benoît Mandelbrot. "The variation of certain speculative prices". In: *The Journal of Business of the University of Chicago* 36 (1963), pp. 394–419.

[MHL14]   Shiwen Mao, Yingson Huang, and Yihan Li. "On developing a soft-
           ware defined radio laboratory course for undergraduate wireless
           engineering curriculum". In: *121st American Society Engineering
           Education Annual Conference and Exposition*. Illinois, United States,
           June 2014.

[Mas12]   Abdelbasset Massouri. "Modélisation comportamentale SystemC-
           AMS d'interfaces RF et liaisons radio multipoint pour réseaux de
           capteurs". PhD thesis. Université de Lille 1, 2012.

[MP13]   Muneya Matsui and Zbynek Pawlas. "Fractional absolute moments
           of heavy tailed distributions". In: *Brazilian Journal of Probability and
           Statistics* 30 (Jan. 2013). DOI: 10.1214/15-BJPS280.

[Mei+17]   Z. Mei et al. "Performance Analysis of LDPC Coded Diversity Com-
           bining on Rayleigh Fading Channels With Impulsive Noise". In:
           IEEE Transactions on Communications 65.6 (June 2017), pp. 2345–
           2356.

[Mid79]   D. Middleton. "Canonical non-Gaussian noise models: Their im-
           plications for measurement and for prediction of receiver perfor-
           mance". In: *IEEE Trans. Electromagn. Compat.* 21 (Aug. 1979), pp. 209–
           220.

[Mid73]   D. Middleton. "Man-made noise in urban environments and trans-
           portation systems". In: *IEEE Trans. Commun.* 21 (Nov. 1973), pp. 1232–
           1241.

[Mid77]   D. Middleton. "Statistical-physical models of electromagnetic in-
           terference". In: *IEEE Trans. Electromagn. Compat.* 19.3 (Aug. 1977),
           pp. 106–127.

[Mid72]   D. Middleton. "Statistical-physical models of urban radio-noise
           environments, Part 1: Foundations". In: *IEEE Trans. Electromagn.
           Compat.* 14 (May 1972), pp. 38–56.

[Mid99]   David Middleton. "Non-Gaussian noise models in signal processing
           for telecommunications: new methods and results for class A and
           class B noise models". In: *IEEE Transactions on Information Theory*
           45.4 (May 1999), pp. 1129–1149.

[Mih+05]   Lyudmila Mihaylova et al. "Particle filtering with alpha-stable distri-
           butions". In: *IEEE/SP 13th Workshop on Statistical Signal Processing*.
           Bordeau, France, July 2005.

[Mor+17]   N.A. Moreira et al. "Heterogeneous networks: experimental study
           of interface between IEEE 802.11 and IEEE 802.15.4 technologies".
           In: *Journée Scientifique URSI France 2017*. Feb. 2017, pp. 9–16.

[Mye+07]   Steven Myers et al. "Experimental investigation of IEEE 802.15.4 transmission power control and interference minimization". In: *Proceedings of 4th Annual IEEE Communications Society Conference on Sensor, Mesh and Ad Hoc Communications and Networks*. San Diego, CA, USA, 2007, pp. 294–303.

[Nam+06]   S. Nammi et al. "Effects of impulse noise on the performance of multidimensional parity check codes". In: *IEEE Wireless Communications and Networking Conference, WCNC 2006*. Vol. 4. Apr. 2006, pp. 1966–1971.

[ND07]   Marcel Nassar and Marcus DeYoung. *Receivers for Digital Communication in Symmetric Alpha Stable Noise*. 2007.

[Nas+12]   M. Nassar et al. "Cyclostationary noise modelling i narrowband powerline communications for smartgrid applications". In: *Proceedings of IEEE International Conference on Acoustics, Speech and Signal Processing (ICASSP)*. (Mar. 2012). Kyoto, Japan, Mar. 2012.

[Nas+09]   M. Nassar et al. "Mitigating near-field interference in laptop embedded wireless transceivers". In: *J. Signal Process. Systems* (2009).

[Ngu13]   Duc Toan Nguyen. "Implementation of OFDL systems using GNU Radio and USRP". MA thesis. University of Wollongong, 2013.

[NB08]   S. Niranjayan and N.C. Beaulieu. "A Myriad filter detector for UWB multiuser communication". In: *Proceedings of ICC 2008*. 2008.

[NB10]   S. Niranjayan and N.C. Beaulieu. "BER optimal linear combiner for signal detection in symmetric alpha-stable noise: small values of alpha". In: *IEEE Trans. Wireless Commun.* 9.3 (Mar. 2010), pp. 886–890.

[NB09]   S. Niranjayan and N.C. Beaulieu. "The BER optimal linear rake receiver for signal detection in symmetric α-stable noise". In: *IEEE Trans. Commun.* 57.12 (Dec. 2009), pp. 3585–3588.

[Nol01]   John P. Nolan. "Maximum Likelihood Estimation and Diagnostics for Stable Distributions". In: *Lévy Processes: Theory and Applications*. Ed. by Ole E. Barndorff-Nielsen, Sidney I. Resnick, and Thomas Mikosch. Boston, MA: Birkhäuser Boston, 2001, pp. 379–400. ISBN: 978-1-4612-0197-7. DOI: 10.1007/978-1-4612-0197-7_17. URL: https://doi.org/10.1007/978-1-4612-0197-7_17.

[Nol97]   John P. Nolan. "Numerical calculation of stable densities and distri-
            bution functions". In: *Communications in Statistics. Stochastic Mod-
            els* 13.4 (1997), pp. 759–774. DOI: 10 . 1080 / 15326349708807450.
            eprint: https : / / doi . org / 10 . 1080 / 15326349708807450. URL:
            https://doi.org/10.1080/15326349708807450.

[NBC17]   Umber Norren, Ahcène Bonceur, and Laurent Clavier. "A study of
            LoRa low power and wide area network technology". In: *2017 In-
            ternational Conference on Advanced Technologies for Signal and Image
            Processing (ATSIP)*. Fes, Morroco, May 2017.

[NXP13]   NXP. *Co-existence of IEEE 802.15.4 at 2.4 GHz Application Note*. Nov.
            2013.

[OC07]   Claude Oestges and Bruno Clerckx. *MIMO Wireless Communications*.
            Academic Press, 2007.

[Pan14]   Wararit Panichkitkosolkul. "A Simulation Study of Estimator for
            the Stable Index". In: *Innovative Management in Information and
            Production*. Ed. by Junzo Watada, Bing Xu, and Berlin Wu. New
            York, NY: Springer New York, 2014, pp. 9–17. ISBN: 978-1-4614-
            4857-0.

[PSK11]   Jintae Park, Georgy Shevlyakov, and Kiseon Kim. "maxmin dis-
            tributed detection in the presence of impulsive alpha-stable noise".
            In: *IEEE Transactions on Wireless Communications* 10.6 (June 2011),
            pp. 1687–1691.

[PC13]   Konstantinos Pelekanakis and Mandar Chitre. "Adaptive sparse
            channel estimation under symmetric alpha-stable noise". In: *IEEE
            Transactions on Wireless Communications* 13.6 (June 2013), pp. 3183–
            3195.

[Pet+06]   Marina Petrova et al. "Performance study of IEEE 802.15.4 using
            measurements and simulations". In: *WCNC 2006 proceedings*. 2006,
            pp. 487–492.

[PW10]   P. Pinto and M. Win. "Communication in a poisson field of interfer-
            ers part II: channel capacity and interference spectrum". In: *IEEE
            Transactions on Wireless Communications* 9.7 (2010), pp. 2187–2195.

[PS02]   John G. Proakis and Mahoud Salehi. *Communication Systems Engi-
            neering*. 2nd ed. United States of America: Prentice Hall, 2002.

[Rac03]   S. T. Rachev. *Handbook of Heavy Tailed Distributions in Finance*. North
            Holland, 2003.

[RAC06]   David Rousseau, G.V. Anand, and François Chapeau-Blondeau.
           "Noise-enhanced nonlinear detector to improve signal detection
           in non-Gaussian noise". In: *Signal Processing* 86 (2006), pp. 3456–
           3465.

[SH12]   Khodr A. Saaifan and Werner Henkel. "A Spatial Diversity Recep-
           tion of Binary Signal Transmission over Rayleigh Fading Channels
           with Correlated Impulse Noise". In: *19th International Conference on
           Telecommunications*. Apr. 2012.

[SME12]   Tarik Shehata Saleh, Ian Marsland, and Mohamed El-Tanany. "Sub-
           optimal detectors for alpha-stable noise: simplifying design and
           improving performance". In: *IEEE Transactions on Communications*
           60.10 (Oct. 2012), pp. 2982–2989.

[ST94]   G. Samorodnitsky and M.S. Taqqu. *Stable non-Gaussian random pro-
           cesses*. United States of America: Chapman and Hall CRC, 1994.

[SM77a]   Arthur D. Sapulding and David Middleton. "Optimum reception in
           an impulsive interference environment - Part I: Coherent Detection".
           In: *IEEE Transactions on Communications* 58.9 (Sept. 1977), pp. 910–
           923.

[Sha12]   Ehab M. Shaheen. "Non-Gaussian MAI modeling to the performance
           of TH-BPSK/PPM UWB ciommunication systems". In: *8th Interna-
           tional Wireless Communications and Mobile Computing Conference
           (IWCMC)*. Limassol, Cyprus: IEEE, Aug. 2012.

[SN93]   Min Shao and Chrysostomos L. Nikias. "Signal processing with
           fractional lower order moments: stable processes and their applica-
           tions". In: *Proceedings of IEEE* 81.7 (July 19993), pp. 986–1010.

[SME10]   T. S. Shehat, I. Marsland, and M. El-Tanany. "A novel framework for
           signal detection in Alpha-stable interference," in: *IEEE Vehicular
           Technology Conference*. May 2010, pp. 1–5.

[Shi+06]   Soo Young Shin et al. "Packet error rate analysis of IEEE 802.15.4 un-
           der IEEE 802.11b interference". In: *IEEE 63rd Vehicular Technology
           Conference*. Melbourne, Australia, May 2006.

[SPV13]   Jorge Silva, Pedro Pinho, and Mário Véstias. "Design of the Alamouti
           scheme for a MIMO receiver and its implementation on an FPGA".
           In: *ISEL Academic Journal of Electronics*, *Telecommunications and
           Computers* 2.1 (2013).

[Sko78]   E.N. Skomal. *Manmade Radio Noise*. Princeton. NJ, 1978.

[SK14]   Lenka Slamova and Lev B. Klebanov. *On discrete approximations of stable distributions*. Mar. 2014.

[Sob09]   I.M. Sobol. *The Monte Carlo method*. Moscow: Mir pusblisher, 2009.

[Sou92]   E. Sousa. "Performance of a spread spectrum packet radio network in a poisson field of interferers". In: *IEEE Trans. Inform. Theory* 38.6 (Nov. 1992), pp. 1743–1754.

[SM77b]   AD. Spaulding and D. Middleton. "Optimum Reception in an Impulsive Interference Environment–Part II: Incoherent Reception". In: *IEEE Transactions on Communications* 25.9 (Sept. 1977), pp. 924–934.

[Tan97]   Mario Tanda. "Random signal detection in correlated non-Gaussian noise". In: *16ème Colloque GRETSI*. Grenoble, France, Sept. 1997, pp. 1261–1264.

[TR95]   A. Tesei and C.S. Regazzoni. "Signal detection in non-Gaussian noise by a kurtosis-based probability function model". In: *IEEE Workshop on HOS*. 1995.

[Tje07]   Jan Magne Tjensvold. *Comparison of the IEEE 802.11, 802.15.1 and 802.15.4 and 802.15.6 wireless standards*. Sept. 2007.

[Tol+16]   Viktor Toldov et al. "Experimental evaluation of interference impact on the energy consumption in wireless sensor networks". In: *2016 IEEE 17th International Symposium on A World of Wireless, Mobile and Multimedia Networks (WoWMoM)*. 2016, pp. 1–6.

[TNS95]   G.A. Tsihrintzis, C.L. Nikias, and M. Shao. "Performance of Optimum and Suboptimum Receivers in the Presence of Impulsive Noise Modeled as an Alpha-stable Process". In: *IEEE Trans. Commun.* 43.2 (Feb. 1995), pp. 904–914.

[Vas84]   Kenneth S. Vastola. "Threshold detection in narrow band non-Gaussian noise". In: *IEEE Transactions on Communications* 32.2 (Feb. 1984), pp. 134–139.

[WM57]   A. D. Watt and E. L. Maxwell. "Characteristics of atmospheric noise from 1 to 100 kc". In: *Proc. IRE* 45 (1957), pp. 787–794.

[WA12]   S. Weber and J. Andrews. "Transmission capacity of wireless networks". In: *Foundations and Trends in Networking*. Vol. 5. 2-3. London: NOW Publishers, 2012.

[WCT88]   Edward J. Wegman, Stuart C. Schwartz, and John B. Thomas. *Topics in non-Gaussian signal processing*. Springer-Verlag, 1988.

[Wei12]   Gu Wei. "Robustness against interference in Internet of Things". PhD thesis. Villeneuve d'Ascq, France: Université de Lille 1, 2012.

[WS11]   Thad B. Welch and Sam Shearman. *AC 2011-2086: Labview, the USRP, and their implications on software defined Radio*. 2011.

[WPS09]   M.Z. Win, P.C. Pinto, and L.S. Shepp. "A mathematical theory of network interference and its applications". In: *IEEE Proceedings* 97.2 (Feb. 2009), pp. 205–230.

[Yan15]   Xin Yan. "Robustness against interference in sensor networks". PhD thesis. Villeneuve d'Ascq, France: Université de Lille 1, 2015.

[YXG11]   Dong Yang, Youzhi Xu, and Mikael Gidlund. "Wireless coexistence between IEEE 802.11 and IEEE 802.15.4-based networks: a survey". In: *International Journal of Distributed Sensor Networks* 7.1 (2011).

[YZ14]   Fan Yang and Xi Zhang. "BER analysis for digital modulation schemes under symmetric alpha-stable noise". In: *2014 IEEE Military Communications Conference*. IEEE Computer Society, 2014, pp. 350–355.

[YP03]   X. Yang and A. Petropulu. "Co-channel interference modeling and analysis in a Poisson field of interferers in wireless communications". In: *IEEE Trans. Signal Process.* 51.1 (Jan. 2003), pp. 64–76.

[Yoo+06]   Dae Gil Yoon et al. "Packet error rate analysis of IEEE 802.11b under IEEE 802.15.4 interference". In: *IEEE 63rd Vehicular Technology Conference*. Melbourne, 2006, pp. 1186–1190.

[YWL07]   Wei Yuan, Xiangyu Wang, and Jean-Paul M. G. Linnartz. "A coexistence model of IEEE 802.15.4 and IEEE 802.11b/g". In: *Proceedings of 14th IEEE symposium on Communications and Vehicular Technology in the Benelux*. Delft, Netherlands, Nov. 2007.

[ZBA06]   S. Zozor, J.M. Brossier, and P.O. Amblard. "A Parametric Approach to Suboptimal Signal Detection in α-stable Noise". In: *IEEE Trans. Signal Processing* 54.12 (Dec. 2006), pp. 4497–4509.

Appendix A

Software and equipment list
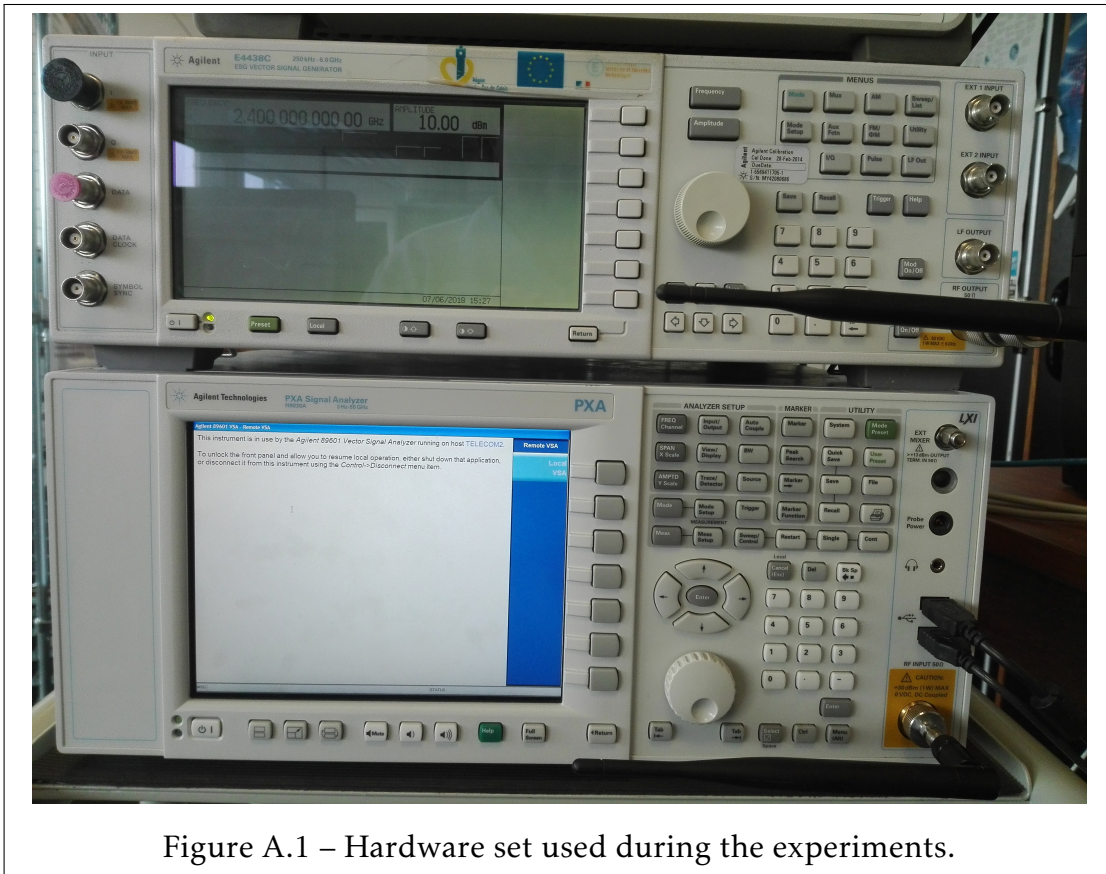
Figure A.1 – Hardware set used during the experiments.
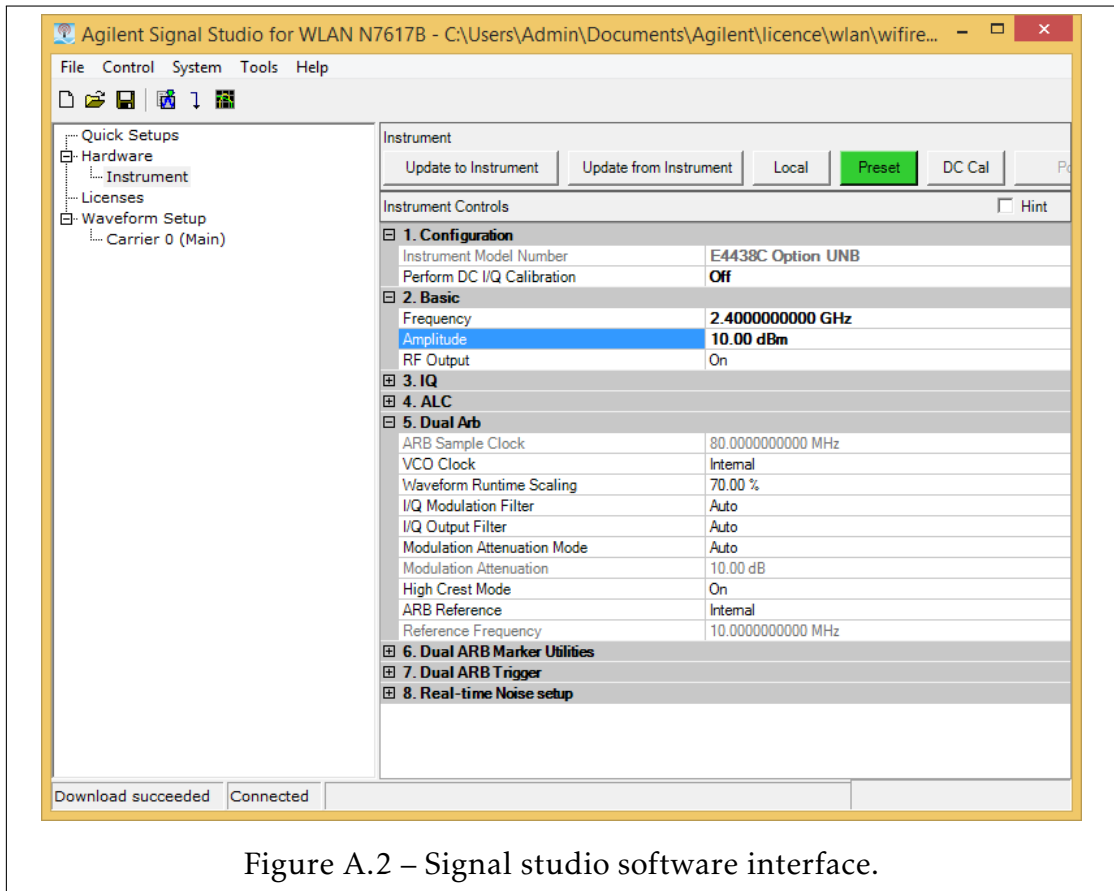
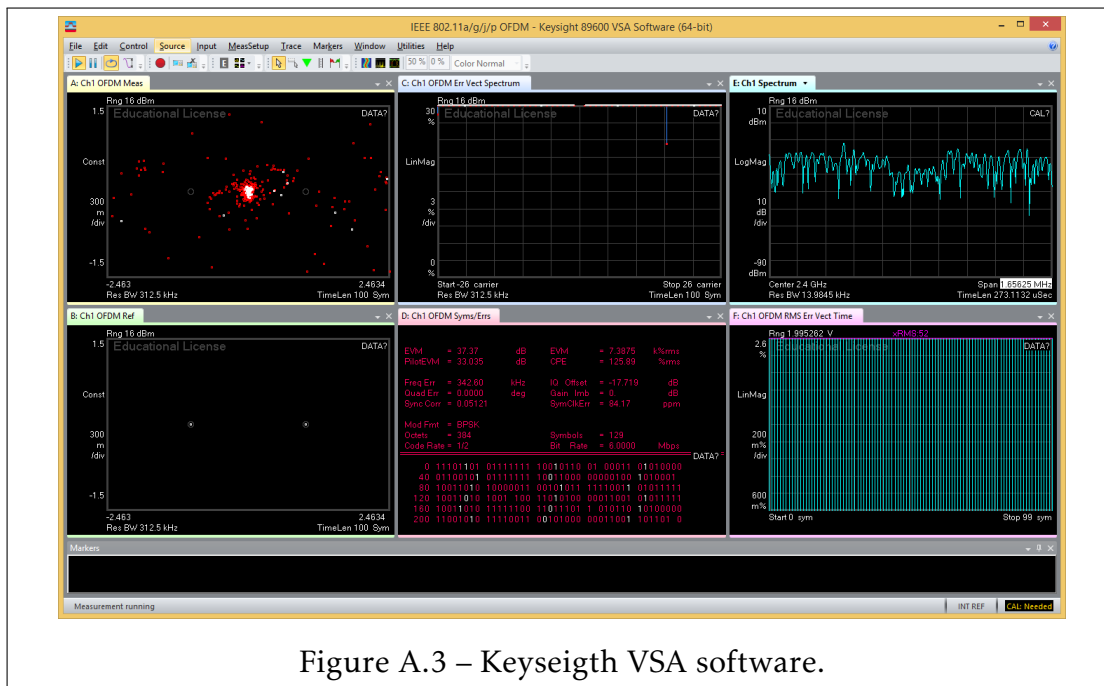Figure A.2 – Signal studio software interface.

Figure A.3 – Keyseigth VSA software.

Materials List: Hardware:

- 2 DIGI Xbee S1 XB24 modules;

- Agilent E4438C ESG Vector Signal Generator (250kHZ - 6.06GHz);

- PXA Signal Analyzer N9030A 3Hz-50GHz

- 1 Netbook and 1 PC Desktop

Software:

- XCTU;

- Keysight Technologies VSA Software;

- Signal Studio (for signal generation).

A.0.1   XCTU configuration
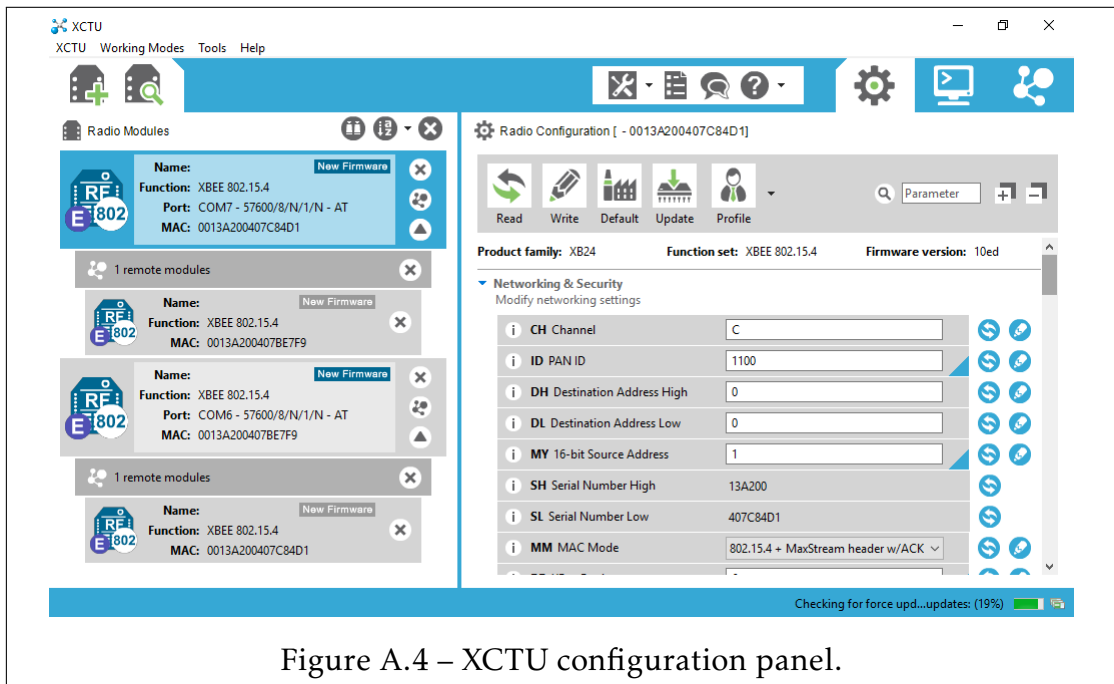
Figure A.4 – XCTU configuration panel.

Emitter Xbee configuration (XCTU):

- **Port:** COM7;

- **MAC:** 0013A200407C84D1;

- **Channel:** C;

- **PAN ID:** 1100;

- **DH destination address high:** 0;

- **DH destination address low:** 0;

- **My 16-bit source address:** 1;

- **SH serial number high:** 131200;

- **SL serial number low:** 407C84R1;

- **MM MAC Mode:** 802.15.4 MaxStream Header with/ ACK;

- **RR XBee retries:** 6;

- **BD interface data rate:** 57600;

- **Parity:** No parity.

Receiver Xbee configuration (XCTU):

- **Port:** COM6;

- **MAC:** 0013A200407BE7F9;

- **Channel:** C;

- **PAN ID:** 1100;

- **DH destination address high:** 0;

- **DH destination address low:** 1;

- **My 16-bit source address:** 0;

- **SH serial number high:** 131200;

- **SL serial number low:** 407BE7F9;

- **MM MAC Mode:** 802.15.4 MaxStream Header with/ ACK;

- **RR XBee retries:** 6;

- **BD interface data rate:** 57600;

- **Parity:** No parity.

Package configuration on XCTU

- **Package content:** Test1;

- **Transmit interval level: 0 or 500ms, depending on test**;

- **Loop ifinitely:** Active.

The test was repeated for the following scenarios:

Test sequence

- Wifi only;

- Wifi and Zigbee signals with 500ms between each Zigbee packet;

- Wifi and Zigbee continuous signals;

- Zigbee only continuous signal;

- Zigbee only signal with 500 ms between each Zigbee packet;

- Only background noise (no signal).

Appendix B

Some additional properties of α-stable RVs

B.1 Fractional Lower Order Moments, Negative Lower Order Moments

As stated on 2.4.6, the second order moments of a SαS random variable with $0 < \alpha < 2$ does not exist, all the FLOMs of order less than α do exist. Let X be a SαS random variable with $a = 0$ and dispersion γ, then [LS95]:

$$\mathbb{E}(|X|^p) = C(p,\alpha)\gamma^{p/\alpha}, 0 < p < \alpha, \tag{B.1}$$

where

$$C(p,\alpha) = \frac{2^{p+1}\Gamma(\frac{p+1}{2})\Gamma(-p/\alpha)}{\alpha\sqrt{\pi}\Gamma(-p/2)}. \tag{B.2}$$

[LS95] presents also the proof of existence of Negative-Order Moments, that can be expressed by:

$$\mathbb{E}(|X|^p) = C(p,\alpha)\gamma^{p/\alpha}, -1 < p < \alpha. \tag{B.3}$$

B.2 Fractional Absolute Moments

[MP13] uses techniques of fractional differentiation to obtain expressions for $\mathbb{E}[|X-\mu|^\zeta]$ with $1 < \zeta < 2$ and $\mu \in \mathbb{R}$ in terms of Laplace transform or characteristic function and gives applications on stable distributions, Pareto law, geometric stable law, Linnik law and combination of stable law with Linnik law.

Let $\zeta = k + \lambda, k \in \mathbb{N}, 0 < \lambda < 1$ and denoting $m_p := \mathbb{E}[|X|^p]$ a fractional absolute

moment of order $0 < p < 2$ and $m_{\mu,p} := \mathbb{E}[|X - \mu|^p]$ a μ-centered moment with $\mu \in \mathbb{R}$. If $0 < \alpha < 1$ and X is a stable with Laplace transform given by $\mathbb{E}[e^{-tX}] = exp\{-\sigma^\alpha t^\alpha\}$, then for $-\infty < \zeta < \alpha$:

$$\mathbb{E}[X^\zeta] = \frac{\Gamma(1 - \zeta/\alpha)}{\Gamma(1 - \zeta)}\sigma^\zeta. \tag{B.4}$$

In symmetric case, i.e. $\beta = 0$, with $\delta = 0$ is shown that:

$$m_\zeta = \frac{2^\zeta \Gamma((1 + \zeta)/2)\Gamma(1 - \zeta/\alpha)}{\Gamma(1 - \zeta/2)\Gamma(1/2)}\sigma^\zeta, -1 < \zeta < \alpha, \tag{B.5}$$

For general β and $\delta = 0$ we have:

$$m_\zeta = \kappa^{-1}\Gamma(1 - \frac{\zeta}{\alpha})(1 + \theta^2)^{\frac{\zeta}{2\alpha}}\cos(\frac{\zeta}{\alpha}arctan\theta)\sigma^\zeta, -1 < \zeta < \alpha, \tag{B.6}$$

where $\theta = \beta\tan(\frac{\pi\alpha}{2})$ and:

$$\kappa = \begin{cases} \Gamma(1 - \zeta)cos(\frac{\zeta\pi}{2}), & \text{if } \zeta \neq 1, \\ \frac{\pi}{2}, & \text{if } \zeta = 1. \end{cases} \tag{B.7}$$

Let X have a stable distribution with real parameters $\alpha > 1, |\beta| \leq 1, \delta = 0$ and $\sigma > 0$. Then, for $0 < \lambda < \alpha - 1$ we have:

$$m_{1+\lambda} = \frac{\lambda\Gamma(1 - \frac{1+\lambda}{\alpha})}{\sin(\frac{\lambda\pi}{2})\Gamma(1 - \lambda)}\sigma^{1+\lambda}(1 + \theta^2)^{\frac{1+\lambda}{2\alpha} - 0.5} \times$$
$$\times\cos[(1 - \frac{1+\lambda}{\alpha})arctan\theta] + \theta\sin[(1 - \frac{1+\lambda}{\alpha}arctan\theta)], \tag{B.8}$$

and for $\mu \in \mathbb{R}$,

$$m_{\mu,1+\lambda} = \frac{\lambda}{sin(\frac{\lambda\pi}{2})\Gamma(1 - \lambda)}\{\mu\int_0^\infty u^{-(1+\lambda)}e^{-\sigma^\alpha u^\alpha}\sin(\mu u - \theta\sigma^\alpha u^\alpha)du +$$
$$+\alpha\sigma^\alpha\int_0^\infty u^{\alpha-\lambda-2}e^{-\sigma^\alpha u^\alpha}[cos(\mu u - \theta\sigma^\alpha u^\alpha) - \theta\sin(\mu u - \theta\sigma^\alpha u^\alpha)]du\}, \tag{B.9}$$

where $\theta = \beta\tan(\frac{\pi\alpha}{2})$. If X is symmetric, i.e. $\beta = 0$, it follows that:

$$m_{1+\lambda} = \frac{\lambda\Gamma(1 - \frac{1+\lambda}{\alpha})}{\sin sin(\frac{\lambda\pi}{2})\Gamma(1 - \lambda)}\sigma^{1+\lambda}, \tag{B.10}$$

and

$$m_{\mu,1+\lambda} = \frac{\lambda\sigma^{1+\lambda}}{sin(\frac{\lambda_p i}{2})\Gamma(1-\lambda)}[\frac{\mu}{\sigma}\int_0^\infty u^{-(1+\lambda)}e^{-u^\alpha}\sin(\frac{\mu u}{\sigma})du+$$
$$+\alpha\int_0^\infty u^{\alpha-\lambda-2}e^{-u^\alpha}\cos(\frac{\mu u}{\sigma})du]. \tag{B.11}$$

For proofs and further information see [MP13]. More information on applications of Fractional Calculus on Probability and Random Variables see: [CD09] and [DP12].

B.3   Covariation, covariation estimation and conditional expectation

As discussed in 2.4.6, due to lack of finite variance, covariance does note exist for SαS RVs with $\alpha \neq 2$. In this section, the concept of covariation is introduced [LS95]. The covariation for SαS RVs plays a similar role to covariance for Gaussian RVs: Given two jointly SαS RVs X and Y with $1 < \alpha \leq 2$, the covariation of X with Y is defined by [LS95]:

$$[X,Y]_\alpha = \int_S xy^{<\alpha-1>}\mu(d\mathbf{s}), \tag{B.12}$$

where S is the unit circle and $\mu(\cdot)$ is the spectral measure of the $S\alpha S$ random vector (X,Y) and

$$z^{<a>} = |z|^a sign(z), \tag{B.13}$$

for any given $z \in \mathbb{R}$ and $a \geq 0$. The covariation coefficient of X with Y is given by [LS95]:

$$\lambda = \frac{[X,Y]_\alpha}{[Y,Y]_\alpha}. \tag{B.14}$$

X and Y play asymmetric roles according to the definition given above. Denoting now γ_y as the dispersion of Y, we have [LS95]:

$$[Y,Y]_\alpha = \|Y\|_\alpha^\alpha = \gamma_y, \tag{B.15}$$

$$\lambda_{XY} = \frac{\mathbb{E}(XY^{<p-1>})}{\mathbb{E}(|Y|^p)}, 1 \leq p < \alpha, \tag{B.16}$$

$$[X,Y]_\alpha = \frac{\mathbb{E}(XY^{p-1})}{\mathbb{E}(|Y|^p)}, 1 \leq p < \alpha, \tag{B.17}$$

B.3.1   Properties of covariations

Linearity in X

Given jointly SαS X_1, X_2 and Y, for any $a, b \in \mathbb{R}$, the covariation $[X, Y]_\alpha$ is linear in X [LS95]:

$$[aX_1 + bX_2, Y]_\alpha = a[X_1, Y]_\alpha + b[X_2, Y]_\alpha. \qquad (\text{B.18})$$

The Gaussian particular case

When X, Y are jointly Gaussian ($\alpha = 2$) with mean zero, the covariation of X with Y reduces to the covariance of X and Y [LS95]:

$$[X, Y]_\alpha = \mathbb{E}(XY). \qquad (\text{B.19})$$

Pseudo-linearity

Usually, $[X, Y]_\alpha$ is not linear with respect to Y. However, if Y_1, Y_2 are independent and X, Y_1, Y_2 are jointly $S\alpha S$, then, for any given constants $a, b \in \mathbb{R}$ [LS95]:

$$[X, aY_1 + bY_2]_\alpha = a^{<\alpha-1>}[X, Y_1]_\alpha + b^{<\alpha-1>}[X, Y_2]_\alpha. \qquad (\text{B.20})$$

X, Y independent

If X, Y are independent and jointly SαS, then [LS95]:

$$.[X, Y]_\alpha = 0 \qquad (\text{B.21})$$

The inverse in not necessarily true.

Cauchy-Schwartz inequality

Let X, Y be any two SαS given RVs, the Cauchy-Schwartz inequality holds [LS95]:

$$|[X, Y]_\alpha| \leq \|X\|_\alpha \|Y\|_\alpha^{<\alpha-1>}. \qquad (\text{B.22})$$

If X, Y have unit dispersion [LS95]:

$$|[X, Y]_\alpha| \leq 1. \qquad (\text{B.23})$$

B.3.2   Proposition

Let U_i independent SαS RVs with dispersion γ_i, for any a_i, b_i with $b_i \neq 0$ $i = 1, 2, ..., n$:

$$X = \sum_{i=1}^{n} a_i U_i. \tag{B.24}$$

$$Y = \sum_{i=1}^{n} b_i U_i. \tag{B.25}$$

Then [LS95]:

$$[X, X]_\alpha = \sum_{i=1}^{n} \gamma_i |a_n|^\alpha, \tag{B.26}$$

$$[Y, Y]_\alpha = \sum_{i=1}^{n} \gamma_i |b_n|^\alpha, \tag{B.27}$$

$$[X, Y]_\alpha = \sum_{i=1}^{n} \gamma_i a_n b_n^{<\alpha-1>}, \tag{B.28}$$

$$\lambda_{XY} = \frac{\sum_{i=1}^{n} \gamma_i a_n b_n^{<\alpha-1>}}{\sum_{i=1}^{n} \gamma_i |b_n|^\alpha}. \tag{B.29}$$

B.3.3   Covariation estimation

Given n independent observations (X_i, Y_i), with $i = 1, 2, ..., n$, the FLOM estimator is given by [LS95; SN93]:

$$\hat{\lambda}_{FLOM(p)} = \frac{\sum_{i=1}^{n} X_i |Y_i|^{p-1} sign(Y_i)}{\sum_{i=1}^{n} |Y_i|}. \tag{B.30}$$

Screened Ratio Estimator (SRE) is an unbiased estimator that can also be used for covariation estimation, and is given by [LS95; SN93]:

$$\hat{\lambda}_{SCR} = \frac{\sum_{i=1}^{n} (X_i Y_i^{-1} \mathcal{X}_{Y_i})}{\sum_{i=1}^{n} \mathcal{X}_{Y_i}}, \tag{B.31}$$

where:

$$\mathcal{X}_Y = \begin{cases} 1 & \text{if } c_1 < |Y| < c_2 \\ 0 & \text{otherwise,} \end{cases} \tag{B.32}$$

for arbitrary $0 < c_1 < c_2 \le \infty$. The LS estimation can also be applied for estimating $\hat{\lambda}$ [LS95; SN93]:

$$\hat{\lambda}_{LS} = \frac{\sum_{i=1}^{n} X_i Y_i}{\sum_{i=1}^{n} Y_i^2}.$$
(B.33)

B.3.4   Conditional expectation and linear regression

Given X_i, with $i = 0, 1, ..., n$ jointly SαS RV with $1 < \alpha \le 2$, spectral measure $\mu(\cdot)$. The regression of X_0 in terms of X_i is the conditional expectation $\mathbb{E}(X_0|X_1, ..., X_n)$, which, usually, in the SαS case is not linear. For the regression estimate to be linear, the following theorem presents a necessary and sufficient condition [LS95]:

Theorem B.3.1 *Let $X_0, X_1, ..., X_n$ be jointly SαS RV with $1 < \alpha \le 2$ and spectral measure $\mu(\cdot)$ on the sphere unit S in $\mathbb{R}^{n+1}$, then*

$$\mathbb{E}(X_0|X_1, ..., X_n) = \sum_{i=1}^{n} a_i X_i \iff \int_S (x_0 - \sum_{i=1}^{n} a_i x_i)(\sum_{i=1}^{n} r_i x_i)^{<\alpha-1>} \mu(d\mathbf{x}) = 0, \forall r_i,$$
(B.34)

with $i = 1, 2, ..., n$.

In other words, if the regression is linear, then the coefficients a_i are uniquely determined by $\mu(\cdot)$ if and only if X_i are linearly independents elements in the space of integrable random variables [LS95].

Corollary B.3.1.1 *If X_0, X_1, X_2 are jointly SαS and*

$$\mathbb{E}(X_0|X_1, X_2) = a_1 X_1 + a_2 X_2,$$
(B.35)

then a_1, a_2 satisfy [LS95]:

$$a_1 [X_1, X_1]_\alpha + a_2 [X_2, X_1]_\alpha = [X_0, X_1]_\alpha,$$
(B.36)

$$a_1 [X_1, X_2]_\alpha + a_2 [X_2, X_2]_\alpha = [X_0, X_2]_\alpha,$$
(B.37)

Theorem B.3.2 *If X_i, with $i = 1, 2, ..., n$ are jointly independent and non-degenerate SαS RVs then [LS95]:*

$$\mathbb{E}(X_0|X_1, ..., X_n) = \sum_{i=1}^{n} \lambda_{0i} X_i,$$
(B.38)

where λ_{0i} is the covariation coefficient of X_0 with X_i, $i = 1, 2, ..., n$.

It is important to observe that a SαS process has the linear regression property if and only if it is sub-Gaussian [LS95].

B.4   Zero-order statistics

FLOM do not provide a universal framework for the characterization of algebric-tailed process: for a given $p > 0$, the processes with $\alpha \leq p$ the associated FLOM does not exist. [GPA06] presents the concept of Zero-Order Statistics (ZOS), introducing three new parameters: geometric power, zero-order location and zero-order dispersion. They play a similar role to those played by power, expected vale and standard deviation in the theory of second-order processes, respectively. ZOS is based on logarithmic moments of the form $\mathbb{E} \log |X|$. Let X be a RV with algebric or lighter tails, then $\mathbb{E} \log |X| < \infty$ [GPA06].

Let X be a logarithmic order RV. We define the geometric power of X as [GPA06]:

$$S_0 = S_0(X) = e^{\mathbb{E} log |X|}. \tag{B.39}$$

B.4.1   ZOS properties

The ZOS have the following properties [GPA06]:

S_0 is a scale parameter

For any logarithmic-order process X, and any constant c:

- $S_0(X) \geq 0$

- $S_0(cX) = |c| S_0(X)$

S_0 is an indicator of process strength

- $S_0 = |c|$

- $0 \geq c_1 < |X| < c_2$ implies $c_1 > S_0 < c_2$

- $S_0(X) = 0 \Leftrightarrow \mathbb{P}(|X| < \epsilon) > 0 \forall \epsilon > 0$, which implies that zero power is only attained when there is a "pile up" of probability mass around zero.

Multiplicity

For any pair of logarithmic order RV X, Y and any real constant c:

- $S_0(XY) = S_0(X) S_0(Y)$;

- $S_0(X/Y) = S_0(X)/S_0(Y)$;

- $S_0(X^c) = S_0(X)^c$.

Absolute value inequality

For any pair of log-arithmetic-order RV X and Y:

$$S_0(|X| + |Y|) \geq S_0(X) + S_0(Y). \tag{B.40}$$

B.4.2 Geometric Power

[GPA06] gives a closed-form expression for the geometric power of SαS RVs:

$$S_0 = \frac{(C_g \gamma)^{1/\alpha}}{C_g}, \tag{B.41}$$

where $C_g \approx 1.78$ is the exponential of the Euler constant. The proof is given in [GPA06]. Let $L_x(p) = \mathbb{E}|X|^p$ a moment function, then [GPA06]:

$$S_0(X) = e^{L'_x(0)}, \tag{B.42}$$

where $L'_X(p)$ denotes the derivative of $L_X(p)$. For the proof and the results for the geometric and second order power of some common distributions, see [GPA06]. An estimation for the geometric power is given by [GPA06]:

$$\hat{S}_0 = \exp(\frac{1}{N} \sum_{i=1}^{N} \log|x_i|) = (\prod_{i=1}^{N} |x_i|)^{1/N}. \tag{B.43}$$

The geometric power is related to FLOM through the following theorem [GPA06]: Let $S_p = (|X|^p)^{1/p}$ denote the scale parameter derived from the p-th order moment of X. If S_p exists for sufficiently small values of p, then [GPA06]:

$$S_0 = \lim_{p \to 0} S_p. \tag{B.44}$$

Signal quality is defined as the ratio between the channel information and noise powers, in the second order-sense, known as Signal-to-Noise Ratio (SNR) of the communication system: high values of SNR indicates good quality, otherwise, indicates poor performance. Due to the infinite-variance of impulsive noises, the SNR is always zero, becoming a meaningless indicator of signal quality. The geometric power gives a universal indicator of signal quality that is meaningful and model-independent: let A be the amplitude of a modulated signal in an additive-noise channel with noise geometric power S_0, the G-SNR is given by

[GPA06]:

$$GSNR = \frac{1}{2C_g}(\frac{A}{S_0})^2. \tag{B.45}$$

B.4.3 Zero-Order Location

Let X be a logarithmic order variable. The zero-order indicator of location, μ_0, as the value that minimizes the geometric power of the shifted variable $X - \mu$, this is [GPA06]:

$$\mu_0 = \mu_0(X) = \underset{\mu}{argmin} S_0(X - \mu). \tag{B.46}$$

Properties

- μ_0 is a location parameter: Let X be symmetric and unimodal with symmetry center c, then $\mu_0(X) = c$.

- Shift and scale invariance: for any constants a, b:

$$\mu_0(aX + b) = a\mu_0(X) + b. \tag{B.47}$$

When locating a logarithmic-order distribution, we refer μ_0 as the center of the distribution and is said that X is zero-centered when $\mu_0(X) = 0$.

Zero-order estimation of location

Defining:

$$\hat{\mu}_\delta = \underset{\mu \in \Delta_\delta}{argmin} \sum_{i=1} N \log|x_i - \mu|, \tag{B.48}$$

where

$$\Delta_\delta = \mathbb{R} - \bigcup_{i=1}^{N}(x_i - \delta, x_i + \delta), \tag{B.49}$$

then:

$$\hat{\mu}_0 = \underset{\delta \to 0}{lim} \hat{\mu}_d. \tag{B.50}$$

Another simples definition is: given a sample of values $x_1, ..., x_N$, the zero-order estimator of location can be calculated as:

$$\hat{\mu}_0 = \underset{x_j \in \mathcal{M}}{argmin} \prod_{i=1, x_i \neq x_j}^{N} |x_i - x_j|, \tag{B.51}$$

where $\mathcal{M} = x_{m_1}, x_{m_2}, ..., x_{m_n}$ is the set of modes, or most repeated values in the sample.

Properties of the ZOS location estimator

- Shift and scale invariance: let $z_i = ax_i + b$ for $i = 1, ..., N$, then:

$$\hat{\mu}_0(z_1, ..., z_N) = a\hat{\mu}_0(x_1, ..., x_N) + b \tag{B.52}$$

- No overshoot/undershoot: $\hat{\mu}_0$ is always bounded by:

$$x_2 \leq \hat{\mu}_0 \leq x_{N-1} \tag{B.53}$$

where x_i denotes the i-th order statistic of the sample. If $N = 3$, $\hat{\mu}_0$ is equivalent to the sample median.

- Unbiasedness: Let X_i, $i = 1, ..., N$ be all independent and symmetrically distributed around the symmetry center c, then $\hat{\mu}_0 = \hat{\mu}_0(X_1, X_2, ..., X_N)$ is also symmetrically distributed around c, in particular, if $\mathbb{E}\{\hat{\mu}\}_0$ exists, then $\mathbb{E}\{\hat{\mu}\}_0 = c$.

Proofs and a discussion about optimality of $\hat{\mu}_0$ in very impulsive environments is given in [GPA06]

B.4.4   Zero-order dispersion

Let X be a logarithmic-order RV, the zero-order indicator of dispersion σ_0 is given by [GPA06]:

$$\sigma_0 = \min_{\mu} S_0(X - \mu) = S_0(X - \mu_0). \tag{B.54}$$

B.5   Multivariate stable distributions

For a stable k-dimensional distribution $F(\mathbf{S}), \mathbf{S} \in \mathbb{R}^k$, its characteristic function is given by [LS95]:

$$\varphi(\mathbf{t}) = \begin{cases} \exp\{j\mathbf{t}^T\mathbf{a} - \mathbf{t}^T A\mathbf{t}\} & \text{if } a = 2 \\ \exp\{j\mathbf{t}^T\mathbf{a} - \int_s |\mathbf{t}^T\mathbf{s}|^\alpha \mu(d\mathbf{s}) + j\beta_\alpha(t)\} & \text{if } 0 < \alpha < 2 \end{cases} \tag{B.55}$$

with

$$\beta_\alpha = \begin{cases} \tan\frac{\alpha\pi}{2} \int_s |\mathbf{t}^T\mathbf{s}|\mu(d\mathbf{s}) & \text{if } 0 < \alpha < 2, \alpha \neq 1 \\ \int_s \mathbf{t}^T\mathbf{s}\,log|\mathbf{t}^T\mathbf{s}|\mu(d\mathbf{s}) & \text{if } \alpha = 1 \end{cases} \tag{B.56}$$

where $\mathbf{a}, \mathbf{t} \in \mathbb{R}^k$. S is the k-dimensional unit sphere. $\mu(\cdot)$ is a finite Borel spectral measure on S and A is positive semi-definite symmetric matrix. α is the characteristic exponent. For the case $\alpha = 2$, we have a multivariate Gaussian distribution with mean $\mathbf{a}$ (the location vector) and covariance matrix. $2A$. $\beta_\alpha(t)$ is called skewed function. If $\beta_\alpha(t) \equiv 0$ we have a symmetric stable distribution, also called Symmetric α Stable, SαS. As in the univariate case, for the multivariate case, there's no closed-form expression for the density function [LS95].

B.5.1   Properties

Stability Property

A k-dimensional distribution function $F(\mathbf{X}), \mathbf{X} \in \mathbb{R}^k$ is called stable if, for any I.I.D. random vectors X_1, X_2 with distribution function $F(\mathbb{X})$ and arbitrary constants a_1, a_2, there exist $a \in \mathbb{R}, \mathbf{b} \in \mathbb{R}^k$ and a random vector $\mathbf{X}$ with the same distribution function $F(\mathbf{X})$ such that [LS95]:

$$a\mathbf{X} + \mathbf{b} \stackrel{d}{=} a_1 \mathbf{X}_1 + a_2 \mathbf{X}_2. \tag{B.57}$$

If $1 < \alpha \le 2$, then, a random vector $\mathbf{X}$ follows a multivariate stable law with characteristic exponent α if and only if all components of $\mathbf{X}$ follows a univariate stable (SαS) law with the same characteristic exponent α. The family of multivariate stable distributions forms a nonparametric set, except for $\alpha = 2$, instead of a parametric one in the case of univariate stable distributions [LS95].

Moments

If $X_1, X_2, ..., X_n$ are independent and α-stable, then [LS95]:

$$\mathbb{E}(|X_1|^{p_1}...|X_n|^{p_n}) < \infty, \tag{B.58}$$

if and only if $p_i < \alpha, i = 1, ..., n$. If $X_1, X_2, ..., X_n$ are dependent and jointly SαS, then the equation B.58 will be true if and only if $0 < \sum_{i=1}^{n} p_i < \alpha$ [LS95].

Index

Contents

On heterogeneous networks under non-Gaussian interferences: experimental and theoretical aspects

Abstract

Internet of Things represents a technical challenge for 5G communications due to its characteristic heterogeneity: the 2.4 GHz ISM band, for example, is shared between different kind of technologies, such Wifi, Bluetooth and Zigbee. In addition to the loss of quality of communication, recent studies show that interference increases significantly the energy consumption. So, dealing with interference becomes an important task to ensure successfull data transmission. The present thesis approaches two aspects of heterogeneous networks. The first part presents an experimental study on the nature of interference between IEEE 802.11 and IEEE 802.15.4 devices, its impacts on the communication reliability and proposes a statistical description of it. The main conclusion of this part is that, on this context, the interference may present a non-Gaussian behavior, more precisely, an impulsive behavior. Recent theoretical works allied with these experimental results show that the α-stable distribution is more adequate to represent impulsive noises. It means that the, once optimal, classical communication architectures based on the Gaussian assumption, particularly the Least Squares based channel estimation and linear receiver, is not optimal anymore, presenting a significant loss of performance. The second part presents a robust MIMO architecutre based on Alamouti coding, supervised channel estimation based on Least Absolute Deviation and p-norm receiver with an estimator for p. The proposed approach outperforms the classical method.

Keywords: internet of things, sensor netowrks, non-gaussian interference

RÉSEAUX DE CAPTEURS SOUS INTERFÉRENCE NON-GAUSSIENNE :
aspects expérimentaux et théoriques

Résumé

L'Internet des Objets représente un défi technique pour la communication 5G à cause de sa hétérogénéité caractéristique : la bande 2.4 GHz ISM, par exemple, est partagée entre différentes types de technologies, comme Wifi, Bluetooth et Zigbee. En plus de la perte de qualité de communication, des études récents montrent que l'interférence augmente de façon significative la consommation d'énergie. Donc, traiter l'interférence devient un tâche important pour assurer la réussite de la transmission de donnés. Cette thèse s'approche de deux aspects différents des réseaux hétérogènes. La première partie présente un étude expérimentale sur la nature de l'interférence entre dispositifs IEEE 802.11 et 802.15.4, ses impacts dans la fiabilité de la communication et propose une description statistique. La conclusion principale est que, dans ce contexte, l'interférence présente un comportement non-Gaussien, plus précisément, impulsif. Des travaux théoriques récents alliés avec ces résultats expérimentaux montrent que la distribution α-stable est plus convenable pour représenter bruits impulsives. Cela signifie que, une fois optimal, les architectures de communication classiques basé sur assomption Gaussienne, particulièrement le méthode des moindres carrés et le récepteur linéaire, ne sont plus optimales et présentent une perte de performance significative. La deuxième partie présente une architecture MIMO basé sur codage Alamouti, estimation de canal supervisée basé sur méthode *Least Absolute Deviation* et récepteur p-norme avec une estimation de p. L'architecture proposée présente une performance supérieure au méthode classique.

Mots clés : internet des objets, réseaux de capteurs, interférences non-gaussiennes